KfK 3941
Mai 1985

Fatigue Data Compilation and Evaluation of Fatigue on Design

A. Nyilas
Institut für Technische Physik

Kernforschungszentrum Karlsruhe

KERNFORSCHUNGSZENTRUM KARLSRUHE
Institut für Technische Physik

KfK 3941

Fatigue Data Compilation and Evaluation of Fatigue on Design

A. Nyilas

Study, performed under the contract No 151/84-4/FU D/NET
for the NET-team.

Kernforschungszentrum Karlsruhe GmbH, Karlsruhe

Kernforschungszentrum Karlsruhe GmbH
ISSN 0303-4003

Abstract

The aim of this report is a review of the available fatigue data of various materials necessary for the design of large superconducting magnets for fusion. One of the primary objectives of this work is to present a broad outline of the low temperature fatigue data of relevant materials within the scope of available data. Besides the classical fatigue data of materials the fatigue crack propagation measurements are outlined widely. The existing recommendations for the design of cryogenic structures are described. A brief introduction of fracture mechanics as well as a historical background of the development of our present day understanding of fatigue has been done.

Zusammenstellung von Materialermüdungsdaten und deren Wirkung auf die Auslegung

Zusammenfassung

Ziel dieses Berichtes ist es, einen Überblick über verfügbare Ermüdungsdaten von verschiedenen Werkstoffen, wie sie für den Bau von großen supraleitenden Magneten in der Fusionsenergiegewinnung verwendet werden, zu geben. Insbesondere wurden alle verfügbaren Tieftemperatur-Ermüdungsdaten der infrage kommenden Werkstoffe zusammengestellt. Neben den klassischen Wechselfestigkeitsdaten von Werkstoffen sind auch im weitesten Sinne die Rißausbreitungsuntersuchungen umrissen. Die zur Zeit bestehenden Empfehlungen zur Bauteilauslegung von kryogenen Strukturen sind dargestellt. Eine kurze Einführung in die Bruchmechanik einschließlich eines historischen Rückblicks auf diese Entwicklung, die zum heutigen Verständnis der Werkstoffermüdung geführt hat, wird gegeben.

Contents

Foreword

The aim of this report is a review of the available fatigue data of various materials necessary for the design of large superconducting magnets for fusion. In general, these magnets are composed of different materials each with a specific task and assembled as an operating unit. Magnet designers, therefore, have to decide for an optimum materials combination due to conflicting requirements in terms of structural and mechanical integrity, suitable electrical and thermal properties and their complex combination to a reliable operating unit for a long period of time. In addition, pulsed operation of the tokamak type fusion machines forces the magnet designers to take into account the fatigue response of the individual materials and the durability of the joined sections under repeated load condition. Basic data of the bulk materials as well as weldments, brazed, soldered, and adhesive joints give the actual fatigue behaviour of the components under design.

One of the primary objectives of this report is to present a broad outline of the low temperature fatigue data of relevant materials within the scope of data available. If low temperature data do not exist, an effort has been made to forecast at least the tendency of the fatigue response of the materials from the known ambient data.

The numerous cracking problems during the fabrication of the components recently shifted the fatigue problem from fatigue initiation to fatigue crack propagation of existing flaws in the materials. Todays engineering approach for critical components is based therefore, on the "damage tolerance" philosophy with respect to the length of time required to propagate a crack to its critical size i.e. that at which fracture occurs. Linear elastic fracture mechanics (LEFM) techniques have been successfully used for stressed members of complex structures. Because of these considerations, both the classical fatigue data of

materials, and the fatigue crack propagation measurements are outlined widely.

The existing recommendations for cryogenic structures are described. The lack of design guidelines to structures subjected to fatigue loading at cryogenic temperatures underlines the necessity of the work towards a low temperature design code. The preparation of such a design code should be carried out by a task group in cooperation with safety authorities. The design code should involve all the recent experience that arose during the construction of low temperature structures e.g. the LCT and MFTF activities.

To facilitate the use of fracture mechanics terminology for design engineers unfamiliar with this field the report has a brief introduction of fracture mechanics as well as a historical background of the development of our present day understanding of fatigue and its use in design [chapters 1 and 2]. Those familiar with this subject should pass chapter 3 where the compiled data is discussed.

1. Introduction to Fatigue

In modern mechanical engineering fatigue is a vitally important design consideration because the great majority of mechanical failures involve fatigue. Engineering applications of structural materials involve a wide variety of different operational modes. Only in a very few cases load bearing members are subjected to constant static loads. Repeated load changes, fluctuations, vibrations, etc. are common for operating modern machinery. In certain cases "safe" load from a static design point may cause sudden and catastrophic failure, and in addition the collapse of the entire structure. Such failures are referred to as "fatigue failures". A more general definition of fatigue can be made as the change of the properties in the materials due to repeated application of stresses or strains, thus leading to cracking, crack propagation and failure. In its broadest use the term "fatigue" refers to material failures as result of recurring loads, which means any structure of a machine subjected to load changes is potentially liable to fail by fatigue.

In contrast to other types of material failures e.g. corrosion, wear, distortion, creep etc . fatigue failures occur often with no prior indication of a deteriorated performance of the structure and without any warning of an impending collapse of the structure. Contrary to fatigue failure, other failures occuring in service cause only a nuisance, they may involve costly and time consuming repairs and in many cases loss of production, but in general no threat to life or other servere conditions. Therefore, any step towards safe designing against fatigue is in the primary interest of a designer.

Historically, the beginning of fatigue considerations is closely related to the development of the steam engines. According to Timoshenko /1/ the term fatigue was introduced by Poncelet of

France in a book published in 1839. Some decades later early locomotive design engineers were involved directly with fatigue failures of axle shafts, which were fractured after some hundred miles of service. In 1849 the British Institute of Mechanical Engineers met to consider this problem of the fracture of railroad axles and Hodgkinson was commissioned to investigate the severe situation. In 1852 the French government called a commission to also determine whether it could be recommended to change the railway axles after a certain period of time. But in that time the most realistic study of this fatigue problem was done by A. Wöhler, chief locomotive engineer of the Royal Lower Silesian Railways, whose name is now almost synonymous with the term fatigue. Between 1852 and 1869 A. Wöhler constructed the first repeated load testing machine, which was able to test the materials durability under load changing conditions. With this test equipment he carried out tests on materials of railroad axles and discovered two important facts of the materials response against recurring loads. He stated that no general relation exists between the load and the elapsed time of materials testing, but a strict correlation between the number of load changes (stress cycles) and the load level. The second important fact he pointed out was the existence of a limiting stress for ferrous materials, where an infinite number of stress cycles could be superposed without any damage of the materials under test.

From these early beginnings the fatigue failure investigations followed two distinct paths. First, investigations are performed to understand the fundamental mechanism of fatiguing of materials, including the static mechanical properties of the materials, microstructural relation, surface finishing, type of loading (random, constant amplitude etc .), size and shaping of the components under test, residual stresses, environmental effects etc. Second, data are collected with the aim of determining empirically the fatigue response of the materials under consideration and the effect of certain parameters, which may influence the fatigue properties.

Much of the modern tools such as X-ray diffraction methods, scanning electron microscope, transmission electron microscope, electron microprobe, helped to understand theoretically the fatigue phenomenon. Contributions to the dislocation theory beginning in the late 1940's influenced fruitfully the fatigue observations. In 1950, Frank and Read /2/ referred to this theory by advancing their proposition regarding the generation of new dislocations under load. This is now known as the Frank-Read sources. However, all these theories and the fundamental research, which give an important basic understanding of the fatigue problem could by no means adequately replace the empirical data for solving engineering problems in practical design. Therefore, empirical investigations will remain the backbone of the fatigue research for a long period of time. Often the theoretical explanation of the materials fatigue response will immediately follow the detailed analysis of the empirical findings of the load and cycle number correlations.

For the design engineer, the fatigue response of the materials means in general to find a compromise between conflicting requirements in terms of structural and mechanical integrity, safety and economy. Today the limiting strength criterion in many advanced designs is the adequate fatigue resistance. It is therefore essential for a designer, early in the design period, to make an effort of the possible influence of the recurring loads and the service environments on the special design problem. In addition, he should consult the metallurgists or the materials engineers to make a proper selection of the most suitable material and the processing of the planned design application. The fatigue failure should therefore be considered in the early stages of the design and not be an afterthought.

1.1 General description of fracture by fatigue

Fracture by fatigue starts generally from an existing small crack, which under repeated changes of the stress level grows in size and, as a consequence the remaining cross section can not sustain the applied load. For high cycle fatigue with stress application below the gross yielding level, fracturing by fatigue occurs without any observation of plastic deformation in macroscopic scale. In submicroscopic level, however, plastic deformation must take place to rearrange the atoms from one place to another and to move the failure in the microstructure.

All crystalline lattice structures have slip planes of different number and orientation, and the plastic deformation is a result of slip or sliding along the slip planes. Slip or plastic strain is irreversible in its nature and this means that there is no tendency to move back to a position of the former atomic arrangement. From the energy viewpoint, the slip is a mechanism by which the atomic plane glides along a preferentially oriented spacing (in general between 45^{o} - 60^{o} relative to the applied main tensile stress direction) where a lower energetic level exists. Accumulation of slip steps result in formation of parallel slipbands in the microstructure. Also mechanical twinning at submicroscopic level is important to the mechanism of fatigue fracture. In most metals at temperatures close to ambient, slip seems to be the predominant factor in fatigue failure. At cryogenic temperatures, especially with ferrous materials mechanical twinning is the more pronounced reason of fatigue fracture. The most obvious difference between slip and twinning is the shape change resulting from the deformations. Slip involves a simple translation across a slip plane such that one rigid portion of the solid moves relative to other, whereas the twinned body undergoes a shape change.

During the mechanism of slip formation mainly two types of microstructural changes in materials are possible. There are materials that can exhibit sufficient strain hardening or precipitation hardening, which create places of local plastic straining with the result of strengthening, thus giving enhanced resistance against further slip formation. In addition, the decrease of slip formation influences the microstructure in a manner, where the microcrack initiation almost stops. Contrary to this, in the absence of strain hardening effects, slip band develop submicorscopic cracks defined as initiation cracks. These initiation cracks may grow to a micro-crack and propagate under repeated load changes until the structure fails.

The origins of fatigue failures are in a majority of cases localized at highly stressed points, in general all types of geometric stress raisers, such as fillets, holes, screw threads etc., but may also involve inclusions embedded in the microstructure.

During the fatigue crack propagation the separated surfaces of the materials show patterns of concentric marks in the vicinity of the initial fatigue start. These marks are called beach marks or oystershells and result from the random characteristics of the load repetitions, from rest periods, intermittent loads, overloads etc.. The surface of this relatively slow crack growth region is defined as "fatigue zone" and its appearance is quite smooth in comparison to the final failure, where a coarse surface, called the instantaneous zone separates from the latter one. The fatigue zone is in general accentuated by the rubbing and hammering of both faces of the crack, as it opens and closes during the crack propagation. The instantaneous zone is similar to that of a static tensile failure (Fig. 1).

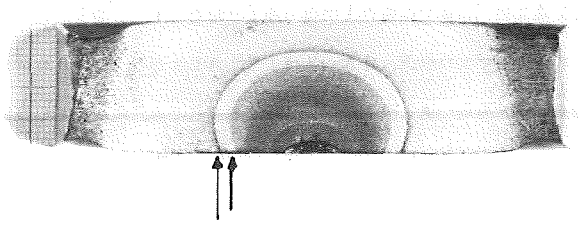

Fig. 1. Fatigue load appearance of an austenitic material. The marks characterize load variations in the "fatigue zone".

From the appearance of the separated surface one may determine the type of loading, which caused the failure. In general an apparent single origin together with a wide fatigue zone suggests a relatively low operational stress. In Fig. 2 the different types of loadings and their resultant fatigue fracture surfaces are schematically shown. The four most common loading types are given here in conjunction with laboratory fatigue tests.

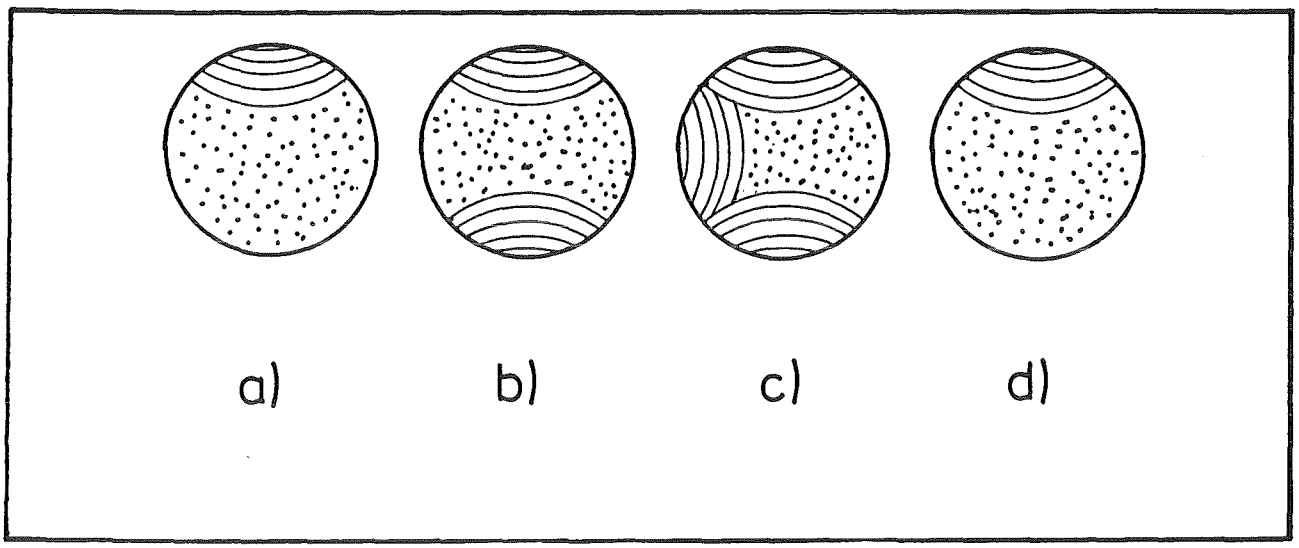

Fig. 2. Appearances of fatigue fracture surfaces for different loadings.
a) cyclic bending, b) completely reversed bending, c) rotating bending and d) axial loading.

In normal engineering application several types of loading are usually present. Moreover, the loading conditions are being associated axial loading with bending loads or with a more complex loading system. However, the fracture will invariably originate at a geometrically sharp corner or at a stress raiser similar to laboratory gained test results.

It should be emphasized that the correct interpretation of each particular fracture must be considered in relation to the materials type, condition of loading, shape and size of the

structure, magnitude of the stresses and the environmental conditions.

1.2 Crack nucleation and propagation

The life of a structure under plane fatigue conditions corresponds mainly to the crack initiation and the growth of the initiated cracks to micro- and macrocracks. No clear definition of microcracks or of initiation cracks exists. Basically an initiation crack or stage I crack can be described as any crack, which can just be observed under high magnification light microscopes. These cracks are able to form themselves into a microcrack, with the possibility of later propagation.

The origin of stage I cracks is closely related to the phenomenon of slip due to static shear stress. Figure 3 shows the slip development schematically.

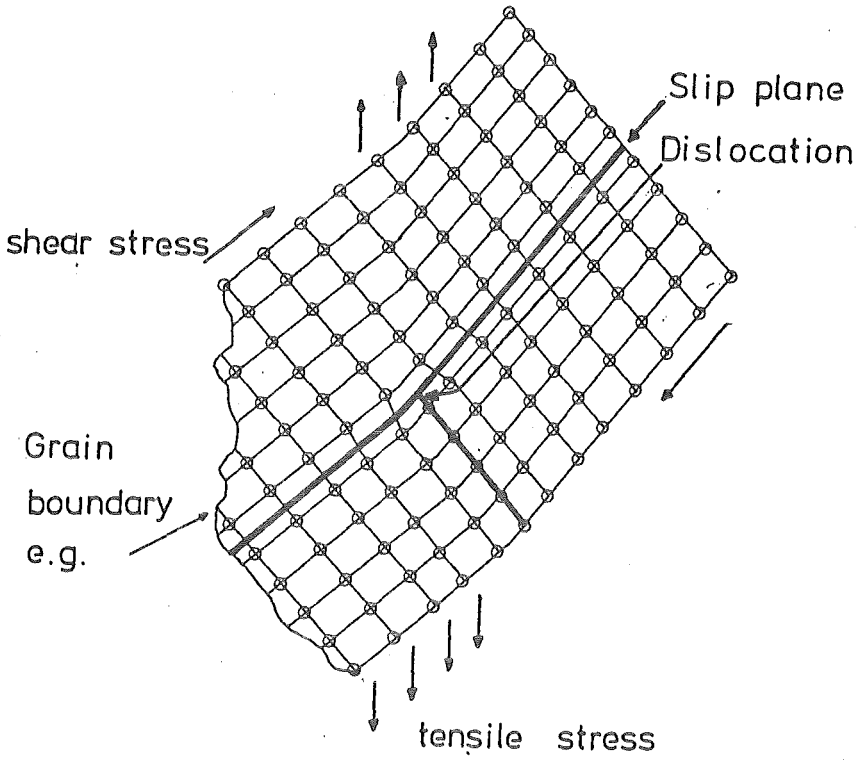

Fig. 3. Translation of atomic arrangements across a slip plane under the effect of shear stress. Starting position is a dislocation source.

The slip happens along a particular slip plane, where a dislocation in an atomic arrangement exists. According to this mechanism, as loading increases, nearly all grains will be involved in the process of slip band formation. The free surface shows parallel shifted slipbands, similar to regions of distortion such as intrusions and extrusions, which can be observed in the microstructure (Fig. 4).

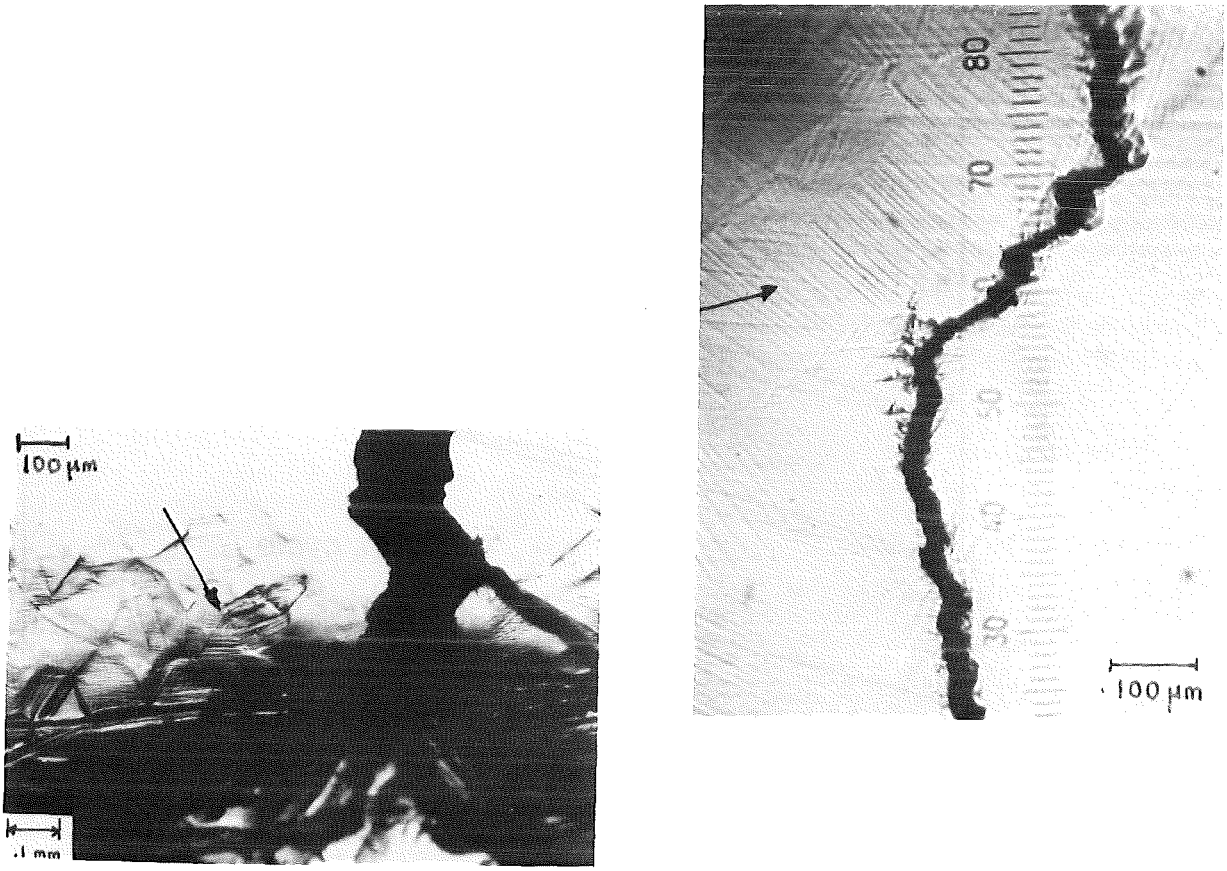

Fig. 4. Crack propagation and the slip band formation in the grains of an austenitic material observed under high magnification light microscope.

This block type nature of the slip produces crystal yieldings at stresses below the nominal yield point of the material. The action itself is localized to a few crystal zones of high

stress concentration. Due to strain hardening or precipitation hardening these local positions may be strengthened with consequence of an eventual stop of further slip motion. The mechanism here is demonstrated in Fig. 5 for a material having strain hardening.

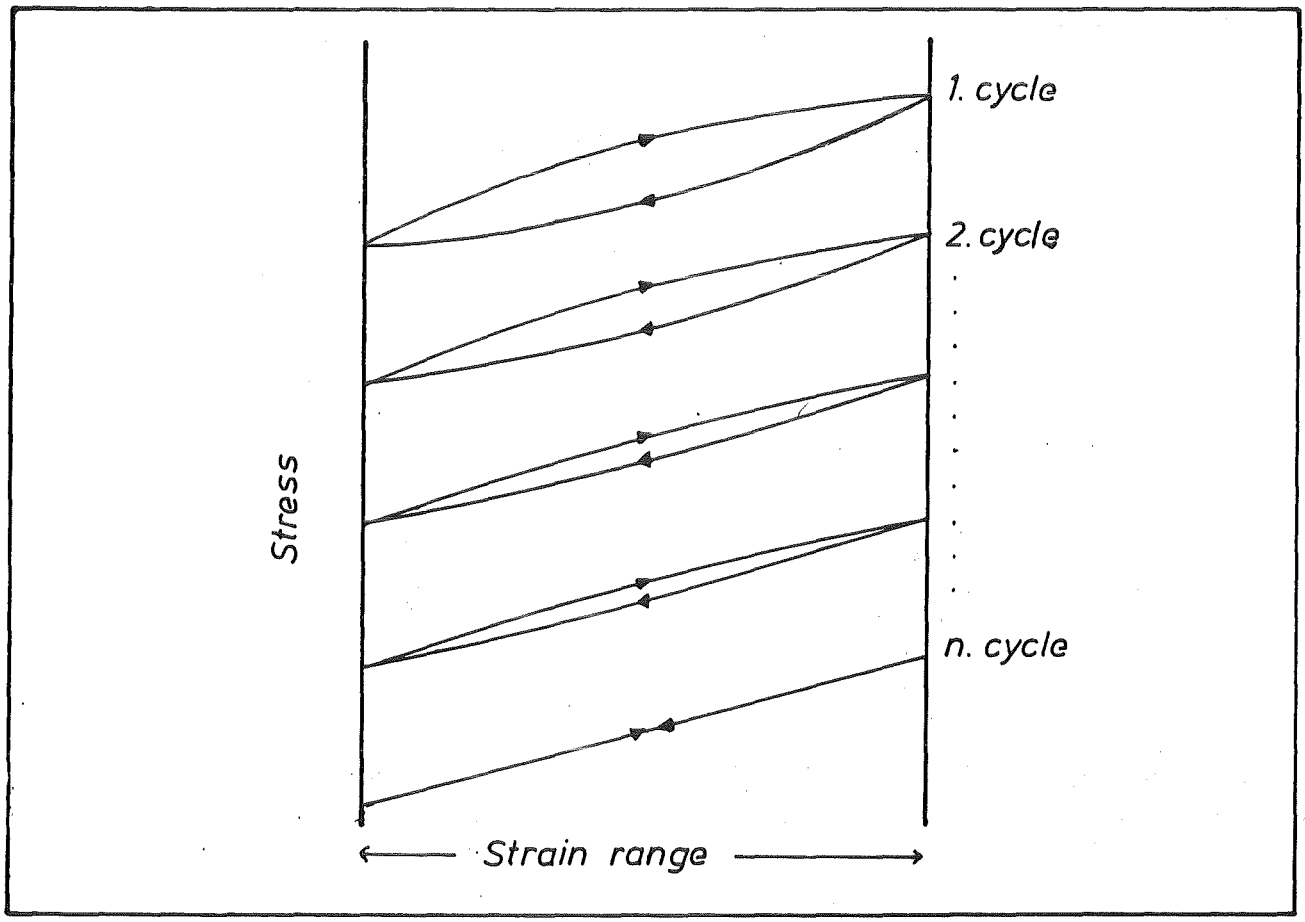

Fig. 5. The stress-strain response of a material under repeated loading. The strain hardening stops after a certain number of cycles and the material behaves itself total elastic

Under cyclic loading condition the stress-strain curve of such a material shows a disappearance of the plastic deformation. The hysteresis loops vanish after a fraction of the end cycle number

and the obtained load-deformation relation thereafter indicates the stopping of slip development. The extent and number of the slip bandes are a function of the applied stress level. In addition, the possibility of the crack nucleation is a competition between the two basic mechanisms, the strengthening effect by strain hardening and the tendency of the development of stage I cracks in the slipbands. Once small stage I cracks have been opened, there is a large probability for the spread of many small cracks to a microcrack.

The development of fatigue slip bands and the subsequent microcrackings is a result of the shear stresses in a small volume fraction of the material. The spatial dimension of the critical volume is within the range of a grain size. According to this phenomenon fine grained materials are in general more susceptible to fatigue weakening by notches than coarse grained materials.The higher strength behaviour of fine grained materials can compensate this fatigue weakening effect due to their low strain and high yield property. In addition, a perfectly brittle material with no ability of plastic deformation will develop no slip bands. Virtually such materials should not fail under fatigue loading. Certain glasses and some ceramics reveal this phenomenon.

The mechanism of fatigue crack propagation differs considerably from the nucleation mechanism of a crack. The main difference is the triaxial nature of the stress at a crack tip, which serves as a stress raiser. The material in front of the crack will be strengthened by strain hardening due to cyclic loading. The resultant normal tensile stresses serve to open the crack.

This means that the direction of the fatigue crack advance changes from the plane of maximum shear stresses, in general 45^{o}, to the plane approximately normal to the existing highest alternating tensile stress. The crack may propagate across the

grain boundaries, passes the grains through and reaches the next grain boundary even though they enhance the fatigue resistance.

The maximum tensile stress during cyclic loading is almost twice as high as the maximum shear stress. In the case of alternating compression stress, where no tensile components exist the crack opening are disturbed and the crack growth occurs along the slip planes subjected to maximum alternating shear stress. Therefore the observed crack growth under alternating compression is much slower than under alternating tension loading.

In combined loading cases, where torsional loading are also present the condition will be somewhat complicated but in general, here also the maximum tensile stresses may be the most important criterion for crack growth.

1.3 Rotating bending tests, S-N-curve

Fatigue testing machines can apply various loading conditions such as single point loading (the bending moment increases toward the fixed end), beam loading with constant moment applied in the gauge section of specimen, and unidirectional tension or tension-compression loading. The test machines most frequently used are the Wöhler type machines, which have a single point cantilever loading (see Fig . 6), and the R.R. Moore testing machines with four point loading (Fig. 7).

In all these machines the specimen rotates and according to the loading, stresses are applied at the top fibers of the specimen´s surface. The standard specimens are 7,5 mm in diamater, and the large fillet radius renders them practically free of stress concentrations. The surfaces are always mirror polished by abrasives to ensure the absence of stress raisers at the surface. The variation of stress with time may be approximated by a sinusoidal type of loading cycle. Modern fatigue testing machi-

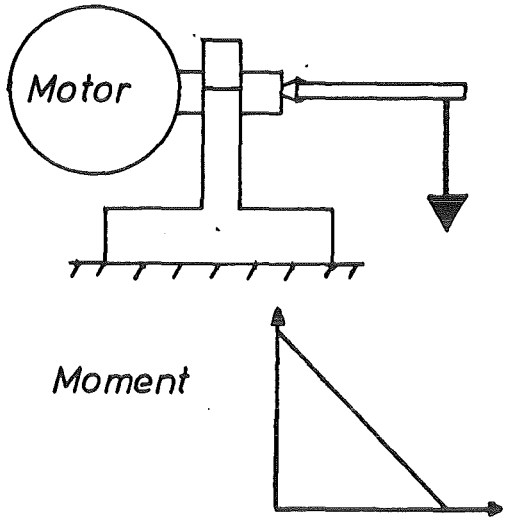

Fig. 6. Single point loaded specimen in a rotating bending test machine.

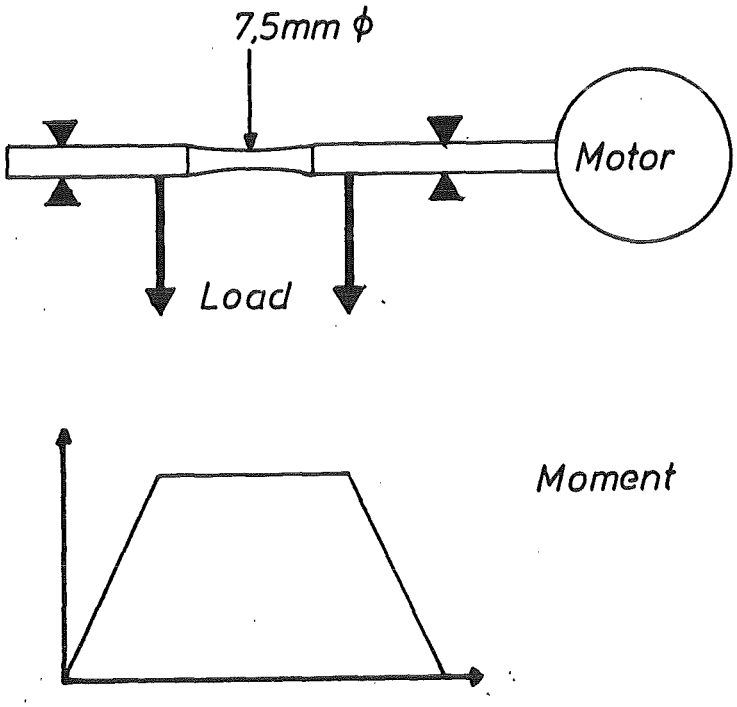

Fig. 7. Beam loaded specimen in a R.R. Moore type testing machine. Standard specimen has 7,5 mm diameter.

nes can also simulate and exactly reproduce the complex service load history, even for non-sinusoidal type of sequences. The rotating bending machines produce completely reversed bending, thus setting each point of the outer fibers of the rotating specimen under alternating compression and stress. In general, the machine´s speed is 1750 rpm and speed variations between 200 and 10 000 rpm doesn´t effect the fatigue results significantly.

A common way to produce stress S vs. number of cycles N data is to mount identical specimens in rotating bending test machines. The applied loads, however, should be selected prior to testing to give stresses, which range slightly above or below the expected materials endurance limit.

The stress S is a nominal stress, which is calculated with the effective section by simple elastic beam theory, disregarding the influence of notches or other geometric discontinuities. This nominal stress of the specimen can be calculated according to the relation

$$S = M \cdot y/I \qquad (1)$$

where M = bending moment at the net test section
I = moment of inertia at the net test section
y = distance from neutral axis to extreme outer fiber at net test section

are. The formula delivers valid stresses in the elastic, but not necessarily in the plastic regims. For circular specimens with $I = \pi \cdot d^4/64$

$$S = 32.M/\pi.d^3 \qquad (2)$$

The fatigue life N is defined as the number of cycles necessary to cause failure under given loading condition. In standard practice the nominal stress S is correlated to the ultimate tensile stress S_u gained by static tension test. The curves S/S_u vs. N are approximated well by straight lines (Fig. 8).

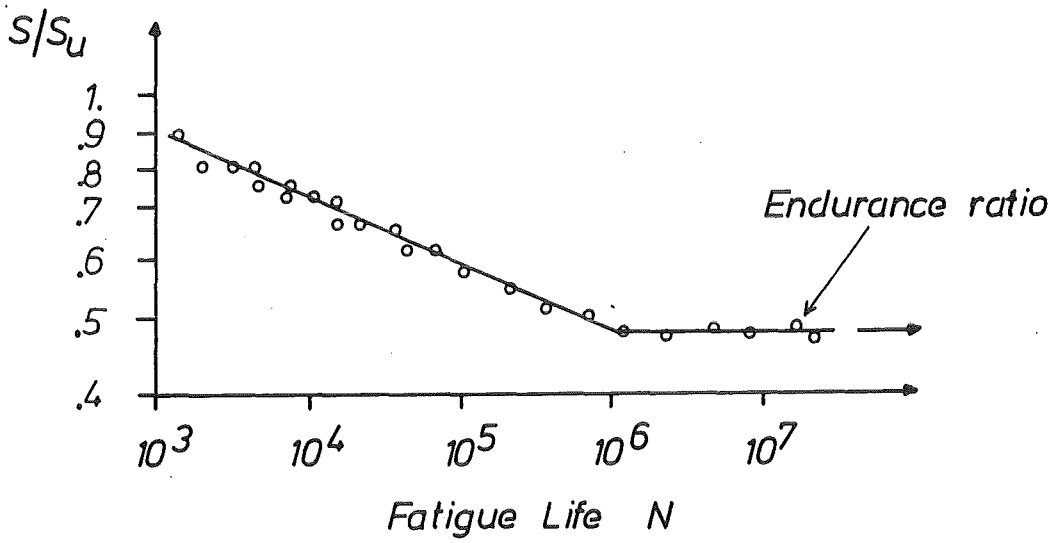

Fig. 8. Representation of fatigue data in logarithmic scale deliver straight lines with a knee. The horizontal portion states the endurance limit of the materials under test.

This is also common to represent the data of the actual calculated nominal stress as a function of fatigue life N, which directly gives the S-N relationship. But the correlation with ultimate tensile strength delivers a deeper understanding of the materials' fatigue behaviour. Figure 8 gives the relation for a hypothetical material. The stress ratio at the "infinite" life portion is defined as the fatigue endurance ratio, an important parameter for the material under consideration. The fatigue life N is an integral quantitiy and comprises the number

of cycles necessary to nucleate a crack, to propagate the crack and final fracture. Approximately 60 - 80 percent of the fatigue life can be attributed to crack nucleation and only the remaining percentage is necessary for crack growth and failure.

1.4 Fatigue response of different materials

Many investigators have developed empirical relationships between the fatigue strength and the mechanical properties of the materials. For both ferrous and nonferrous materials correlations have been found between the strain hardening parameters and the true stress - true strain curves. In addition, hardness of a material is also related to its fatigue strength. For a given type of a material the endurance ratio increases with the increase of the materials hardness, reaches maximum and then drops down at further hardness increase. The mechanical properties, microstructural treatments e.g. coarse or fine grained, duplex structures etc. strongly affect the fatigue strength of materials. In Fig. 9 a rough range of endurance ratios are represented for different types of ferrous materials, some nonferrous materials and engineering plastics. In majority of cases all investigated materials fall in the given ranges, but still there are some extreme cases. Also there are cases, where tests have been recommended to extend the cycle numbers to 2.10^7 or even more to establish endurance limits. The designer must keep this remaining uncertainty in mind.

1.5 Effect of size and surface finish

Under bending and torsional loading conditions a decrease of the endurance strength limit is observed with increasing the size of the specimen. A large diameter increase from the standard 7,5 mm usually reduces the endurance limit by ~ 10%. This reduction remains constant up to ~ 50 mm diameter. The size factor, which must be taken into account is therefore assumed to be ~ 0.9 for parts larger than 10 mm in diameter and 1.0 for smaller parts.

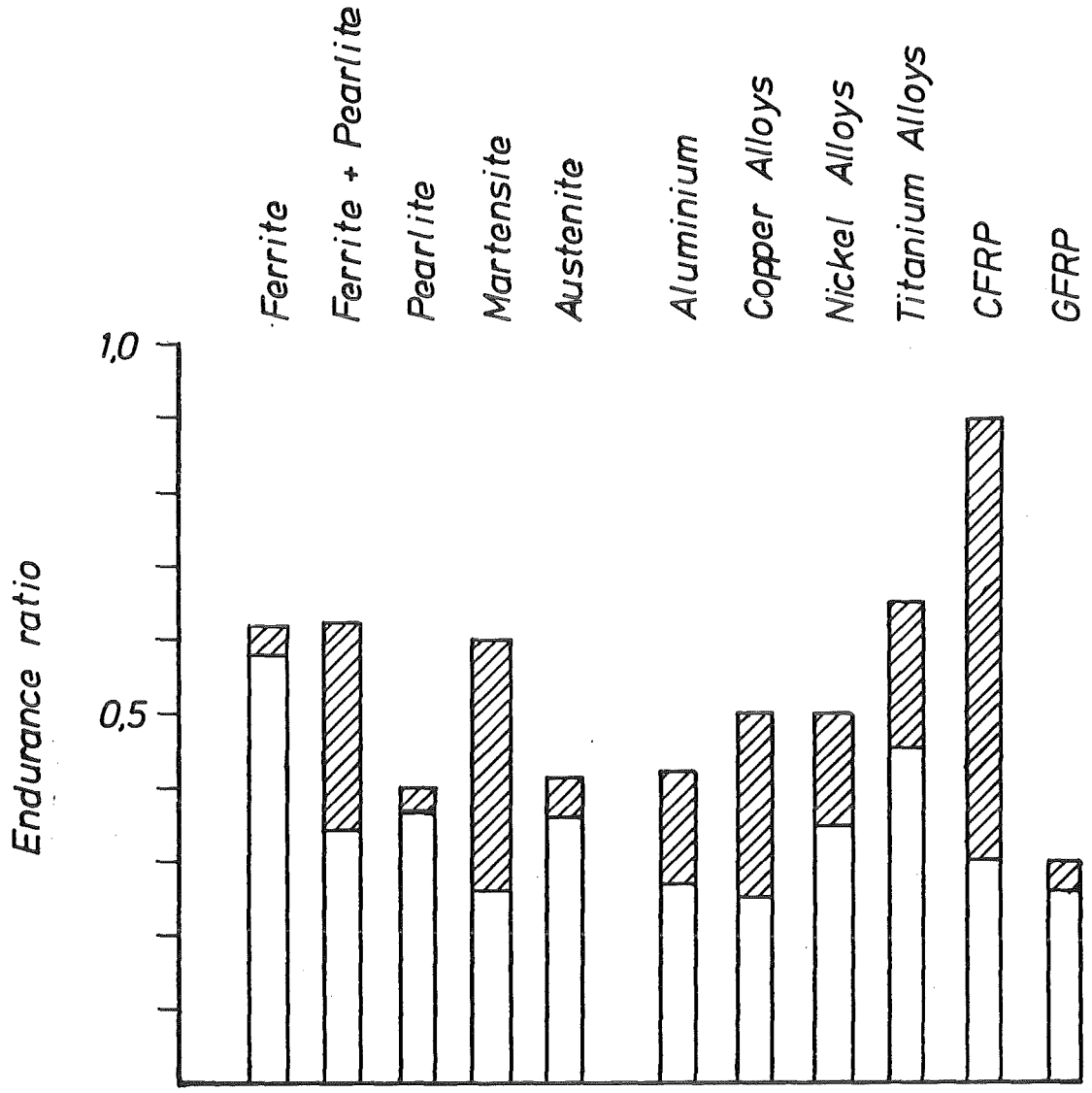

Fig. 9 Endurance ratio of different materials. Dark region represents alloys microstructural influence on the endurance ratio. The endurance cycle limit is for ferrous materials 10^7 cycles, for aluminium alloys ~ $5 \cdot 10^8$ /3/, for copper alloys ~ 10^8 /4/, for nickel alloys ~ 10^8 /5/ and for titanium alloys 10^6 - 10^7 cycles /5/. For engineering reinforced plastics (CFRP and GFRP) the endurance limit is here given with 10^7 cycles, but for this class of materials even beyond of the 10^7 cycles the endurance ratio decreases still /6/.

The size effect is mainly attributed to the stress gradient in the material during the bending load, which is steep for smaller diameters. In loading cases in which no gradient exists, such as in purely axial loading, no size effect could be determined between 7,5 mm to 50 mm diameter. However, for parts above 50 mm size low size factors (0,6 - 0,7) have been observed even for axial loading condition. Here the stress gradients and their effect should be ruled out. The reason for this is the heterogeneous nature of the microstructure, which is more pronounced for larger parts. In addition, the detrimental residual stresses can also strongly affect the fatigue endurance limit. Residual stresses can originate from non-uniform heat treatments of large parts.

The design engineer, therefore, should take into account a size factor for large parts and allow only lower strength limits compared to the laboratory results. A factor of 2 as a design guide is common for designing large components against fatigue, unless specific test data are available to support the use of higher values.

The surface finish, on the other hand, influences the endurance strength by introducing residual stresses at the surface. The grinding with abrasives often creates a layer with residual tension at the surface, which increases the tensile component of the stress at reversed loading. In addition, the metallurgical properties of the surface layer may also be altered, e.g. by removal of the decarburized layer of a forged surface or of the heat treated layer of the near surface. The roughness can change also the properties of the surface concerning the stress concentration. In practical applications, metal surfaces are sufficiently rough enough to cause additional stress raisers compared to the materials' internal defects. Therefore, there may be a difference between determined fatigue strength values of standard mirror polished samples and of the actual parts of the same material. This ratio must be considered in the design as a surface factor.

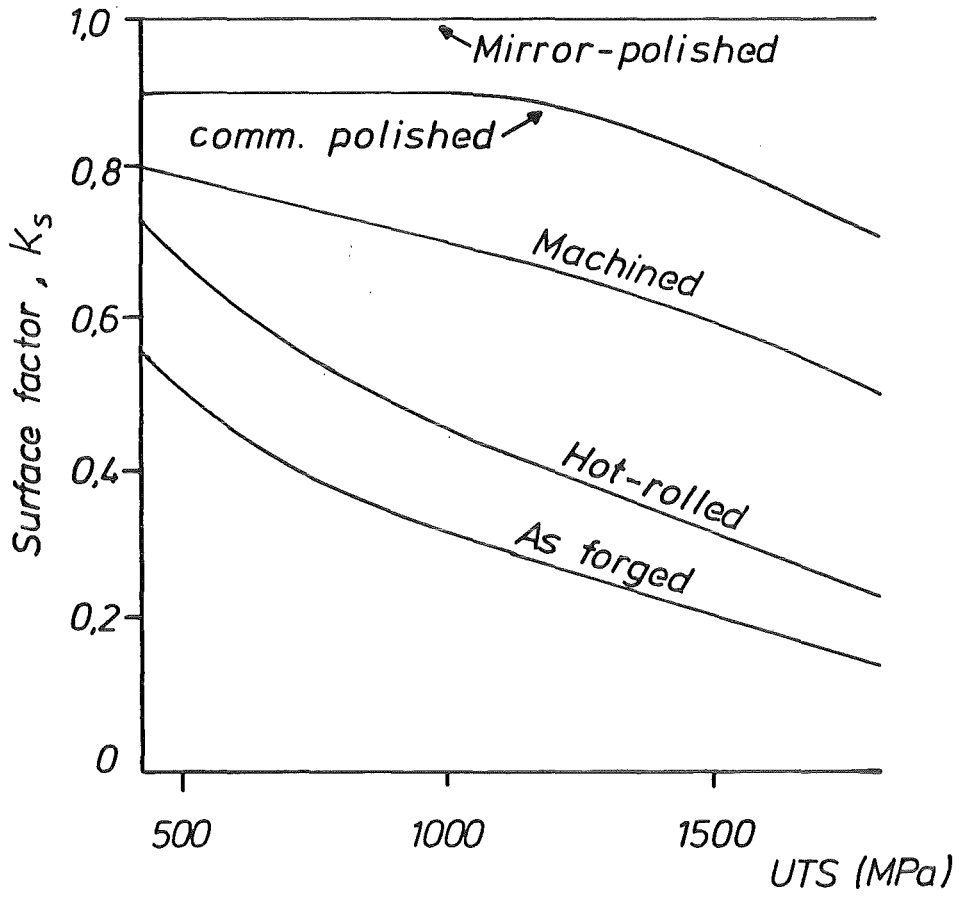

Fig. 10 Surface factor vs. tensile strength of a ferrous material with different kinds of surface finishing.

Figure 10 represents the fractional decrease of the endurance strength of materials due to various fabricated surfaces. The change of the fatigue behaviour between special finished standard fatigue samples and the category of commercial surface finishing practices are represented in this plot with respect to the materials ultimate tensile strength. The commercially polished surface is a high grade industrial finish with carefully controlled grinding and polishing procedures. The surface roughness achieved by this practice is approximately less than 3 µm. In most cases cost will prohibit the use of this

procedure, but for certain high performance parts this method is in use. When surface roughness is taken into account care should be taken to at least produce the surface markings parallel to the main loading direction. This enhances the endurance limit considerably. Harder materials with a uniformly fine-grained microstructure are more susceptible to fatigue weakinging by surface roughness and other geometrical irregularities.

1.6 Constant life fatigue strength diagrams

A sinusoidal type, repeated time dependent stress is characterized by the following quantities (Fig. 11).

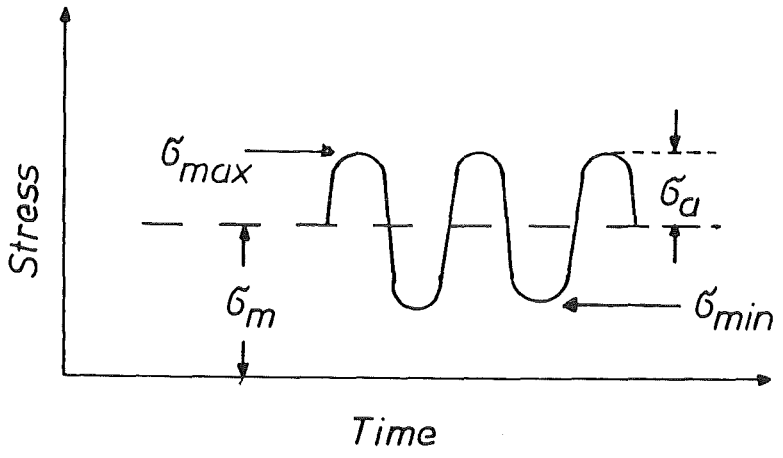

Fig. 11. Stresses in a material under sinusoidal loading.

σ_{max} = Maximum stress of the material
σ_{min} = Minimum stress of the material
σ_a = Alternating stress $(\sigma_{max} - \sigma_{min})/2$
σ_m = Mean stress $(\sigma_{max} + \sigma_{min})/2$
R = Stress ratio $\sigma_{min}/\sigma_{max}$

These variables may be used to construct lines of constant fatigue life.

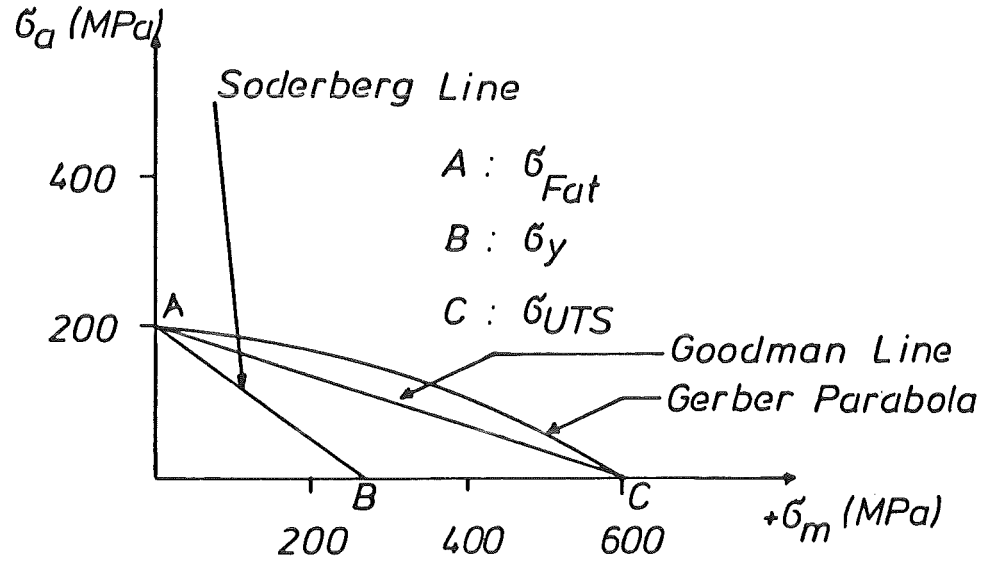

Fig. 12. Constant fatigue life for an austenitic material at ambient temperature.

An example is given in Fig. 12 for infinite fatigue life of an austenitic material at ambient temperature. The reduction of the permissible alternating streess σ_a with increasing mean stress σ_m in the materials is demonstrated: σ_a is largest at zero mean stress (σ_{Fat} at point A) and approaches zero as the mean stress is raised to the ultimate tensile stress at point C. Experimental data scatter in the region between the "Gerber-Parabola", which represents an empirical upper bound and

the "Goodman-Line" for the corresponding lower bound. The "Soderberg-Line" is used for very conservative designs as it excludes the possiblity of failure by general yielding. It is a straight-line interpolation between the experimentally determined value of σ_{Fat} and the yield strength σ_y of the material at point B.

The simplified diagram of Fig. 12 represents the portion of the fatigue loading under tensile mean stress conditions only. The compression mean stress side of the diagram would be symmetrical if the failure mechanisms between tensile and compression loading were identical. In general, materials behaviour under compression mean stress is not as critical as in the case with tensile mean stress. Therefore, the diagram is distorted towards largest allowable mean compression stress as Fig. 13 shows this schematically.

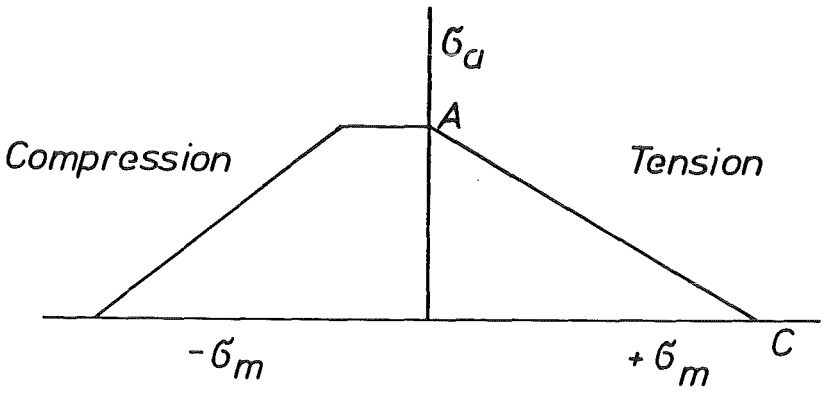

Fig. 13. Compression side of the constant fatigue life diagram.

A variation of the σ_a-σ_m-diagram is shown in Fig. 14 for arbitrary stress units.

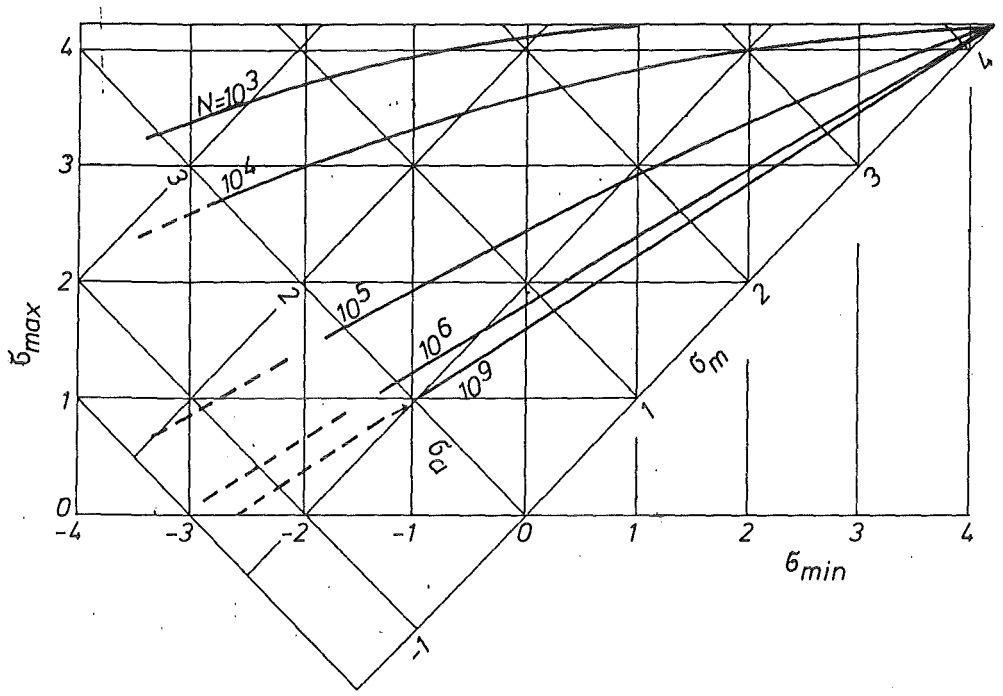

Fig. 14 Constant fatigue life diagram for a material of different fatigue lifes. Arbitrary units.

To gain maximum possible information the common way to represent the actual fatigue analysis is to plot the measured data with reference to Fig. 12 as shown in Fig. 14. The mean-stress and the alternating stress coordinates are turned 45^{o} anticlockwise, to introduce the parameters minimum and maximum stresses as new coordinates. The iso-fatigue lines are lines between Gerber parabola and Goodman line. In Fig. 12 σ_{Fat} at point A refers to the line for $N \geq 10^{9}$ cycles. The compression side of the diagram is represented by dashed lines.

1.7 Low-cycle fatigue

Fatigue problems in engineering applications are mainly concerned with adequate life under many millions of stress cycles which is essentially identical to infinite life. In certain situations, however, only short or finite fatigue life

is required. With respect to short life, one may reduce the mass of components increasing the allowable stress limits, if weight is a critical parameter (e.g. high pressure vessels, pipe works, aircraft components and submarine hull structures) a relaxation of the infinite life design concept is advantageous, especially with regard to elasto-plastic properties of the materials. The basis for this reasoning is that structures exposed to a limited number of high stress cycles are in general subjected to plastic deformations. The materials resistance against failure will be dictated by its resistance to so called low-cycle fatigue.

It is generally agreed that low-cycle fatigue for metallic materials is concerned with lifetimes of less than one million cycles and in practical design even less than ten thousand cycles. The word "low" refers to the number of cycles to failure and not to the magnitude of the applied stresses. Mainly, the nominal stresses are above the initial yield strength of the material and drive it to failure after a short sequence of cycling. Thus, low-cycle fatigue normally involves plastic deformation of the material and it may be also called strain fatigue. A good literature survey is available from Yao et al. /7/. Only a short discussion to understand the relevant results is given in the following. Low-cycle fatigue is a function of strain:

$$\varepsilon \cdot N^{m} = c \qquad (3)$$

with

ε = true strain range

N = cycles to failure

m and c = material constants

Sometimes "true strain" refers only to the strain in the plastic range, but in many other applications to the total strain range. There is also no complete agreement, whether to take into account the "true strain ε" or the engineering strain e. They

are related by the simple equation

$$\varepsilon = \ln(1+e). \qquad (4)$$

The difference is marginal for engineering applications and is usually below 5 percent.

Manson et al. /8/ estimated the fatigue resistance of the materials subjected to straining by superposition of the elastic and plastic strain components.

According to this estimation the relation becomes:

$$\Delta e_T/2 = \Delta e_E/2 + \Delta e_p/2 = \sigma_F/E \cdot (2\,N_F)^b + e_F \cdot (2\,N_F)^c \qquad (5)$$

where

Δe_T = total strain
e_F = fatigue ductility coefficient, definged by the strain intercept at one load reversal ($2\,N_F = 1$)
σ_F = fatigue strength coefficient, defined by the stress intercept at one load reversal ($2N_F = 1$)
$2N_F$ = total strain reversals to failure (cycles)
E = Young´s modulus
c = fatigue ductility exponent, the range for metals is between -0.5 to -0.7
b = fatigue strength exponent.

The constants b and c may be determined by tests according to the functions stress amplitude (σ_a) vs. $2N_F$,

$$\sigma_a = \sigma_F \cdot (2N_F)^b \qquad (6)$$

and correspondingly for the plastic strain amplitude (Δe_p) vs. $2N_F$

$$\Delta e_p/2 = e_F(2N_F)^c. \qquad (7)$$

The scheme in Figures 15, 16 and 17 illustrates the procedure for the determining a material's finite life. All tests are carried out under strain control with specially prepared specimens. The diagrams are plotted for σ_a vs. $2N_F$ and $\Delta e_p/2$ vs. $2N_F$ as given in Fig. 15 and in Fig. 16. From these diagrams values of b, c, σ_F and e_F are determined according to the logarithmic relationship. Figure 17 demonstrates the general response of a material under various strain conditions.

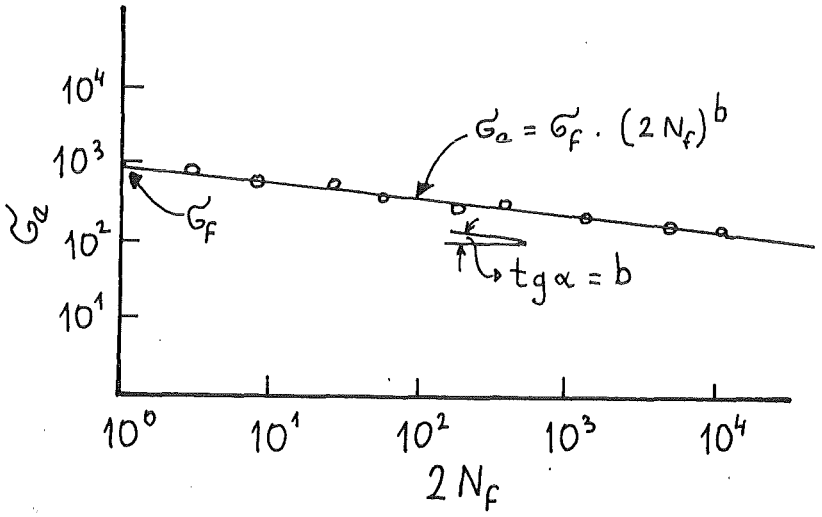

Fig. 15. Alternating stress amplitude vs. materials life. Slope is equal to b.

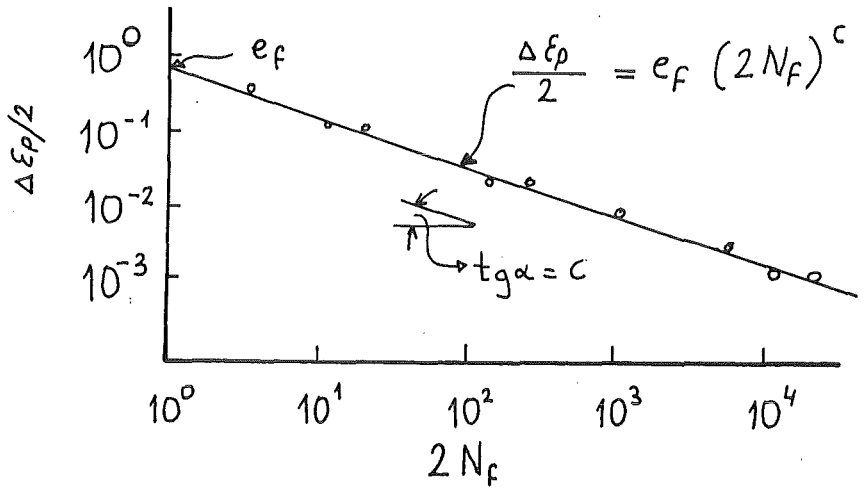

Fig. 16. Plastic strain range vs. materials life. Slope is equal to c.

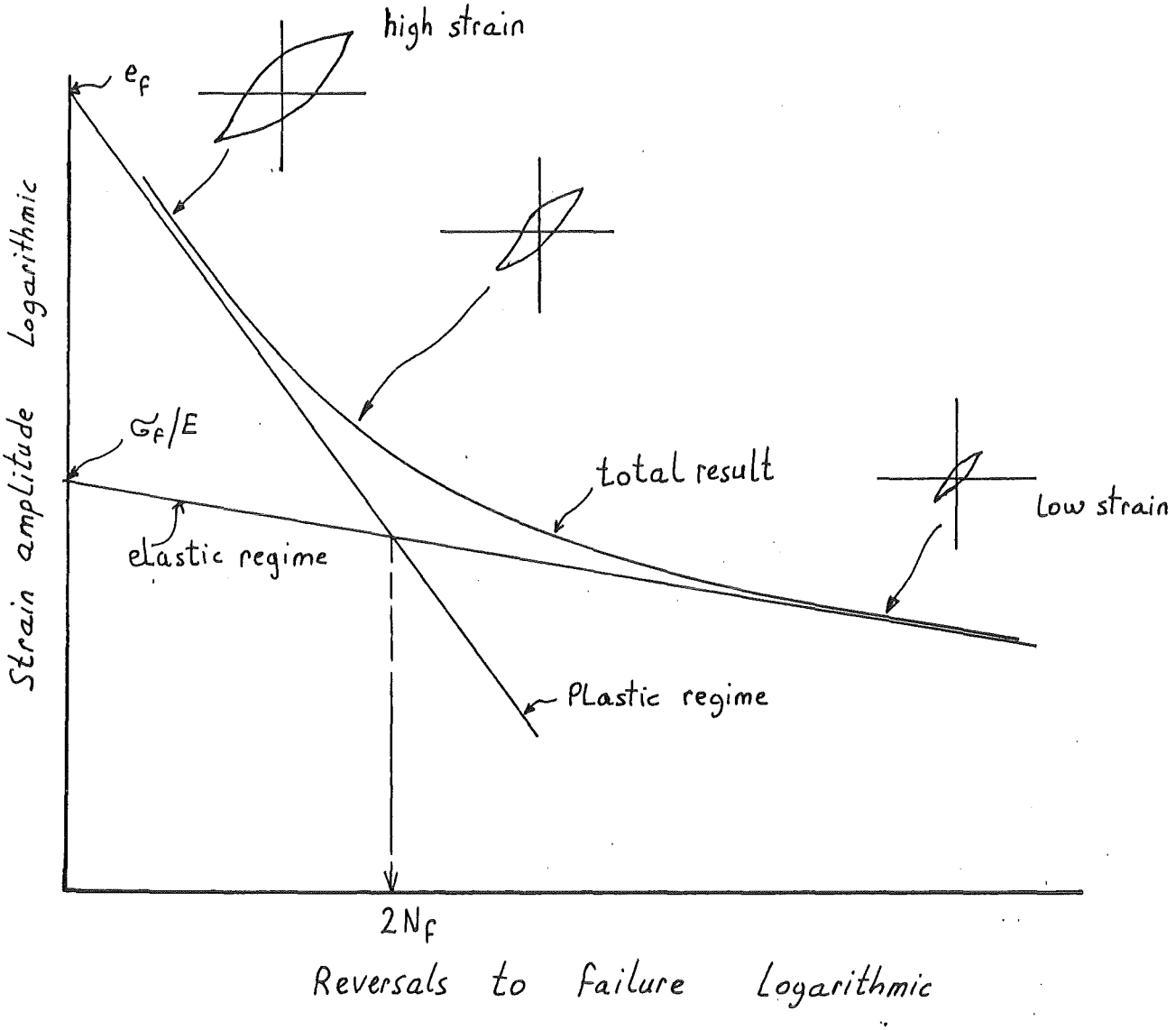

Fig. 17. Strain vs. materials life. Superposition of plastic and elastic strain life curves, which produce the total strain life.

2. Fatigue crack propagation

In the classical fatigue design procedure two sets of data are required - a definition of the fatigue environment (loads, stresses, strains, temperature, etc.), and fatigue life data for the particular material or component being considered. This multitude of parameters requires simplification of both the complex history of a fatigue process and the definition of suitable fatigue life-data of materials for engineering applications.

As previously described, fatigue data consist of graphs of alternating stress versus life-to-failure under constant amplitude conditions with the effects of mean, minimum and maximum stresses incorporated. The most striking difference between the data needed for cyclically loaded engineering structures and the S-N data of the particular materials is due to the discrepancy between the reality of a fabricated structure which is complex in its design, and the simple rotating bending tests. In general, engineering structures contain fabrication-related defects in the material in form of cracks, which therefore have to be considered as already initiated. From an engineering point of view, the question on the life of a material with initial flaws in the broad sense becomes essential.

The classical fatigue strength analysis can deliver only limited information on the situation with flawed members of a structure. Some efforts were made by introducing notched fatigue rotating bending specimens in which the effects of stress raising flaws on the material's fatigue behaviour are determined. In addition, specimens machined from welded sections also give some information about the weld metal fatigue properties. A large number of detailed information exists in handbooks from which the designer can take valuable data for the particular case /9/. Key relationships, however, such as the crack growth in service, crack size and load correlations, or the allowable initial crack

size cannot be given correctly by the qualitative way of a Wöhler type analysis. To close the gap between the traditional knowledge and the service-requirements, designers are often forced to select proper safety margins, very often resulting in bad utilization of the materials.

Modern fracture mechanics is capable of quantitative decisions about the materials' response under fatigue loading in case of preexisting flaws in the structure. It deals with the problems of subcritical cracks, crack propagation and total failure of the material in a quantitative way allowing the crack propagation to be calculated a priori. Starting with Griffith's theory of fracture under static load in 1920 fundamentals of fracture mechanics were developed, and during the 1960's the first crack growth rate relationships became available. In addition, defects in materials can be detected today by a number of sophisticated nondestructive test (NDT) procedures and the breakdown of the structure can be forecast quite exactly by the fracture mechanics analysis. Fatigue crack growth is still a young branch of engineering science and further developments might be expected.

2.1 Stress and crack size correlation during cyclic load

Two types of specimen are frequently used for cyclic load investigations with the purpose of establishing fatigue crack growth rate (FCGR) data. In the "compact tension" (CT) type specimen a machined deep notch exists prior to fatigue crack initiation, and in the "centre cracked plate" (CCP) specimen a small diameter center hole exists as fatigue crack starter. Figures 18 and 19 represent these two specimen with their geometrical notations.

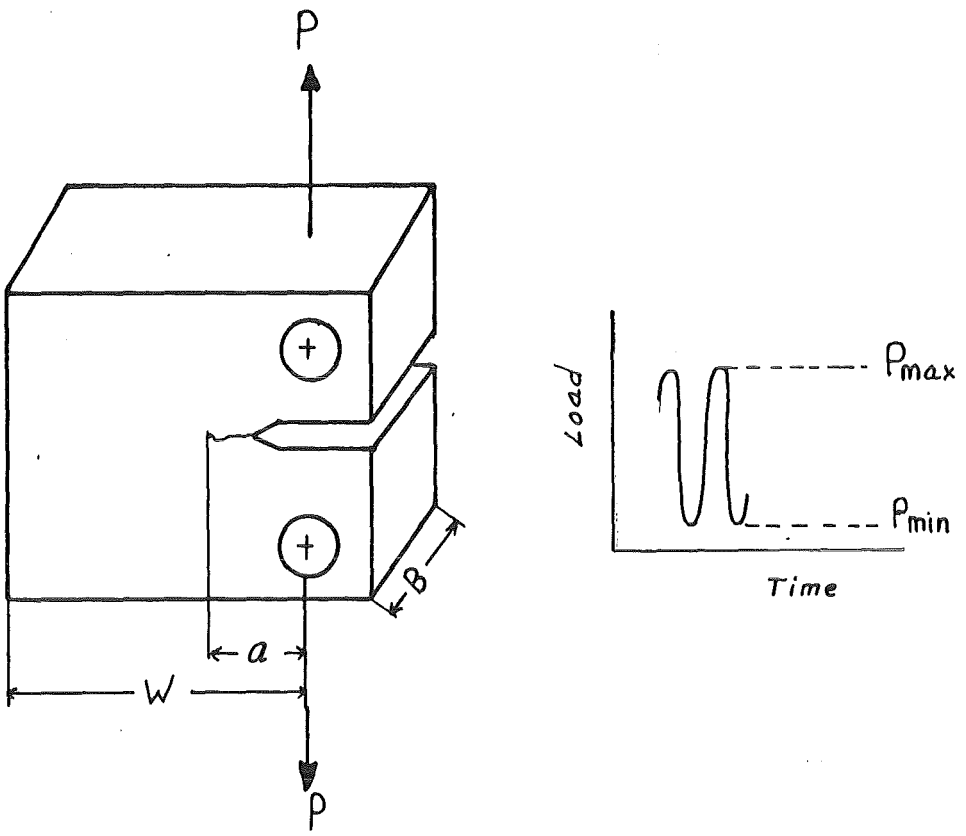

Fig. 18. Compact tension specimen. Relations between width W, crack length a and thickness B are given in /11/.

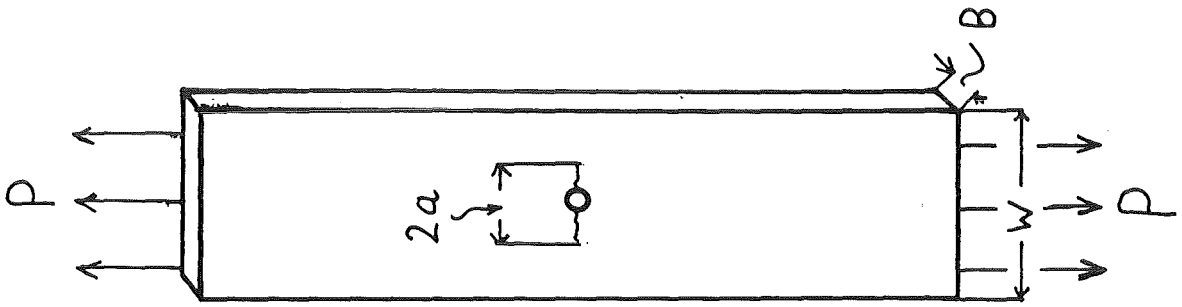

Fig. 19 Centre cracked plate specimen. Recommended for thin sheet investigations.

To avoid non uniform loading, the samples should be loaded with special finished grippings allowing for unidirectional loading; in certain cases even gimbal type of loading is recommended. Crack propagation data may be obtained with these specimen, starting from predefined flaw and recording the crack advance by applied cyclic loads. The change of the crack length can be monitored by various techniques, e.g. calibrated travelling microscope, eddy current techniques, electro-potential drop method, compliance measurements, ultra-sonic crack monitoring. The direct method with a travelling microscope is the simplest one, but it exhibits some disadvantages in certain instances, e.g. with non-parallel crack propagation, crack branching, crack tunnelling in the specimen under test. The other techniques, however, require high effort on exact calibration of electronic signals versus real crack advance and sophisticated electronics with computorized control. In addition, some materials are in certain cases not qualified to be monitored by one of the special technique, because of low signal to noise ratio.

Plotting the readings of crack size increase at a given average stress level vs. the number of cycles delivers diagrams as given in Fig. 20.

The slopes represent the crack size change with number of cycles at that stress level. The crack advance is therefore a function of crack size and the magnitude of the applied stress. The relationship between these parameters results in an empirical power law. By introducing the fracture mechanics concept one is able to derive general relationships with specific constants for the material under consideration.

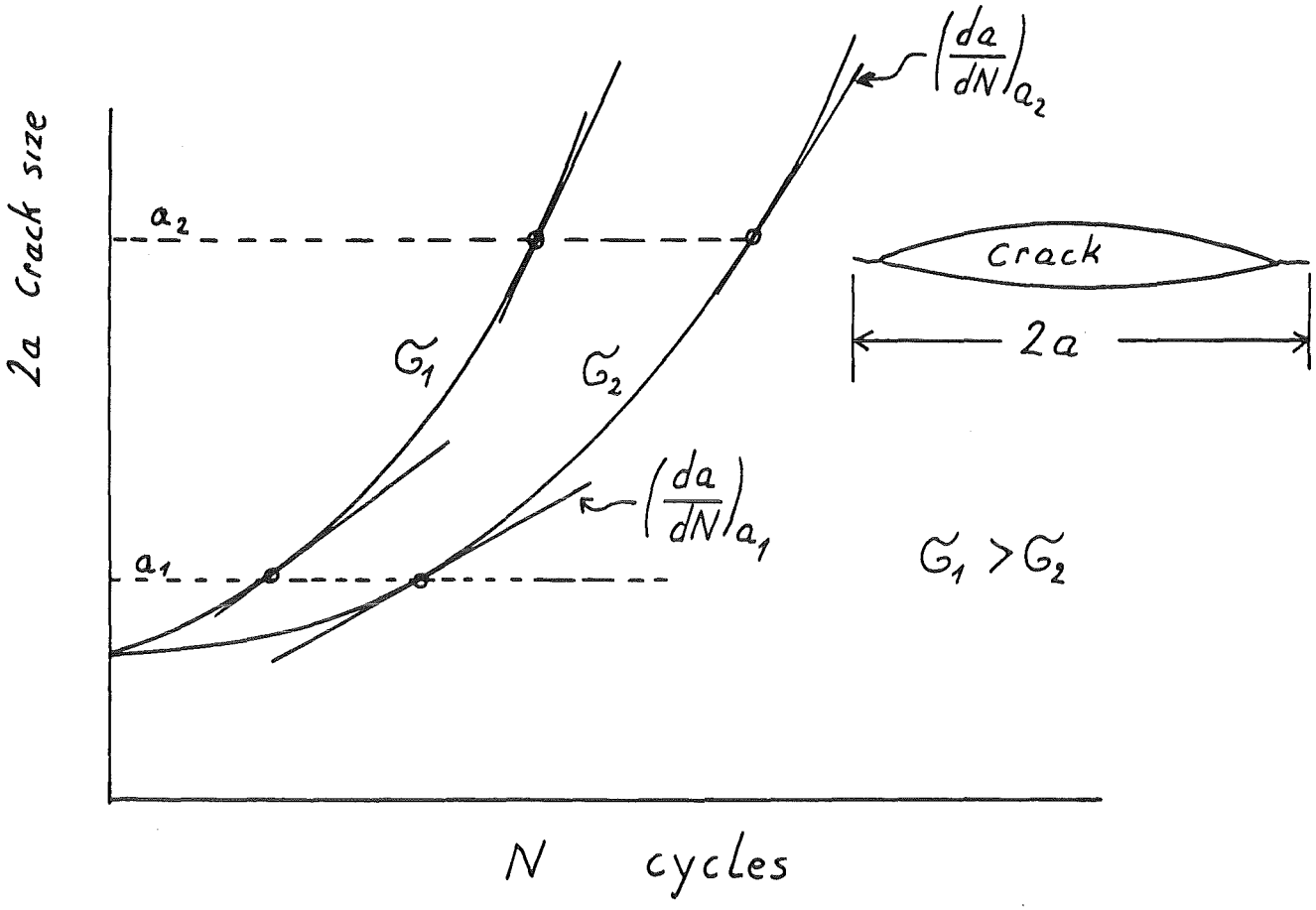

Fig. 20 Record of crack size increase vs. number of cycles. The slopes give the crack propagation rate for the given stress range.

Based on the stress analysis of the elastic theory concepts Westergaard /10/ was first able to determine the nature of stress distribution at a crack tip. According to the linear elastic mechanics (Hookian portion) he described the stress components in the vicinity of the crack tip as shown in Fig. 21:

$$\sigma_y = \frac{K}{\sqrt{2\pi r}} \cdot \cos\frac{\Theta}{2} \cdot \left[1 + \sin\frac{\Theta}{2} \cdot \sin\frac{3\Theta}{2}\right] \qquad (8)$$

$$\sigma_x = \frac{K}{\sqrt{2\pi r}} \cdot \cos\frac{\Theta}{2} \cdot \left[1 + \sin\frac{\Theta}{2} \cdot \sin\frac{3\Theta}{2}\right] \qquad (9)$$

$$\tau_{xy} = \frac{K}{\sqrt{2\pi r}} \cdot \left[\sin\frac{\Theta}{2} \cdot \cos\frac{\Theta}{2} \cdot \cos\frac{3\Theta}{2}\right] \qquad (10)$$

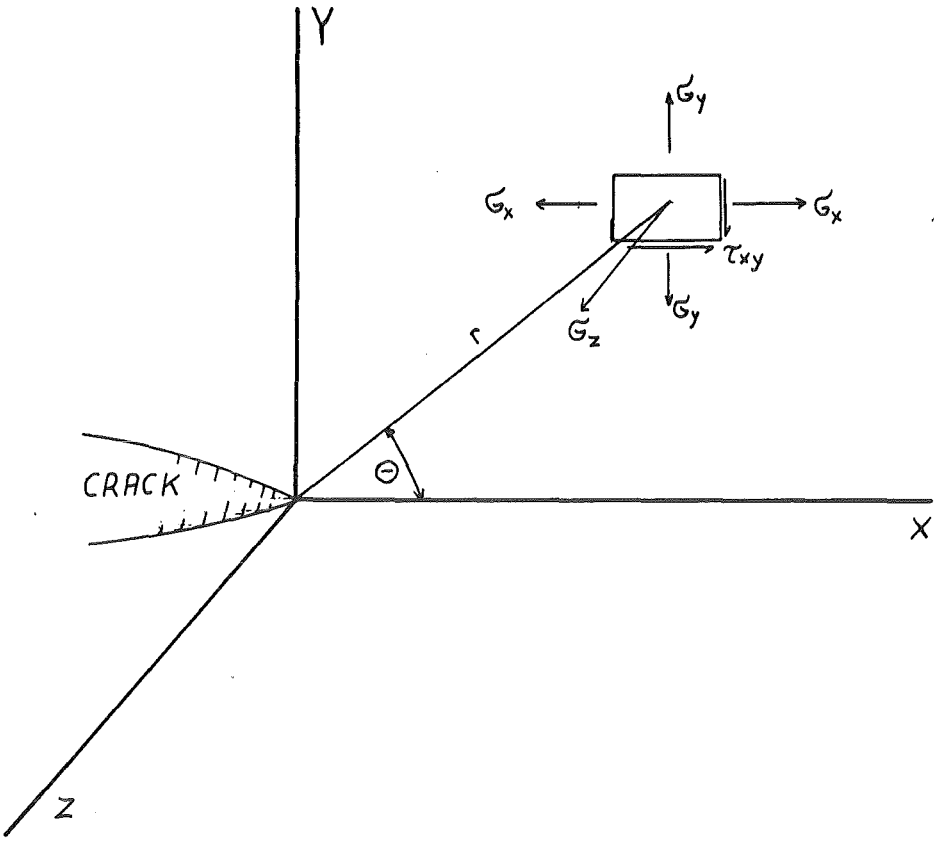

Fig. 21. Stress components in the vicinity of crack tip.

K is here a material constant and the local stresses do not rise to infinity as r approaches to zero, because the material begins to yield by plastic deformation and the validity of the equations is lost.

An important feature of the above equations, however, is the fact that the stress distribution around any crack is independent of the macroscopic structure for the same K value. The stress distribution depends only on the parameters r and θ and the difference between two cracked components is only the magnitude of the stress intensity field parameter K. The so called stress intensity factor K is a single parameter, which determines the relationship between crack size and the magnitude of

the stress, unless the functionality of the configuration of the cracked component geometrical dependency is known. For various geometrical shapes of specimens the functional dependency between the acting overall stresses and the crack size were investigated and solutions in form of graphs exist /12/. The functional relation is in general given between stresses normal to the crack plane, crack length and the geometry of the specimen.

For the CT specimens the stress intensity K is calculated according to the expression /11/:

$$K = \frac{P}{B\sqrt{W}} \cdot \frac{2+\alpha}{(1+\alpha)^{3/2}} \cdot \left(0{,}886 + 4{,}64\alpha - 13{,}32\alpha^2 + 14{,}72\alpha^3 - 5{,}6\alpha^4\right) \quad (11)$$

with

- ΔP - the difference between load maximum and minimum
- α - the ratio between crack length and the specimen width (a/w)
- B - specimen thickness.

The equation is valid for $a/W \geq 0{,}2$ and in linear elastic regime in the sense of fracture mechanics. This means that the specimen behaviour is elastic with the exception of a small region in the vicinity of the crack tip, where plastic deformation may occur.

For the CCP specimens the stress intensity K is represented by the equation /11/:

$$K = \frac{P}{B}\sqrt{\frac{\pi\alpha}{2W} \cdot \sec\frac{\pi\alpha}{2}} \quad (12)$$

Here α is 2a/W and the equation is valid below $\alpha = 0{,}95$. The right handside of both equations contains the specimen related geometrical correction function Y(a/W), which is the solution of the special specimen configuration. Inserting P in KN, B and W in cm the above equations deliver for K a dimension of $MPa\sqrt{m}$.

Based on these suggestions P.C. Paris /13/ postulated in 1964 that the stress intensity factor is the key parameter controlling the FCGR. This assumption is reasonable because by plotting (da/dN) values and the corresponding ΔK values in a log-log coordinate system, three distinct regions can be distinguished as shown in Fig. 22, and discussed in more details in chater 2.4. The linearized portion of the relationship gives an equation in the form

$$da/dN = C \cdot \Delta K^m \qquad (13)$$

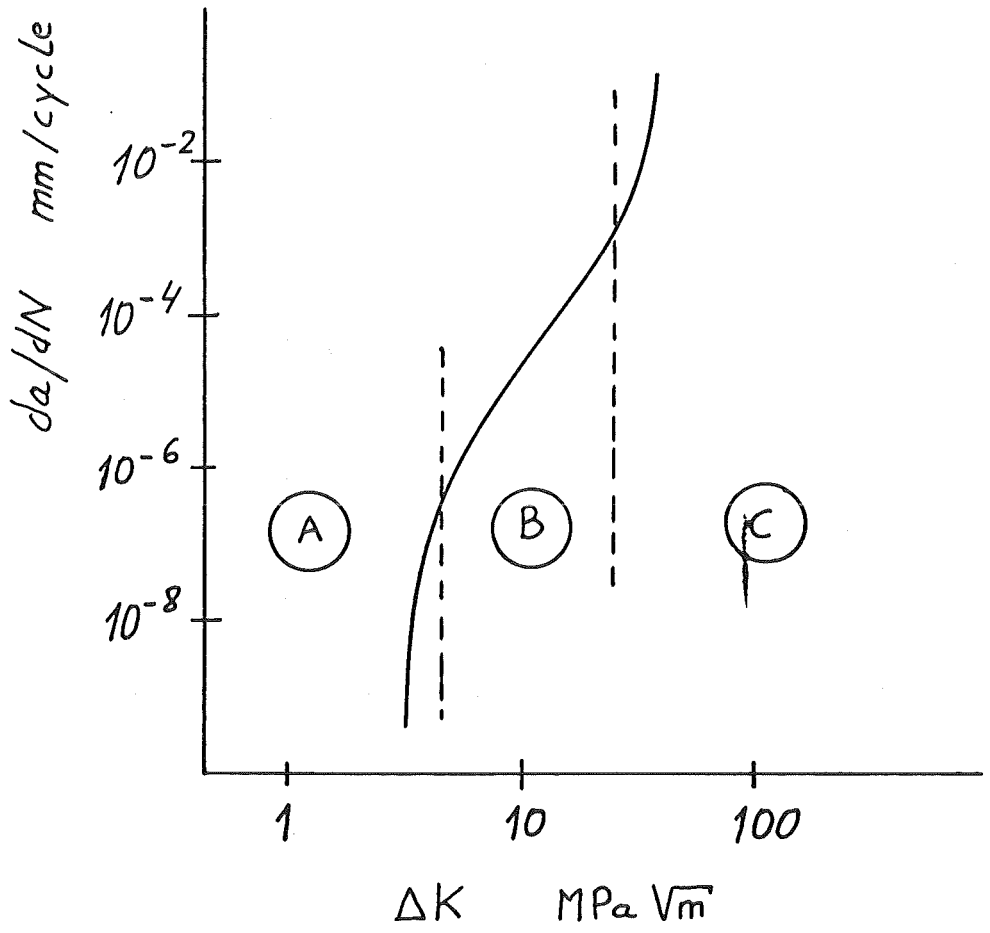

Fig. 22. Generalized relationship between crack growth rate and stress intensity range.

where

da/dN = fatigue crack growth rate

ΔK = Stress intensity range ($\Delta K = K_{Max} - K_{min}$)

C, m = f(material, environment, frequency, temperature, stress ratio R, etc.).

This law is known as "Paris" law. Data for various materials fit well into this form.

2.2 Fatigue life calculations

Fatigue life of the flawed members in a structure can be calculated by integration of the Paris law. Inserting for the stress intensity range the relationship

$$\Delta K = Y \cdot \Delta\sigma \cdot \sqrt{a} \qquad (14)$$

which can be derived from the equations 11 and 12, the formula can be integrated in an analytic way, and the number N_F of cycles between an initial flaw size a_o and a final flaw size a_F can be calculated:

$$N_F = \frac{2}{(m-2) \cdot C \cdot Y^m \cdot \Delta\sigma^m} \cdot \left[\frac{1}{a_o^{\frac{m-2}{2}}} - \frac{1}{a_F^{\frac{m-2}{2}}} \right] \qquad (15)$$

$m \neq 2$

where

Y = geometrical correction value

$\Delta\sigma$ = stress range.

The geometrical correction value depends on the location of the defect in the material. For deeply buried flaws in the material Y is approximately 1,2. Correct analysis require a numerical computation of the fatigue life.

Figure 23 gives the calculation performed for a buried flaw of the material 304 at 4K. Material data m and C have been taken from R.L. Tobler et al. /14/ and are valid between 23 and 71 MPa$\sqrt{m}$ of stress intensity range ΔK. Starting with 2 and 1 mm flaw sizes, respectively, the flaw size increases with the applied stress cycles. The limitation of this particular structure is assumed to be 6 mm flaw size, where static collapse may occur. The calculation shows the strong dependency of the

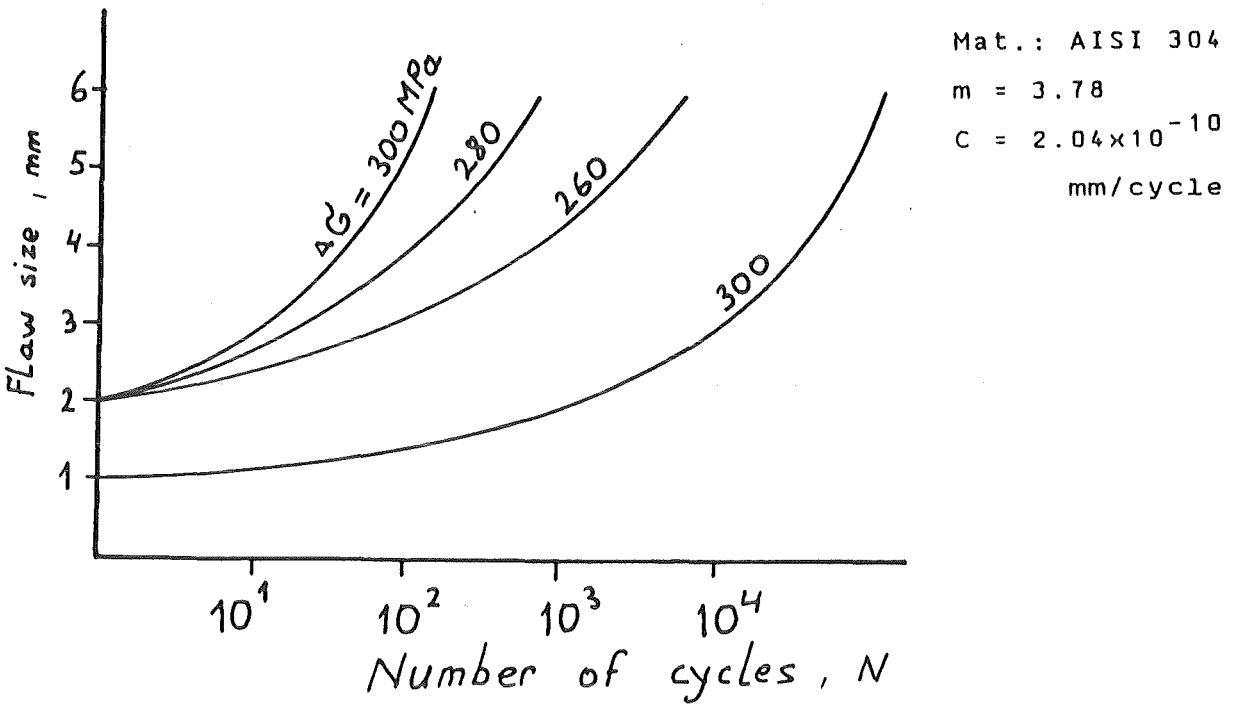

Fig. 23. Life prediction for different initial crack sizes and different stress ranges calculated according to the Paris law.

lifetime on the starting initial flaw size. Therefore, the exact size determination of the preexisting defects in a material should be a primary objective of the failure analysis for a structure.

2.3 Crack growth at high ΔK level

As shown in range C of Fig. 22, at extremely high ΔK levels a material's crack growth rate increases compared to the previously described Paris relationship. At these high growth rates, which are almost the end of the materials fatigue spectrum, the deformed plastic zone becomes very large and therefore the simple procedure by elastic fracture mechanics doesn't apply.

The maximum stress intensity K_{max} of the stress intensity range may also approach to the specimen's fracture toughness K_c, which raises the probability of a local collapse by instabilities. Cleavage type of fracture can be observed on fatigue surfaces as shown in Fig. 24 for an austenitic weld material, which was fatigued at this extreme ΔK level. The same material exhibits quite a different fracture appearance at ΔK-regimes in which the Paris law is valid (Fig. 25).

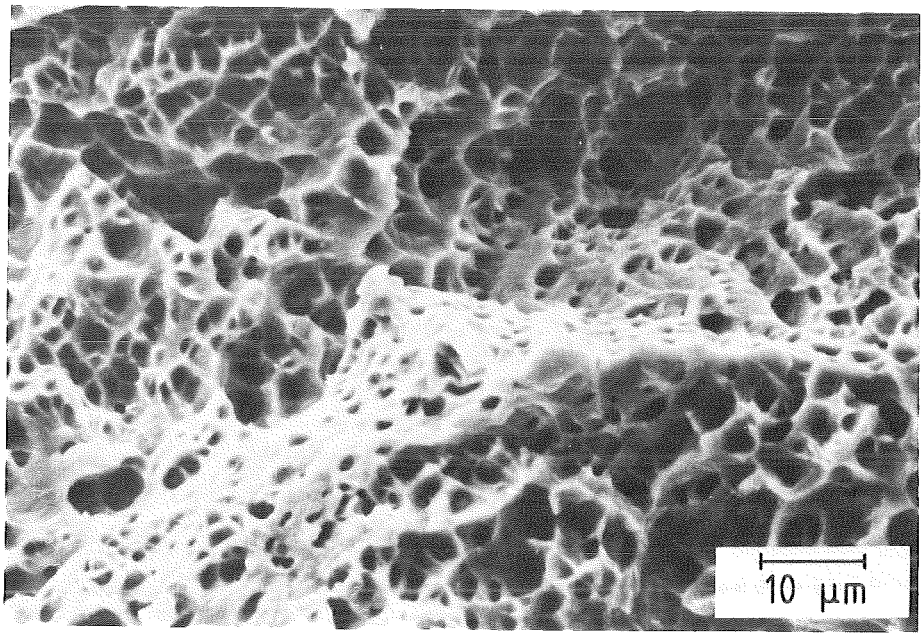

Fig. 24 SEM fracture surface of a specimen fatigued at high ΔK regime.

The high ΔK-levels are also very sensitive to mean stress variations compared to the medium ΔK regime. Therefore, attempts have been made to describe this region by expressions, which consider the mean stress level characterized by the stress ratio:

$$R = K_{min}/K_{max} \qquad -1<R<1 \qquad (16)$$

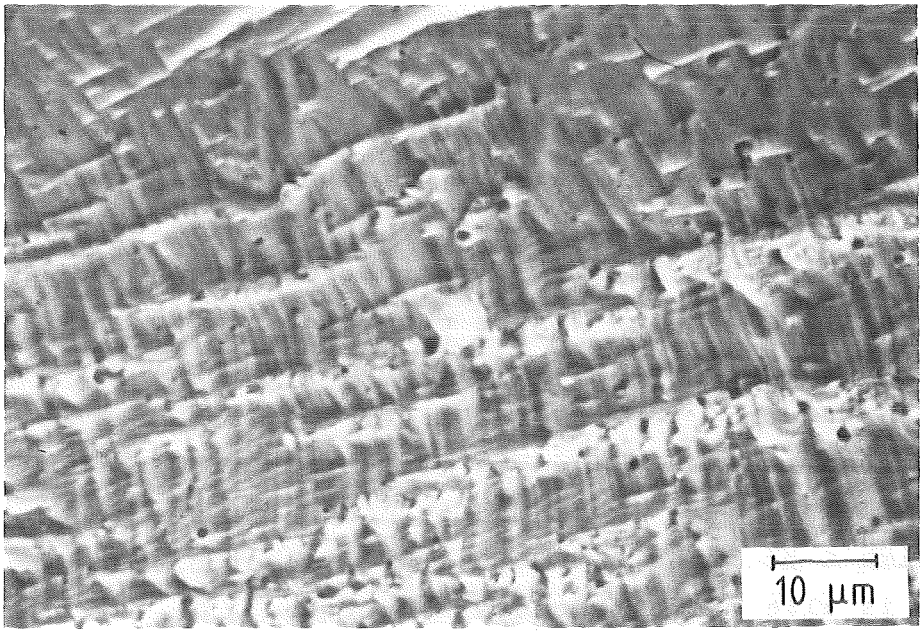

Fig. 25 SEM fracture surface of the same specimen.
Fatigue crack growth for low ΔK regime.

Forman et al. /15/ proposed a relationship for high ΔK levels in the form

$$\frac{da}{dN} = \frac{C \cdot \Delta K^m}{(1-R) \cdot K_c - \Delta K} \qquad (17)$$

where

C, m = material constants

K_c = fracture toughness.

Here, K_c is the fracture toughness of the test specimen and not the materials critical plane strain fracture toughness K_{IC}. K_{IC} is a measure of the resistance of the material to crack extension during static load increase. K_c must be therefore determined prior to the use of the above equation. The procedure is difficult depending on planar and thickness dimensions of the test specimen.

The above equation states that at a given ΔK level an increase of R results in an increase of the crack growth rate.

2.4 Crack growth at low ΔK level

As stated before, plotting the data of da/dN vs. ΔK results a sigmoidal curve in the log-log coordinate, where three regimes dictate the crack growth behaviour of materials (Fig. 22). The low ΔK-regime is sometimes defined as regime A, stage 1 or threshold regime. This regime is microstructurally and environmentelly sensitive and the effect of grain size on threshold properties has been investigated extensively showing a strong grain size dependency for several materials. Regime B or stage 2 has been already characterized as microstructure insensitive and the microstructures show serrated or faceted appearance. As mentioned regime C or stage 3 involves K_{max} induced cleavage of the grains and is also microstructure sensitive.

From Fig. 22 a limiting stress intensity factor range, the threshold level ΔK_{th}, can be defined, below which fatigue failure is quite unlikely. ΔK_{th} of engineering materials, however, are in the order of 2 - 5 % of their fracture toughness K_{IC} value and therefore an operation of the structure below this level is in certain cases non economic.

This ΔK_{th} concept is quite similar to the fatigue endurance limit of the classical fatigue theory. However, in the concept of ΔK_{th} the material has preexisting cracks contrary to the fatigue strength definition where the material is in an unnotched situation. In addition, the endurance limit is related strongly to the strength of the material and to the inverse square root of the grain size. It decreases for large grain sizes. To the contrary grain size increase for materials with preexisting flaws shifts the ΔK_{th} to higher values. So in that context a large grain is bad because the endurance limit will tend to go down. In the context of fracture mechanics where material have preexistent flaws big grains are better. The

reason for this conflicting situation is the fatigue crack nucleation mechanism of materials. Most probably the endurance limit is dominated by the nucleation of a crack and here the microstructure with small grains plays a positive role, whereas for the threshold limit the crack propagation mechanism is adversly affected by the microstrucure, because there a crack is already present.

2.5 Influence of load transients

In general FCGR data are gained by constant amplitude patterns, which doesn't account for effects of sudden load variations. A number of engineering applications, however, demand the response of materials under varying load excursions. It has been demonstrated that a significant delay FCGR can occur after the superposition of a single peak overload on a constant cyclic amplitude. The amount of delay increases with the magnitude and number of overload cycles /16/. The retardation of the crack growth is attributed to the corresponding new overload plastic zone as pointed out in Fig. 26.

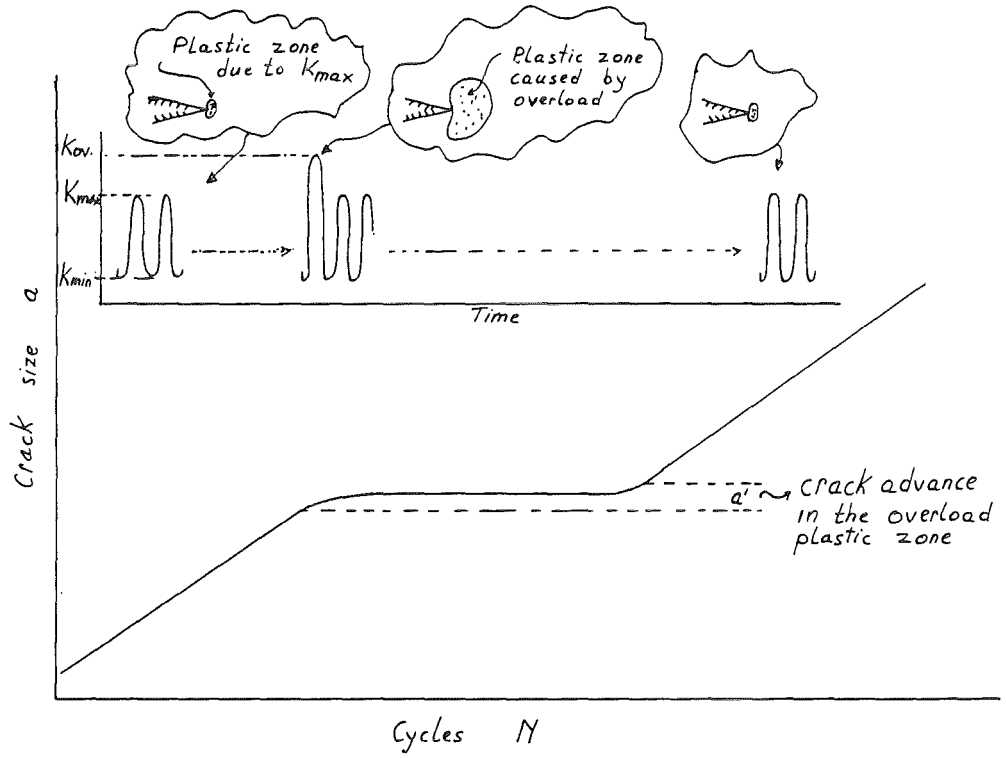

Fig. 26 Retardation mechanism as a consequence of a single overload.

The slope da/dN is constant for a constant stress intensity range ΔK in regime B as long as the plastic zone size ahead of the crack tip has a certain geometrical dimension. When the overload (here the single peak) increases the plastic zone size drastically, the material properties ahead of the crack tip change (residual stresses, strain hardening etc.), and the crack advance afterwards with prevous stress intensity range ΔK is delayed for a crack length of a'. After passing the plastic zone, the original conditions are reestablished, and for the same ΔK the slope da/dN becomes the identical value as before the overload.

3. Compiled fatigue data of engineering materials

3.1 Fatigue data of ferritic materials

The measured FCGR data of several ferritic steels are represented in form of da/dN vs. ΔK diagrams. The load ratio (R) insensitivity of ferritic steels for the stage 2 crack growth regime are demonstrated by Barsom /17/ for A514-B type ferritic steel, which is a low alloy steel, frequently used for structural applications in bridge constructions with the chemical composition given in Table 1.

Table 1. Chemistry of A514-B in wt%

C	Mn	P	S	Si	Ni
0,21	0,91	0,009	0,023	0,26	0,066

Cr	Mo	V	Ti	Al	N
0,56	0,19	0,048	0,017	0,044	0,006

The tests with CT-type specimens are carried out at different R-levels, varied between 0,05 and 0,825. The constant amplitude cyclic load tests presented in Fig. 27 show that stage 2 FCGR data at ambient fall within a narrow scatter-band and agree well with the established behaviour of martensitic steels given by Barsom /18/.

The load ratio sensitive regime is the near threshold and the threshold regime. FCGR measurements at R-levels 0.1 to 0,8 carried out by Bucci /19/ for 10 Ni steel are given in Fig. 28. A marked difference of FCGR is confirmed according to these tests at near threshold regime of ~ 10^{-6}-10^{-7} mm/cycle.

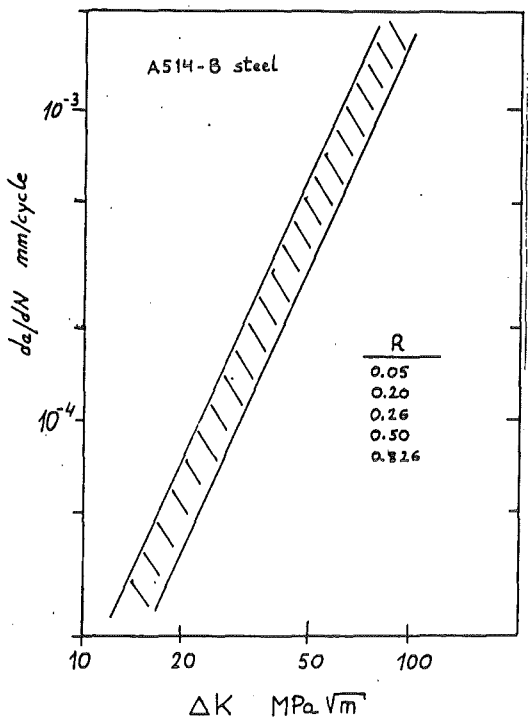

Fig. 27
FCGR measurements carried out with A514-B ferritic steel at different load ratios /17/.

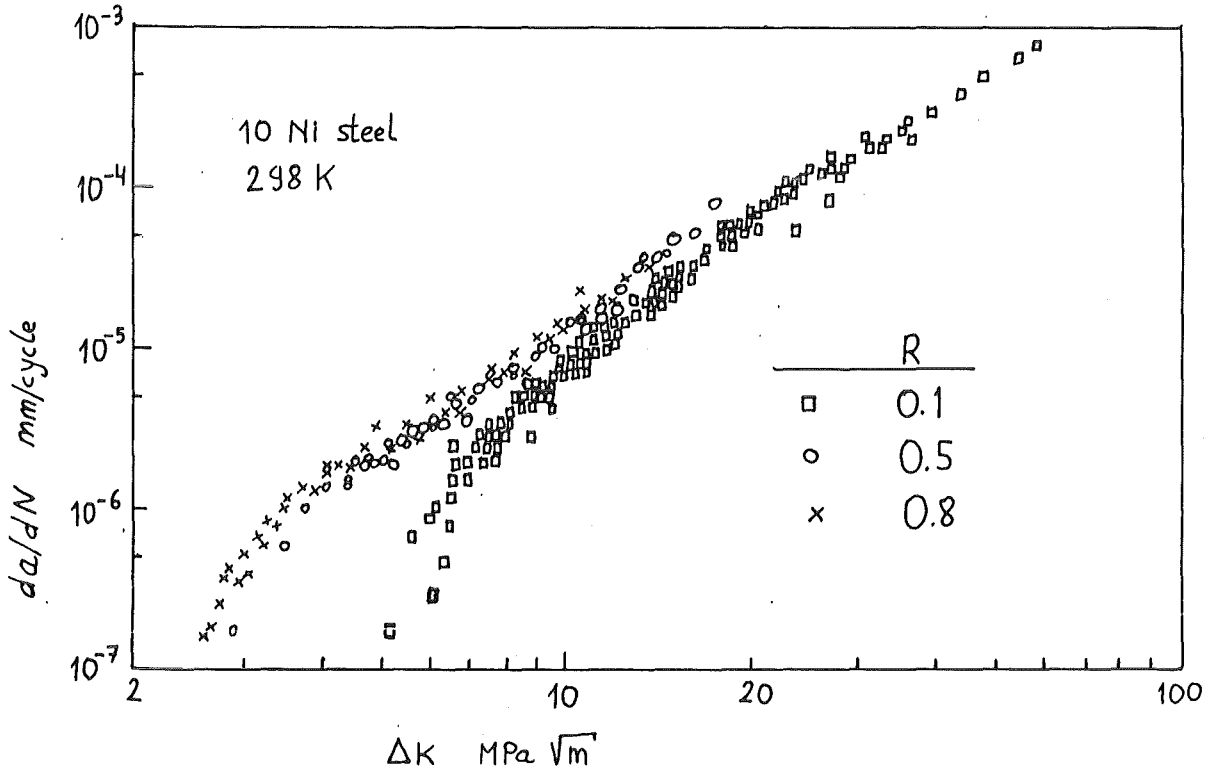

Fig. 28 FCGR data of 10 Ni steel at ambient for different load ratios /19/.

For stage 2 FCGR the influence of yield strength is expected to be small and the collected data shown in Fig. 29 fits well within a narrow scatterband, although the yield strengths of these investigated martensitic steels vary markedly /20/. The same is also true for other types of alloys as found for brass and stainless steels in both cold worked and annealed condition, where 4 to 10-fold differences in static yield strength were reported /21/.

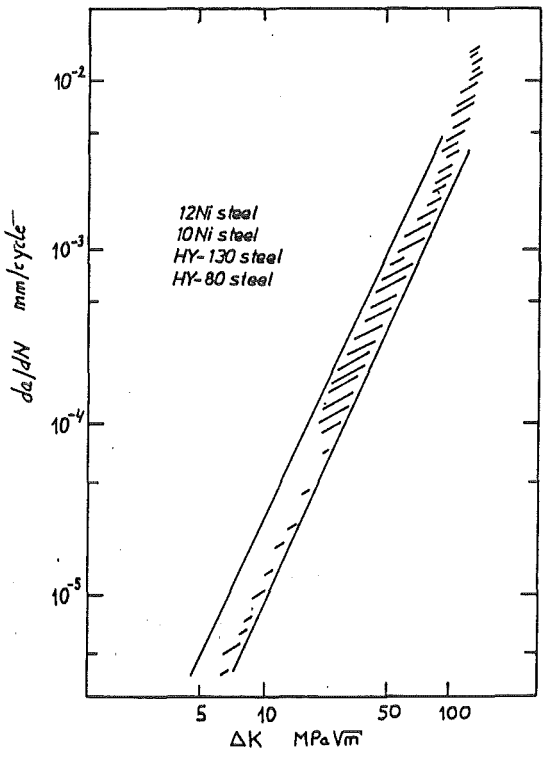

Fig. 29
FCGR behaviour of several martensitic steels at ambient /20/.

This demonstrates that the plastic zone ahead of crack tip is the controlling mechanism for FCGR at stage two. After a few cycles this zone is strain hardened and therefore there should be little difference between cold worked materials and the annealed one.

In ferritic nickel steels the nickel quantity doesn't influence much the properties of FCGR as shown by the results of Bucci et

al. /22/ in Fig. 30. Table 2 gives the chemical composition of the investigated materials.

Table 2 Chemistry of the Ni-steels in wt%

Material	C	Mn	P	S	Si	Cr
5 Ni steel	0,06	0,64	0,011	0,003	0,39	0,06
9 Ni steel	0,08	0,62	0,011	0,003	0,25	0,06

Ni	Mo	Cu	V	Al	N
5,0	0,34	0,24	0,008	0,07	0,013
8,8	0,34	0,24	0,008	0,07	0,013

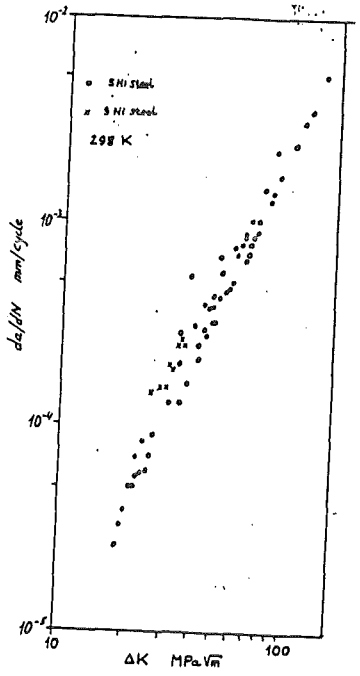

Fig. 30
FCGR data for 5 Ni and 9 Ni steels at ambient with constant load ratio of R = 0.1 /22/.

The properties of different zones in a ferritic welded material have been investigated by Sandifer et al. /23/. The material was a pressure vessel plate material "A 537 M" and was welded by a semiautomatic inert gas-shielded metal arc-spray transfer weld process. Tests were carried out with standard CT-specimens and materials chemical compositon is given in Table 3.

Table 3. Chemistry of A 537 M steel and the weldment in wt%

Material	C	Si	Mn	P	S	Ni	Mo
Base metal	0,12	0,30	1,47	0,018	0,011	0,24	0,07
Weld metal	0,06	0,91	1,47	0,009	0,011	-	-

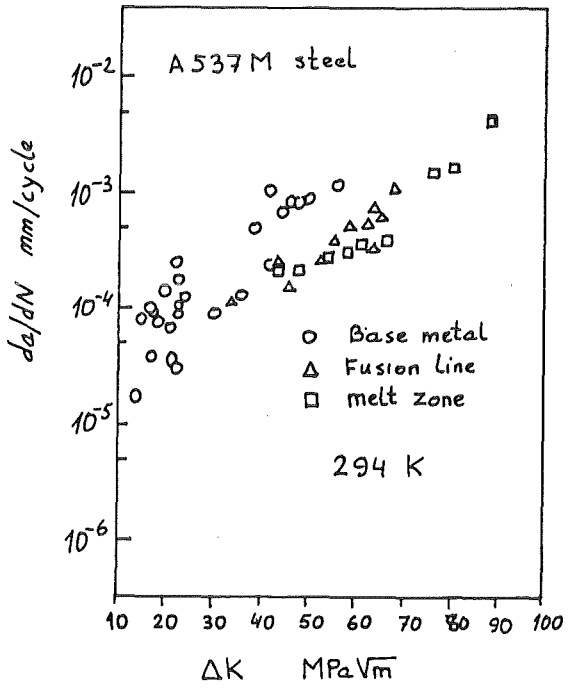

Fig. 31 FCGR data of type A 537 M ferritic steel. Measured crack growth rates at ambient for base metal and weldment. Cracks were propagated in different regions of the welded material /23/.

Figure 31 gives the variation of the FCGR at ambient for different crack orientations in the metal in a semi-log plot.

Elevated temperatures may influence the FCGR markedly. This is shown in Fig. 32 for a low alloy ferritic steel, "A 212 B". Increasing the temperature increases the FCGR at a given ΔK. For a long period of time, a controversy existed concerning the origin of this FCGR temperature sensitivity. The question was whether the creep component or the environmental (corrosion) component is responsible to this effect. In a series of experiments carried out at elevated temperatures but in inert environmental conditions and in vacuum neither temperature nor frequency showed any effect on FCGR. The results of FCGR were all comparable to ambient results. According to these findings, the main parameter can be attributed to environmental aspects such as the corrosion rather than to, for instance, the creep mechanism.

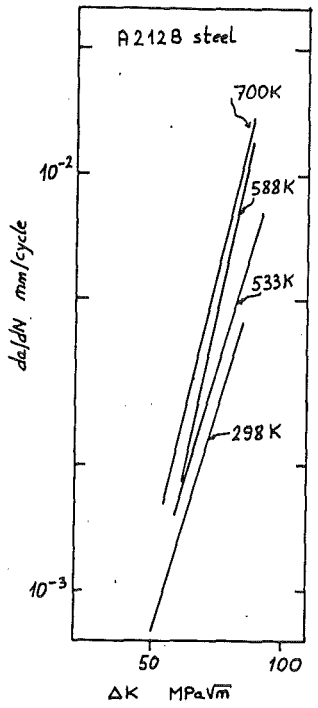

Fig. 32
Influence of temperature measured for A 212 B class material. Data were taken from /24/.

For a high temperature application material Udimet 700 the FCGR at elevated temperature has been determined by Sadananda et al. /25/. The chemistry of this material is given in Table 4.

Table 4. Chemistry of Udimet 700 in wt%

C	Cr	Co	Mo	Ti	Al	B	Ni
0,07	15	18,5	5	3,5	4,4	0.025	bal.

Figure 33 represents the FCGR measured at 1123 K.

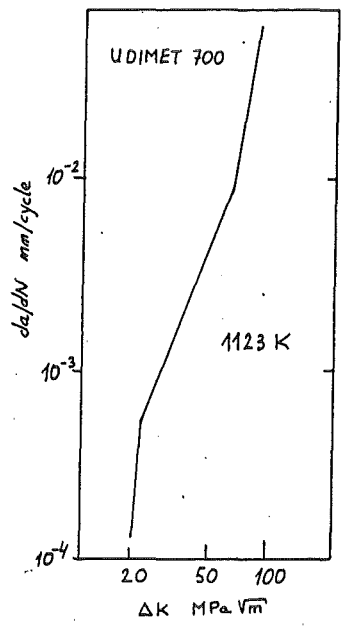

Fig. 33
Udimet 700 crack growth rate measured at 1123 K /25/.

For a 9% Ni ferritic steel designated with ASTM A 553 the effect of cryogenic temperatures on FCGR has been determined by Tobler et al. /26/. The chemical composition of the investigated material is given in Table 5.

Table 5. Chemistry of A 553 in quenched and tempered condition in wt%

C	Si	Mn	P	S	Ni	Fe
0,08	0,19	0,62	0,01	0,01	8,99	bel

These tests (Fig. 34) revealed relatively high FCGR at 4 K. It is assumed by these authors that the increased growth rate can be attributed to the ductile-to-brittle transition of the ferritic materials. However, below a ΔK of 30 MPa$\sqrt{m}$, FCGR could not be obtained and therefore extrapolations to lower ΔK should not be made. In addition, one specimen was subjected to 30 000 cycles at 4 K and ΔK = 20 MPa$\sqrt{m}$ and no detectable crack extension was measured.

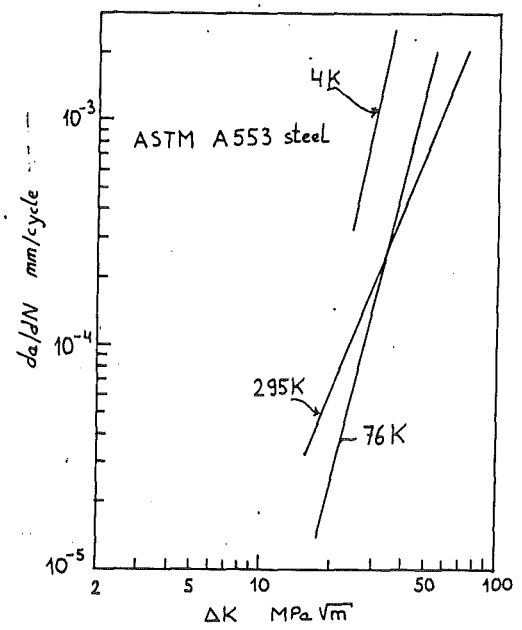

Fig. 34 Influence of cryogenic temperatures for the material A 553 /26/.

The findings at 76 K can be supported by Bucci et al. /22/ who carried out similar tests with CT-specimens at 110 K and 77 K. Figure 35 gives the test results with 5% Ni and 9% Ni steels at cryogenic temperatures. The load ratio was 0.1 and tests with R = -1 at 110 K showed a little tendency towards higher crack growth rates for stage two FCGR.

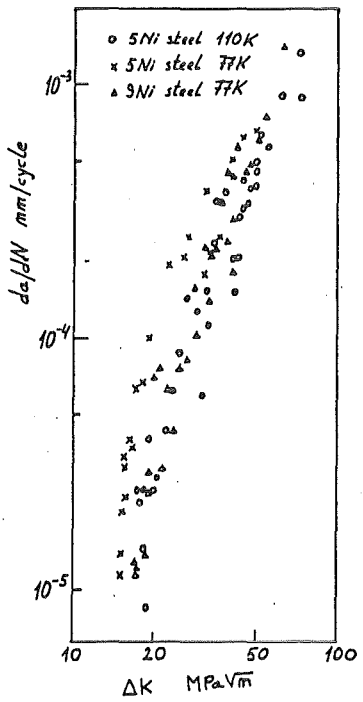

Fig. 35
FCGR of 5 Ni and 9 Ni steels at 110 K and 77 K /22/.

FCGR of pressure vessel materials type SA 533 grade B were investigated by Nakajima et al. /27/ for different types of wave forms during cyclic loading. Figure 36 gives the results of different forms of waves (sinusoidal and triangular). No wave form sensitivity could be determined for stage two FCGR and these data fit well in the scatterband of other martensitic steels.

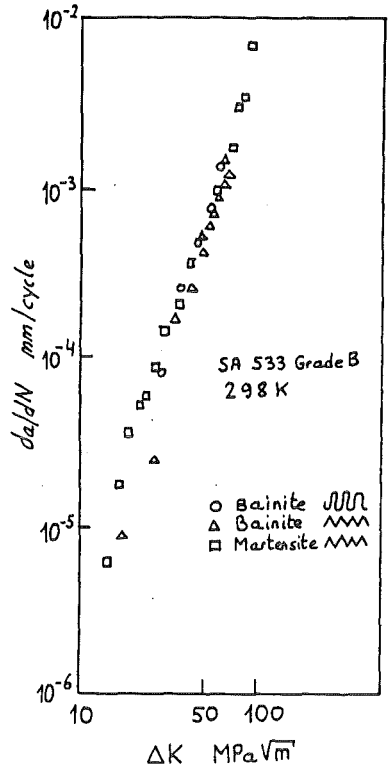

Fig. 36
Tests with different forms of waves carried out for SA 533 grade B steel at ambient /27.

The chemical composition of the investigated steels are given in Table 6.

Table 6. Chemistry of SA 533 grade B in wt.%.

Material	C	Si	Mn	p	S	Ni
Bainite	0,19	0,25	1,28	0,009	0,013	0,61
Martensite	0,17	0,02	1,48	0,011	0,006	0,58

Material	Cr	Mo	Cu	V	Sb	As	Sn
Bainite	0,04	0,55	0,13	0,004	-	-	-
Martensite	0,16	0,52	0,13	0,003	0,0041	0,015	0,008

Investigations at the threshold regime were carried out by Metzner /28/, where growth rates down to 10^{-10} mm/cycle were detected. The material tested was a ultrahigh strength 18 Ni ferritic maraging steel. Material composition is given in Table 7.

Table 7. Chemistry of 18 Ni maraging steel in wt.%.

C	Mo	Ni	Co	Ti
0,03	5,2	18, 5	12,0	0,9

The results at near threshold regime were compared with those of other martensitic steels at ambient.

Figure 37 shows the data points superposed with the results of Fig. 29. The tests reveal the comparability of the values determined. The threshold level investigations are also pointed out in this diagram, which give the entire FCGR band from 10^{-10} to ~ 10^{-2} mm/cycle.

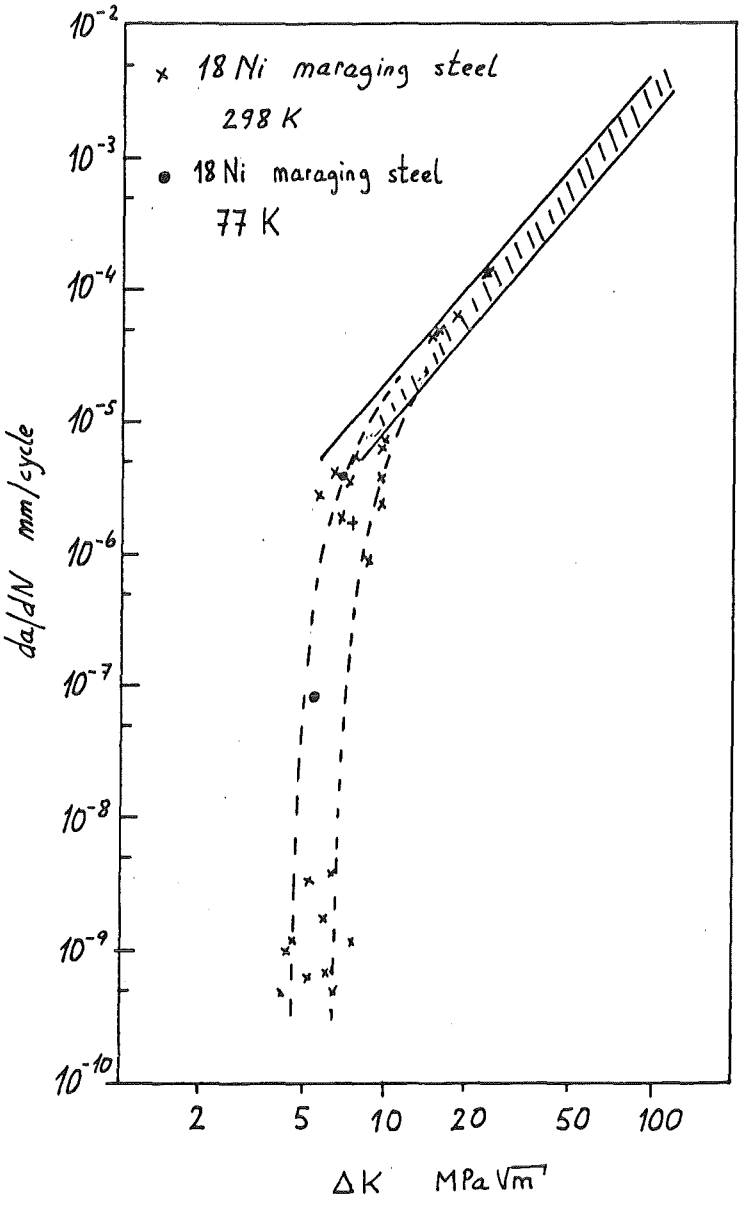

Fig. 37
FCGR tests carried out with 18 Ni maraging steel at ambient and at 77 K /28/.

3.2 Fatigue data of austenitic materials

3.2.1 Low temperature investigations

Complex structures with requirements such as high corrosion resistance, high toughness, non-magnetic behaviour and high microstructural stability at low temperatures demand the use of austenitic materials. These materials belong to the group of stainless steels and the important types of which are outlined in the following with respect to their fatigue properties. Table 8 summarizes these materials and their chemical compositions. Many of them are already in use for cryogenic applications, the stable austenitic FCC-phase being the main requirement. A high nickel content with some special austenit stabilizing elements (such as Mn, C, N) are the key variable for microstructural stability.

Recent investigations carried out at Kernforschungszentrum Karlsruhe /29/ supplied information about the fatigue response of these special alloyed stainless steel systems. One of the candidate material (German Werkstoff number 1.4429) used for superconducting coil case structures was investigated thoroughly in form of the parent material and the weldment. The tested parent material was supplied as 50 mm thick plate material in as solution treated and water quenched form. The tests carried out at ambient with 23 mm thick CT-type specimens revealed for T-L and L-T (T = Transverse, L = Longitudinal) orientations no significant difference of fatigue crack growth in stage II regime (Fig. 38).

All tests were carried out with different types of tensile testing machines operated at different frequencies. Therefore tests were necessary to reveal the influence of the frequency on the crack growth rate behaviour of the materials. The determined FCGR data for the material (Werkstoff number 1.4301) type 304 showed no frequency effect between 5 to 50 Hz. This was also confirmed later for type 1.4429 stainless steel. Figure 39 shows

Table 8 Chemical composition of austenitic materials in wt.%

Material Designation	C	Si	Mn	P+S	Cr	Ni	Mo	N	others	Ref
1.4301	0.036	0.7	1.6	0.036	17.1	8.6	0.2	-	-	/29/
1.4429	0.032	0.4	1.3	0.02	16.7	13.7	2.7	o.16	-	/29/
1.4455	0.o39	0.3	5.4	0.025	19.3	15.4	2.9	0.17	-	/29/
C748 (Mn-Cr)	0.04	0.44	40.3	0.019	17.9	-	-	0.28	-	/28/
305	< 0.07	<1.00	<2.00	< 0.075	17-19	10-13	-	-	-	/34/
304L	0.03	0.44	1.2	0.049	18.6	9.5	0.23	-	-	/37/
A-453	0.05	0.54	1.52	0.023	14.0	24.9	1.3	-	-	/36/
316L SMA	< 0.03	< 1.00	< 2.00	< 0.075	16.5-18.5	11-14	2-2.5	-	-	/39/
Nitronic 40	0.03	0.56	8.97	0.018	20.1	6.34	-	0.29	-	/44/
308-16	0.056	0.32	1.88	0.035	19.7	10.3	0.05	0.07	-	/46/
316	< 0.07	<1.00	<2.00	< 0.075	16.5-18.5	10.5-13.5	2.0-2.5	-	-	
301	< 0.12	<1.00	<2.00	< 0.075	16-18	7-9	-	-	-	
Fe-13Cr-19Mn	0.055	0.38	19.0	0.021	13.4	0.82	-	0.16	-	/34/
Fe-Mn (Kobe steel)	0.02	-	18	-	16	5	-	0.22	-	/33/
Fe-6Mn-21Cr-15Ni	0.045	0.05	6.14	0.029	21.2	15.6	-	-	-	/31/
JBK-75	0.014	0.08	0.02	0.010	13.9	29.3	1.24	-	Ti = 2.11 V = 0.28 Al = 0.29	/38/

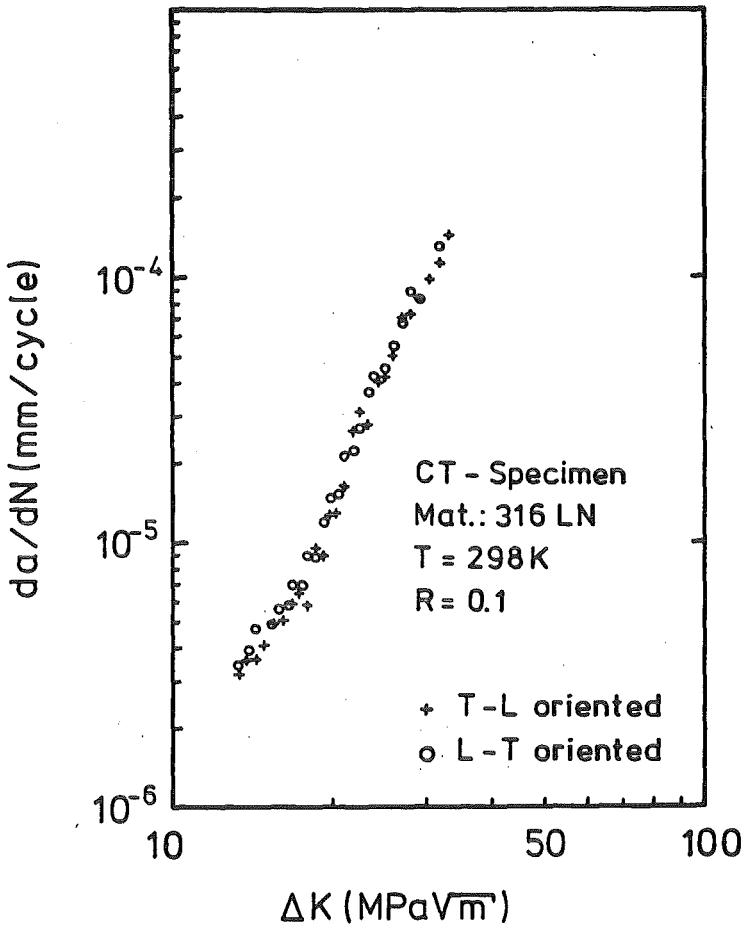

Fig. 38
Fatigue crack growth of the material 1.4429 (~ 316 LN type) show no influence of crack propagation for different crack orientations /29/.

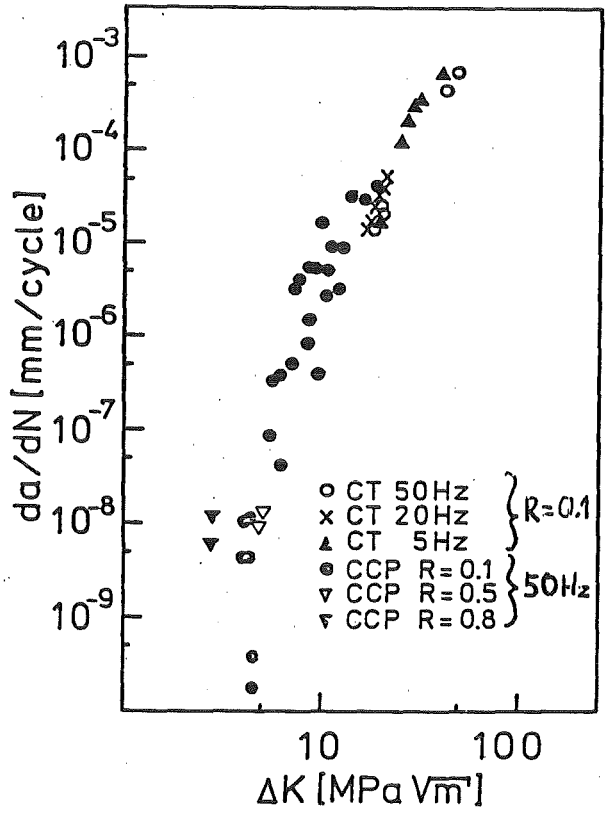

Fig. 39
Material 1.4301 tested with various frequencies and with different specimens at ambient /29/.

the results with 10 mm thick CT-type specimens and 2 mm thick CCP-typs specimen. The overlapping of the data gained with different types of specimens confirms also the validity of the chosen specimens.

In the threshold regime, the load ratio R did not affect the FCGR up to R = 0.5. Above R = 0.5, the crack growth shifts to the left, thus increasing the crack growth rate.
Cryogenic FCGR data were established for the material 1.4429 as shown in Fig. 40.

The results show a slight shift of the cryogenic FCGR data towards lower crack growth rates compared to the ambient data. This can be attributed to the decreasing probability of the slip motion at low temperatures. The more pronounced effect of the low temperatures is, however, the increase of the fatigue resistance generally for all materials. At low temperatures the slip motion will be decreased and the twinning mechanism takes place to nucleate a crack. Fig. 41 shows the fatigue strength of various even not widely used materials and their response to the temperature decrease.

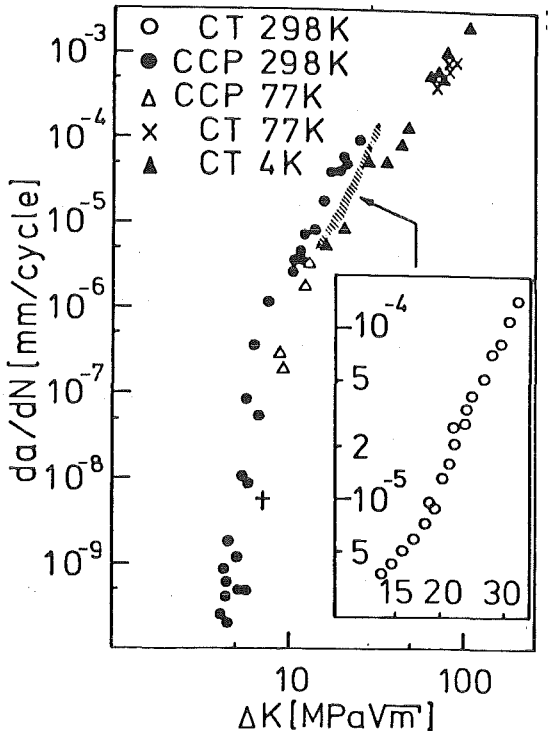

Fig. 40
FCGR measurements at ambient and at low temperatures. Each point gained at 77 K and 4 K refers to an individual specimen. + refers to 77 K FCGR test where for 10^5 cycles no crack advance were observed /29/.

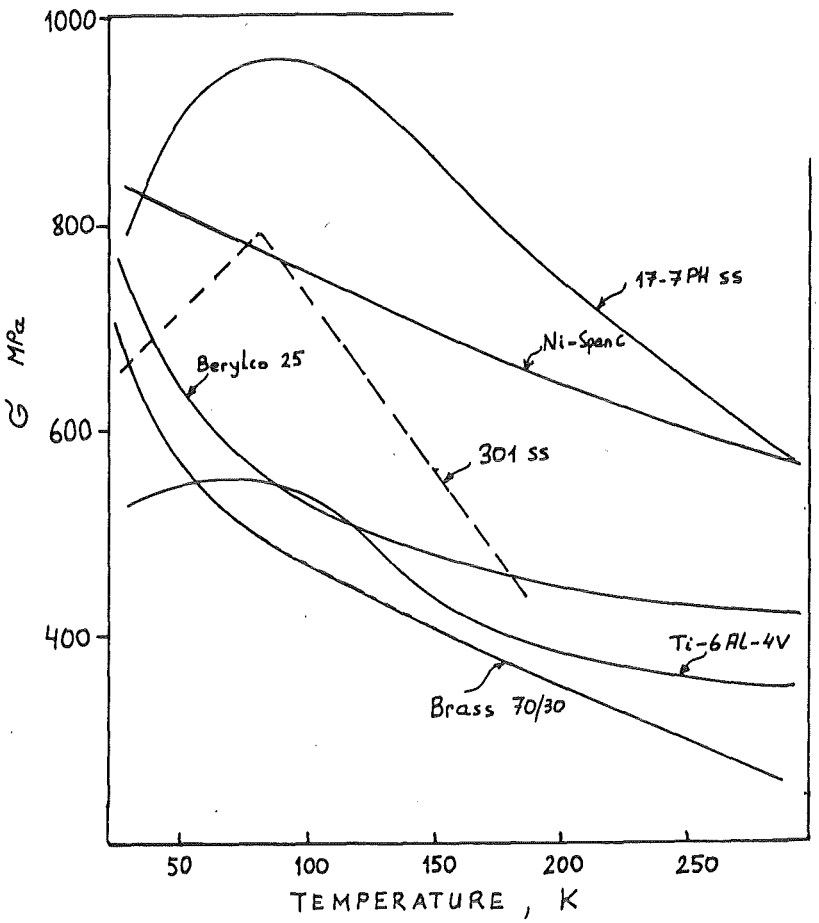

Fig. 41
Fatigue strength vs. Temperature for an endurance limit of 10^6. The data were taken from /30/.

The fatigue strength of materials as shown in Fig. 41 increase with decreasing temperature. The same is true for the ultimate tensile strength which generally increases at lower temperatures. But the increase of fatigue strength of materials due to the temperature decrease cannot be related purely to the enhanced ultimate tensile strength. It is rather assumed that the nucleation process of the fatigue crack initiation stage is largely responsible. Fig. 41 shows also the behaviour of two stainless steels 301 and 17.7 PH which have a ductile to brittle transition point at low temperatures, being not fully austenitic phase stabilized materials. The transformed FCC-phase to α´-martensite behaves quite different concerning the fatigue procedure.

Fig. 42 gives the relationship of fatigue strength for similar type of stainless steel materials with different microstrucures at 11 K and 293 K.

For both heats, the fatigue strengths at 10^6 cycles are much larger at 11 K than at ambient. Heat 2 with a lower inclusion

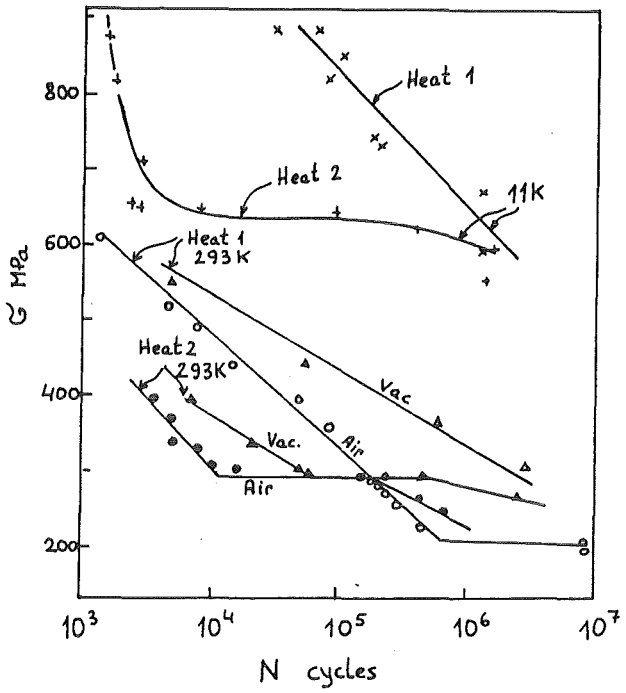

Fig. 42
S-N curve of the material Fe-6-Mn-21Cr-15Ni. Heat 2 was additionally electro stag remelted. Data were taken from /31/.

content due to the electro slag refinement shows a lower fatigue resistance at low cycle numbers in comparison to heat 1. Increasing the steel purity (heat 2) favours the increase of grain sizes and decreases the cyclic fatigue life. Here again, the competition between crack nucleation and the crack growth process and their dependency on microstructure becomes obvious.

The weld metal crack growth behaviour were tested for the material 1.4429 /29/. The weldment was produced by the shielded metal arc process with consumable stick electrodes. The weld material chemical content is given in Table 8 under the weld metal designation 1.4455. The higher manganese as compared to the bulk metal 1.4429 is necessary to suppress the hot cracking of the weldment /32/. The weldment thickness was ~ 50 mm and two types of joints were investigated: double U-type and T-type. Figure 43 summarizes the obtained data of the double U-type joint at ambient.

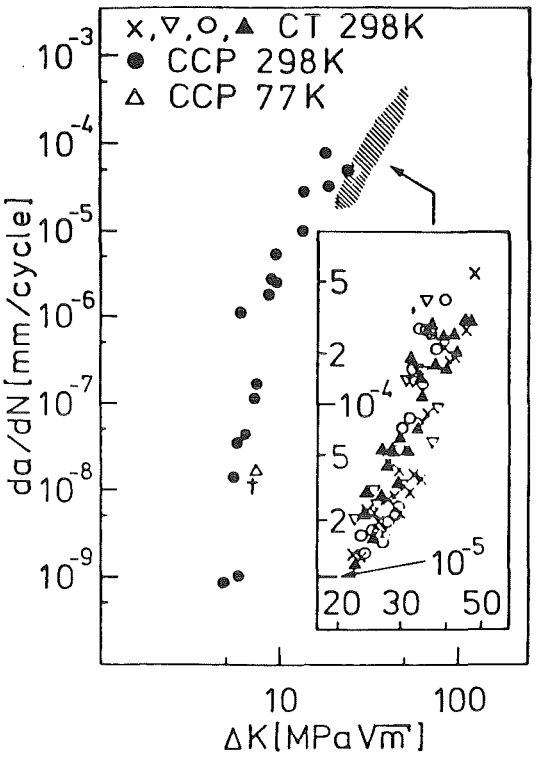

Fig. 43
Measured fatigue response of the weld metal. CT and CCP specimen were machined out of 50 mm thick double U-joint. + refers to 77 K FCGR test where for 10^5 cycles no crack advance were observed /29/.

The specimens were machined from the 50 mm thick weld metal. The 77 K measurements with CCP-specimens show the slight shift of the crack growth rate to lower values. The dashed line is the range of results gained with CT-specimen at room temperature. Figure 44 shows similar results with tests of T-type joints. The results gained with a high manganese Cr-Mn (C 748) austenitic steel are shown in Fig. 45.

4 K investigations of Fe-Mn austenitics have shown that these materials have advantages compared to the high strength 304 LN type materials. The results given in Fig. 46 indicate this behaviour.

Compared to the ambient tests of the Fig. 45 the Fe-Mn material at 4 K shows better FCGR behaviour, which makes this material important for future uses at low temperature. But still there are uncertainties with high manganese austenitics as shown in Fig. 47 in certain cases the materials FCGR increases with decreasing the temperature.

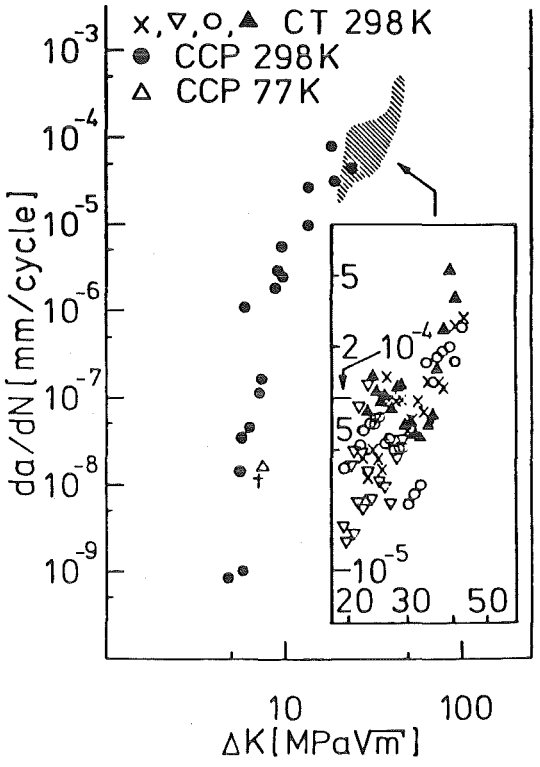

Fig. 44
FCGR data of T-type weldment of material 1.4455. Dashed lines show the range of the results with CT-specimens. + refers to 77 K FCGR test where for 10^5 cycles no crack advance were observed /29/.

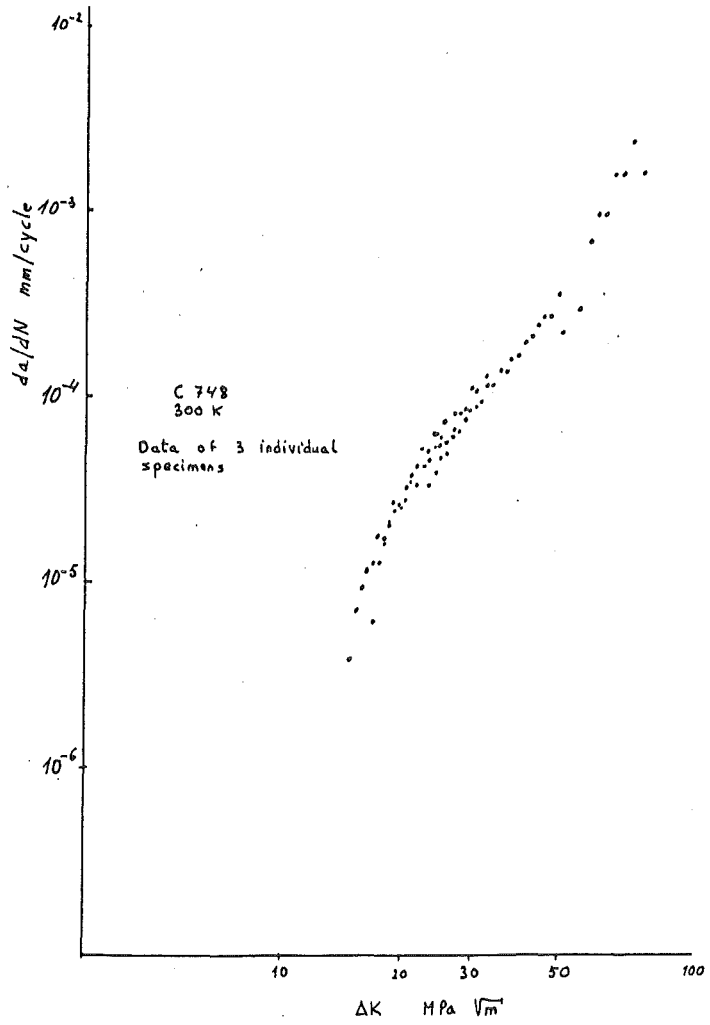

Fig. 45
FCGR results with a Fe-Mn-Cr type stainless steel at ambient. Data were taken from /28/.

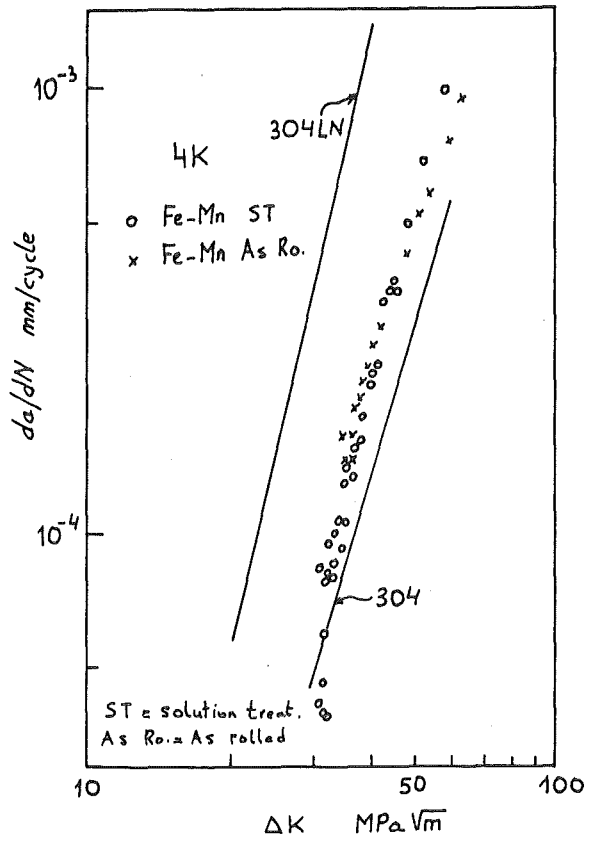

Fig. 46
High manganese stainless steel austenitic and its FCGR results compared to 304 and 304 LN material. This material was fabricated at Kobe steel and data were taken from /33/.

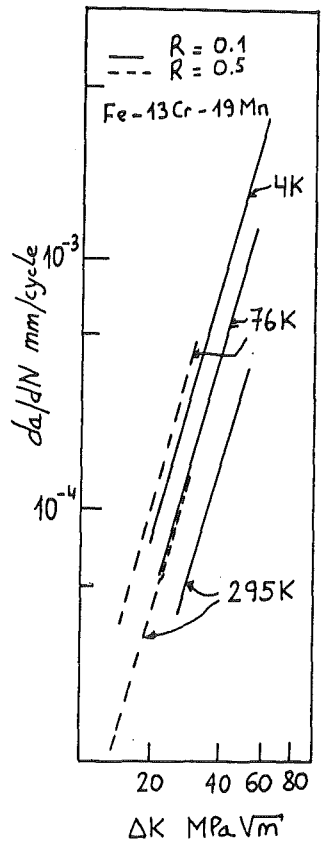

Fig. 47
Fe-13Cr-19Mn material and its FCGR response concerning the temperature decrease. Data were taken from /34/.

Possibly, the non-balanced chemical composition of the elements cause this behaviour. The data in Fig. 47 also show the increased load ratio R sensitivity for stage II FCGR.

For the same load ratio R (here R = 0.1) materials 304L, 304 and 305 reveal an enhanced crack growth resistance at low temperatures. Figures 48 and 49 show this dependency.

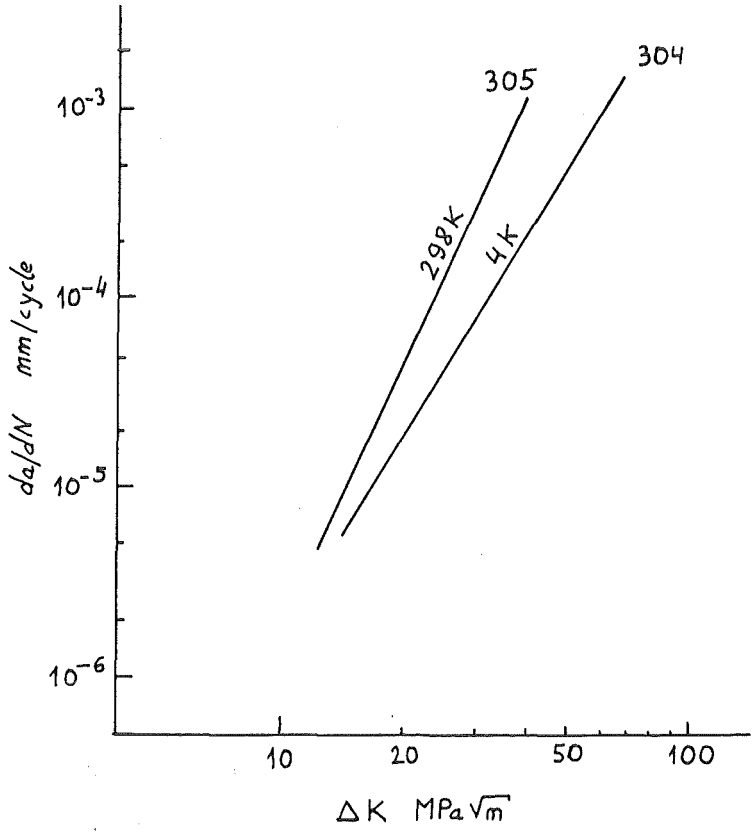

Fig. 48
304 and 305 type austenitic stainless steel. Data were taken from /35, 36/. 4 K FCGR show a higher FCGR compared to the ambient.

As shown in Fig. 50 for a high nickel content iron based austenitic material, the FCGR results show at ambient a high influence of load ratio in the near-threshold regime, but little influence in the stage II regime.

This influence, however, decreases at low temperatures as indicated in Fig. 51. The explanation for this phenomena were given by the authors /38/ by introducing an "environmental assisted crack growth mechanism" at ambient, which is sensitive to load ratio variation.

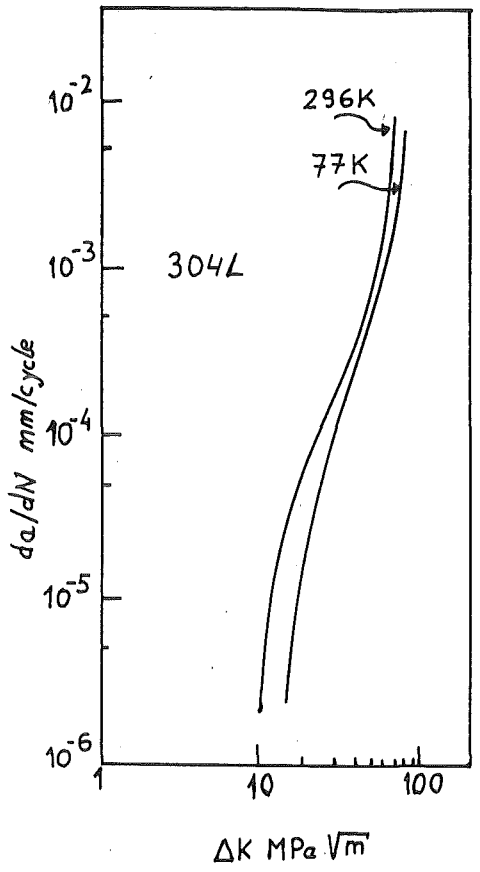

Fig. 49
304L material investigated by Katz et al. /37/ at 77 K and at ambient.

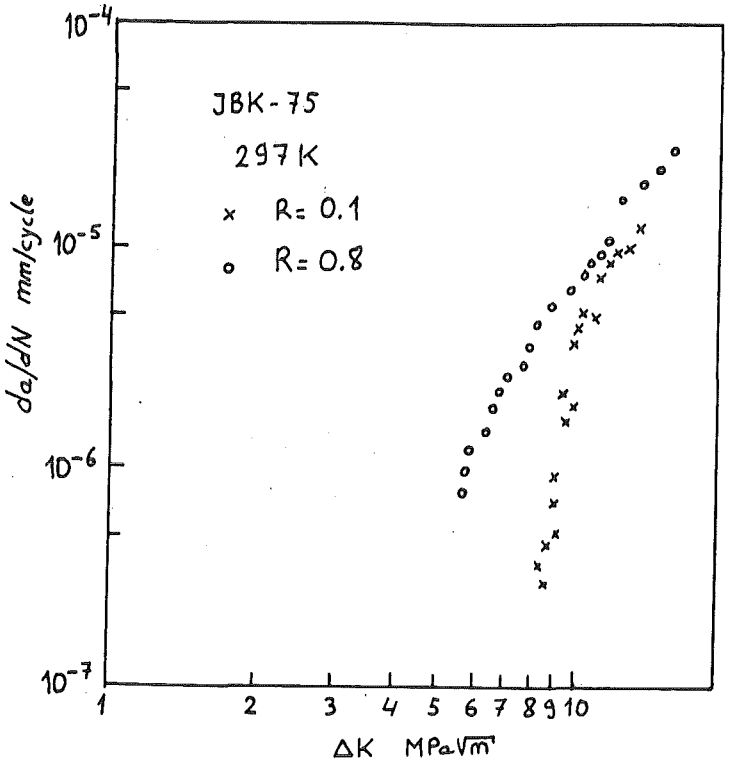

Fig. 50
Near threshold measurements with JBK-75 material. Data were taken from /38/.

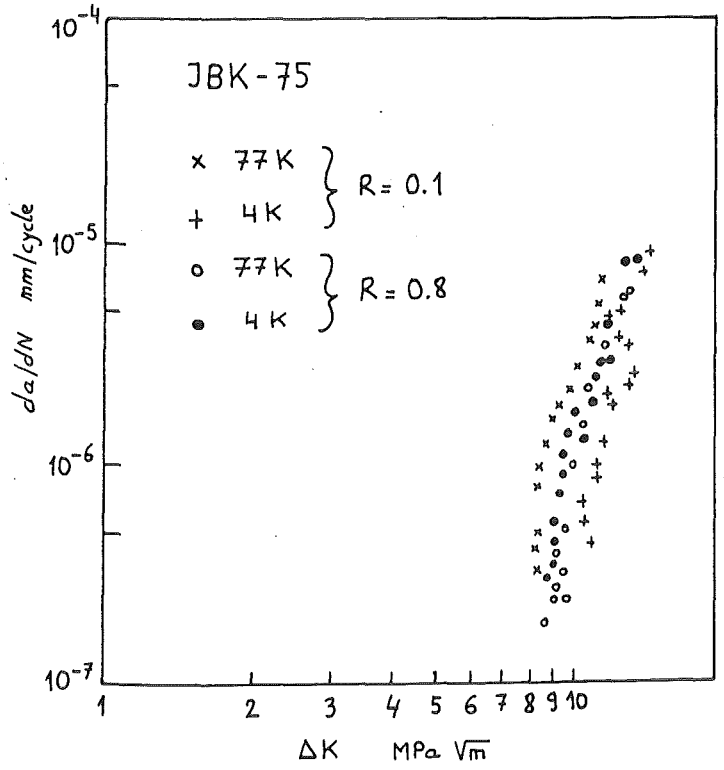

Fig. 51
FCGR of JBK-75 alloy at 77 K. Little influence of the load ratio. After /38/.

Weldments of 316L type material welded by shielded metal arc process were investigated by T. A. Whipple et al. /39/. Cracks penetrated from different positions showed little difference with respect to their 4 K FCGR behaviour (Fig. 52).

The difference between the parent and weld material used in the Japanese Large Coil case were investigated at 4 K /40/. The results show the shift of the weld metal results to lower FCGR. This can be attributed to the grain size properties of the weld/bulk metal (Fig. 53).

The materials ASTM A-453 was investigated at NBS, Boulder /41/ The results give a significant difference of FCGR at near threshold regime measured at low and ambient temperatures. In stage II regime there is no influence of the temperature. As comparison the 4 K data of a similar material (A-286) were plotted in the same Figure 54. A-286 and A-453 are fully austenitic stable materials and therefore there are differences as compared to the materials 304 and 305 (Fig. 48 and Fig. 49).

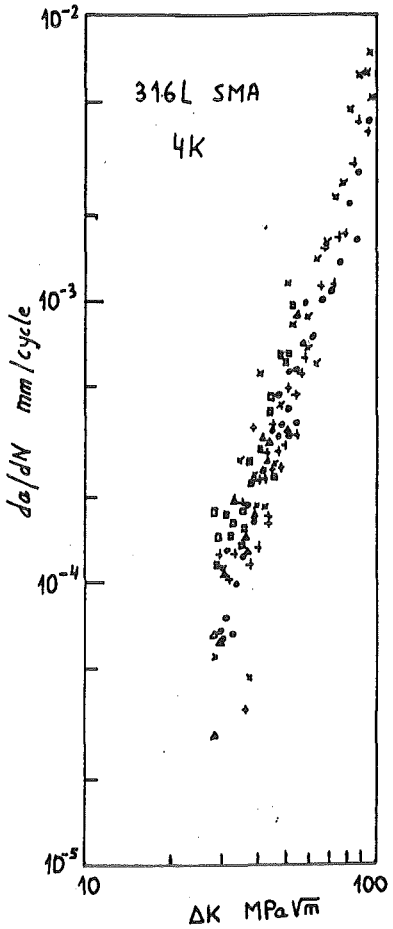

Fig. 52
Four different weldments of material 316L tested at 4 /39/.

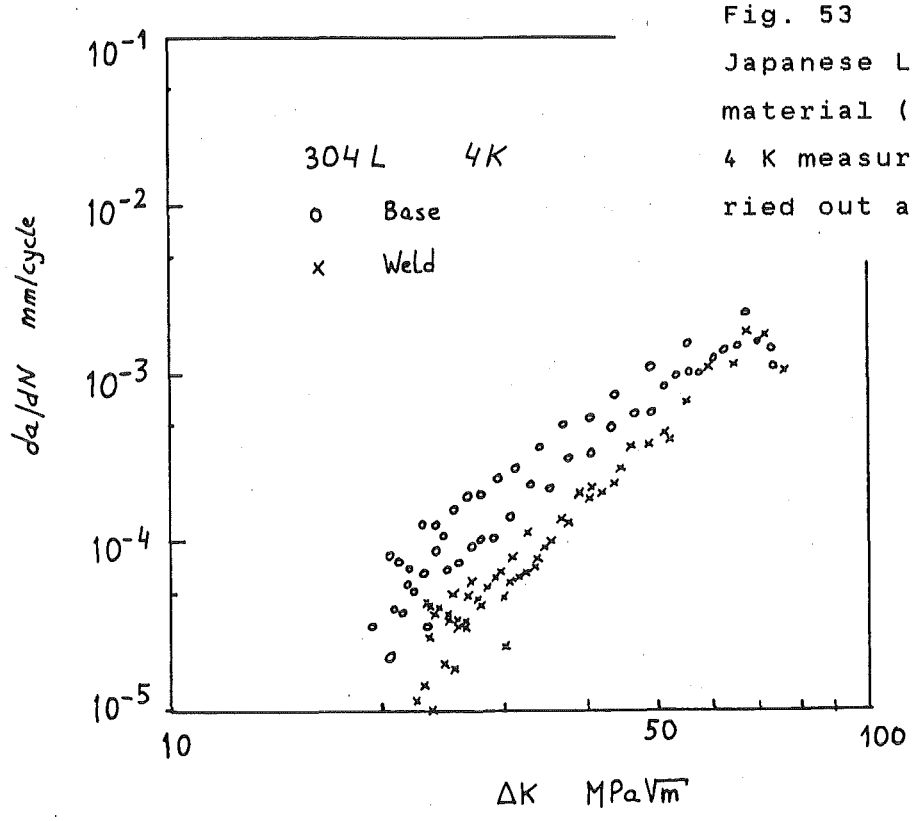

Fig. 53
Japanese LCT coil case material (304L) and the 4 K measurements carried out at JAERI /40/.

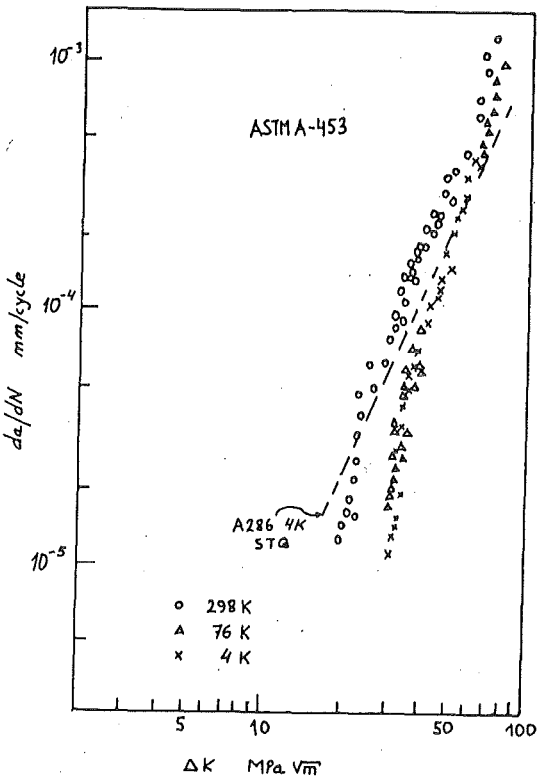

Fig. 54
Measurements of the material ASTM A-453 at ambient, 77 K and 4 K. Data were taken from /41/.

At 4 K several austenitics used for large scale cryogenic applications were investigated by different laboratories. The results of these measurements are shown in Fig. 55. Out of this diagram one can see that large differences (factor of 20 - 50) of crack growth rates exist among the austenitics.

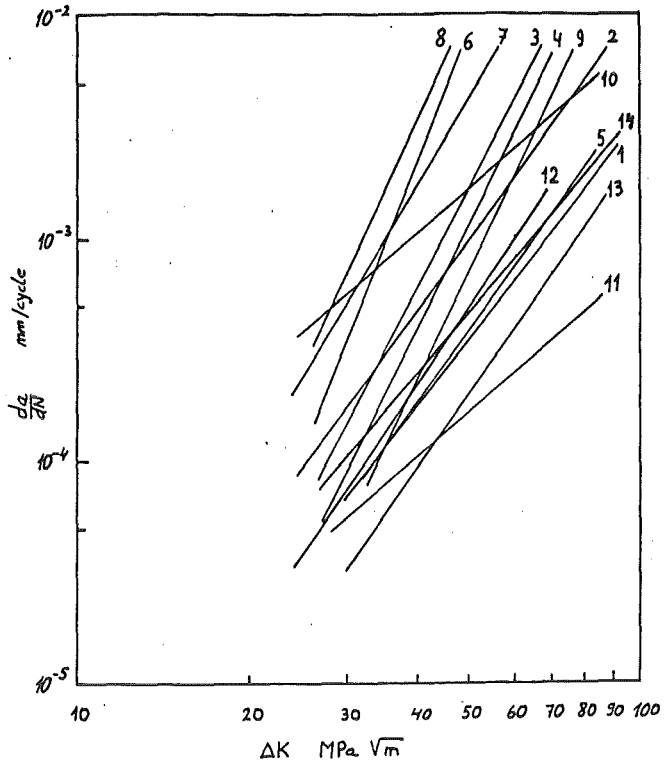

Fig. 55 FCGR data of austenitics measured at 4 K.

1) 316 LN Plate /42/; 2) 316 LN weld /42/;
3) 304 L Plate /43/; 4) 304 L weld /43/;
5) 304 /44/; 6) Nitronic 40 /44/;
7) 304 LN /44/; 8) 304 L /44/;
9) 310 S /44/;
10) A 286 40 % cold worked aged /44/;
11) A 286 sol. treated, quenched /44/.

3.2.2 Influence of radiation on fatigue at low temperature

Low temperature application of austenitic materials under neutron irradiation requires fatigue data concerning there special circumstances. Up to now no cryogenic FCGR data measured in irradiation environment have been published. The establishment of a testing facility operating under neutron irradiation at 4 K is a major demand as stated in a proposal by /45/. Nevertheless one should be able to predict the effect of radiation on the fatigue behaviour at cryogenic temperatures from relevant high temperature measurements. There are numerous investigations concerning the irradiation fatigue behaviour of austenitics at high temperature. These data were gained during the design period of sodium cooled fast breeder reactors. The material AISI 305 (Werkstoff Nr. 1.4948) was most thoroughly investigated for this purpose. The fatigue strength performance was determined with bend type samples /46/. The accumulated fluence during 19 days at 823 K was 5×10^{20} n/cm^2 at E > 0.1 MeV.

The findings (Fig. 56) result in an endurance ratio of about 0.43. The fatigue strength of the irradiated material increased

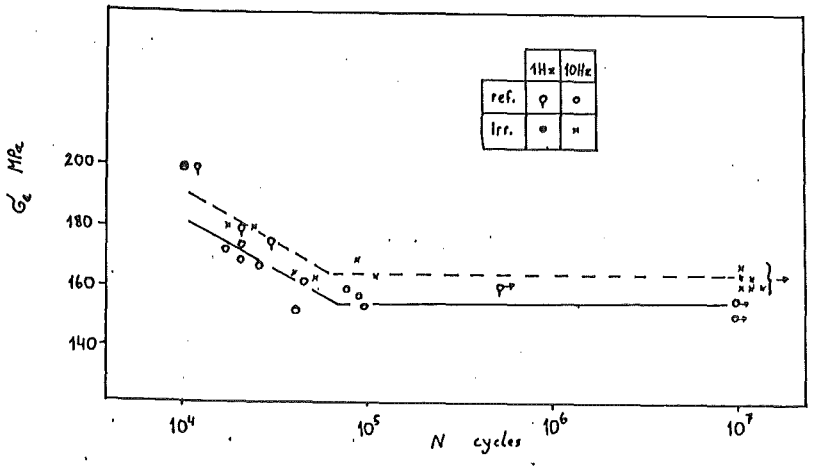

Fig. 56
Fatigue strength vs. cycles to failure at 823 K for the material 305 /46/.

slightly from 152 MPa (reference material) to 162 MPa. Both in reference and irradiated condition the measured fatigue curve has a horizontal part for about $N > 8 \times 10^4$ cycles and thus real fatigue limits could be established.

The slightly increasing characteristics of the fatigue strength can be explained by the increase of the yield strength of this material after the irradiation. Austenitic materials, on the other hand, show a significant decrease of fracture toughness under irradiation environment at high temperatures /47/. One can, therefore, argue that both these effects together may enhance the fatigue strength but decrease the FCGR in general. The decrease of FCGR for irradiated austenitic materials (at 700 K) has already been reported /48/.

For some cryogenic austenitic materials, the mechanical properties have been investigated at low temperatures after irradiation. The neutron fluence in this case were ~ 10^{18} n/cm^2 at high neutron energy levels E > 1.0 MeV. Figure 57 shows the effect of irradiation on the mechanical properties for the austenitic

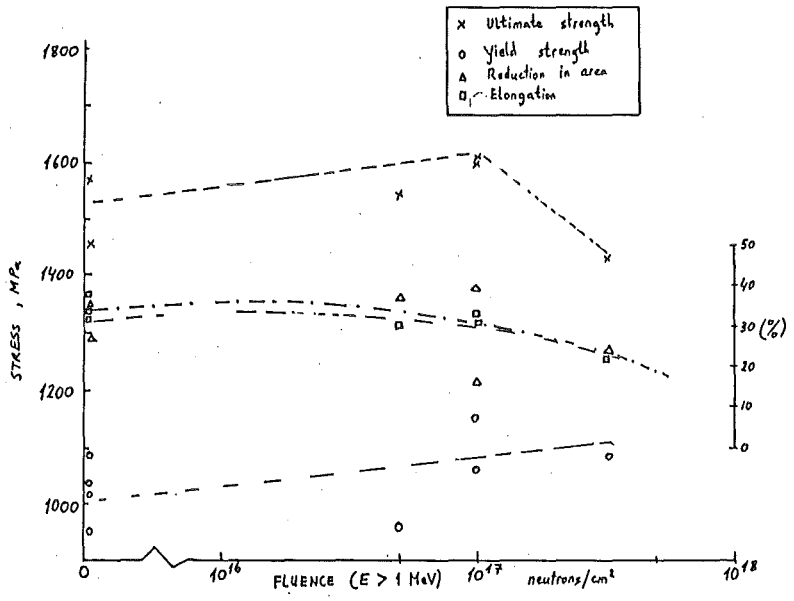

Fig. 57
Mechanical properties of the material A-286 (plate and forging) vs. the neutron fluence at 17 K /49/.

material A 286. A slight decrease of ductility accompanied with an increase of yield strength is obvious.

In Figure 58, 77 K test results of fracture toughness measurements after irradiation are given. The tested material is an austenitic material with 22 % Cr, 13 % Ni and 5 % Mn.

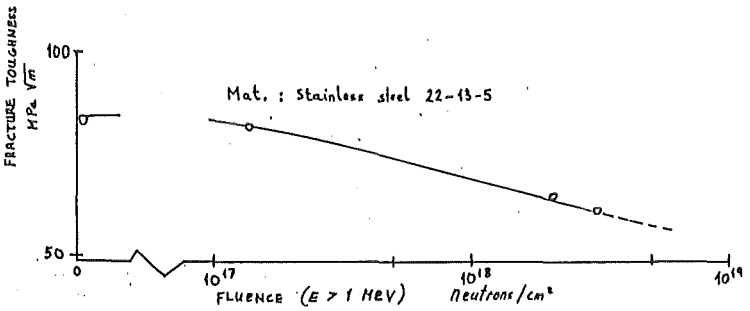

Fig. 58
Influence of the irradiation on the fracture toughness performance of an austenitic material at 77 K /49/.

A marked decrease of the fracture toughness performance is revealed according to these tests. The FCGR response is expected to be reduced after the irradiation. Beyond a fluence of 5×10^{18} n/cm^2 there exist no actual low temperature data, but a prediction can be made towards drastic increase of the crack growth rate with further neutron accumulation.

3.3 Fatigue behaviour of non-ferrous materials

3.3.1 Aluminium alloys

Among the non-ferrous materials aluminium alloys represent an important candidate material, whenever requirements such as low weight, good workability, non-magnetism, high electrical and thermal conductivity and moderate strength and toughness are needed. In this review three different series will be considered concerning their fatigue crack behaviour.

The 2000 series requires solution heat treatment to obtain optimum mechanical properties, but the corrosion resistance (intergranular corrosion) is low compared to other aluminium alloys. To achieve resistance against corrosion, this alloy in form of sheets usually cladded with an aluminium alloy of the 6000 series (Mg-Si alloy) to protect the core material. The best known alloy in this series is the alloy 2024 which is the most widely used aircraft alloy.

Table 9 Chemical composition (wt.%) limits for wrought Aluminium alloys

Material	Si	Fe	Cu	Mn	Mg	Cr	Zn	Ti
2024	0.50	0.50	3.8-4.9	0.3-0.9	1.2-1.8	0.10	0.25	-
5083	0.40	0.40	0.10	0.3-1.0	4.0-4.9	0.05-0.25	0.25	0.15
7075	0.50	0.70	1.2-2.0	0.3	2.1-2.9	0.18-0.40	5.1-6.1	0.20

Table 9 gives the chemical composition of this alloy which shows that copper is the principal alloying element. Figure 59 shows the ambient FCGR data of 2024 aluminium alloy for two different load ratios.

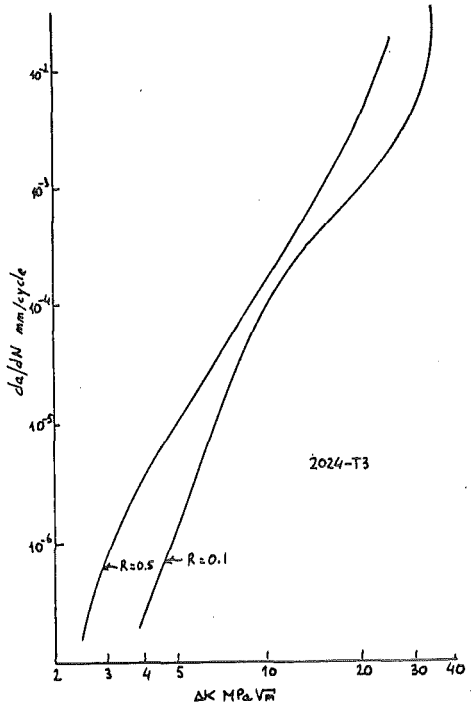

Fig. 59
2024 series aluminium alloy and the measured FCGR at ambient for R = 0.1 and R = 0.5. Data were taken from /50/.

The results show the trend to higher crack growth rate with increasing the load ratio from R = 0.1 to 0.5. It is assumed that in the near future this commercial aerospace material is replaced by newly developed aluminium lithium alloys. One of such a candidate material is the alloy 2.5 Li-1.2Cu-0.7Mg-0.12Zr. Besides copper, the major alloying elements are Lithium and Zirconium. The density of this alloy is ~ 10 % lower and the stiffness ~ 10 % higher compared to the 2024 series alloy.

Under laboratory air the measured ambient FCGR of this Al-Li alloys are significantly lower than in 2000 series alloy as shown in Fig. 60.

At low ΔK the rate of crack growth for Al-Li is about an order of magnitude lower than for the 2000-series. At higher levels of

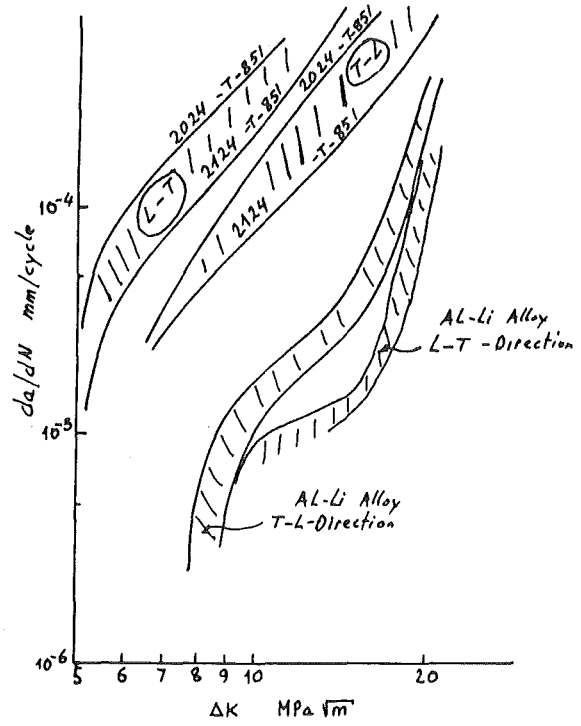

Fig. 60
FCGR data of 2024 and 2124 alloy compared to Al-Li-alloy. The effect of crack orientation is obvious. Data were taken from /51/.

ΔK the growth rates of the Lithium alloy merge with those of 2024 reflecting their similar levels of fracture toughness.

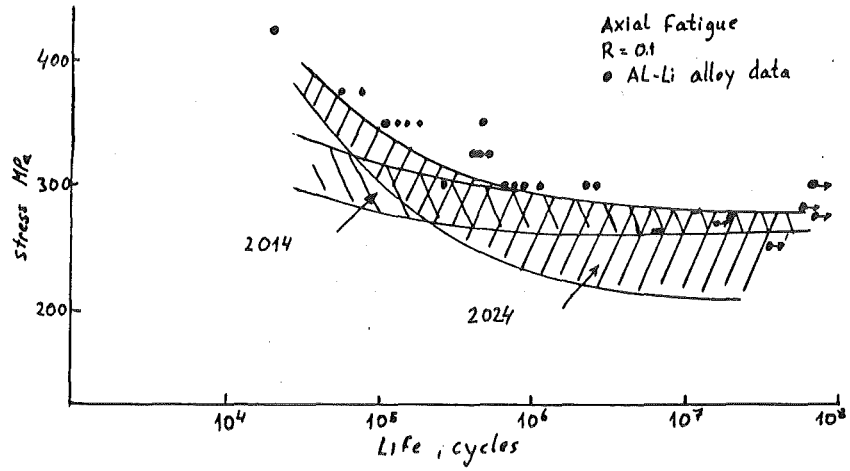

Fig. 61
Fatigue strength data of 25 mm thick plate Al-Li alloy and conventional aluminium alloys. Data were taken from /51/.

For the same material Fig. 61 shows fatigue strength test results for fatigue specimens axially loaded with R = 0.1. In all the tests carried out at ambient the Al-Li alloys matched or outperformed the control alloys in both the longitudinal and transvers test orientations.

For aluminium alloys the interaction between the effects of microstructure and environment on fatigue crack growth are important. The results obtained on a 7075 alloy (chemistry is given in Table 9) in four aged conditions representing different microstructures are given in Fig. 62.

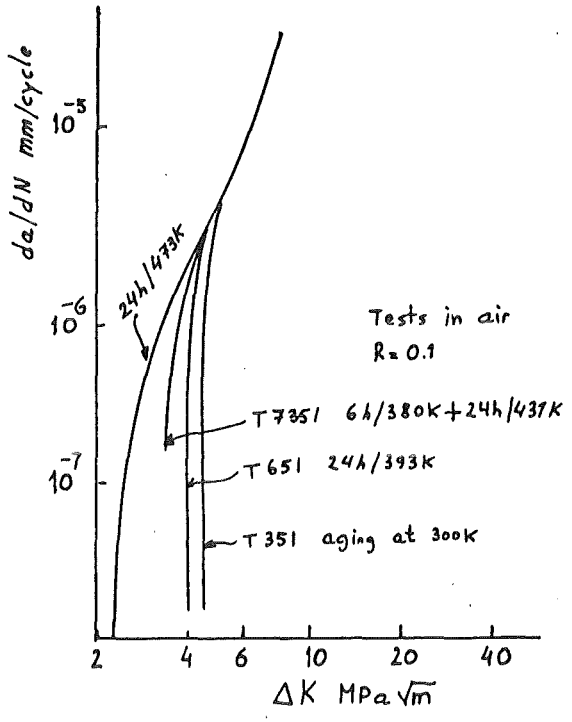

Fig. 62
FCGR data for 7075 alloy with different heat treatments. Data were taken from /52/. Tests were carried out in air.

The tests reveal a strong influence of different heat treatments at the near threshold and the threshold regime. The same specimens, however, exhibit quite different values at vacuum (Fig. 63). The FCGR data of 7075 alloys with similar aged conditions are improved in this case. This can be attributed to the environmental effect such as water vapour adsorption of the crack tip /52/.

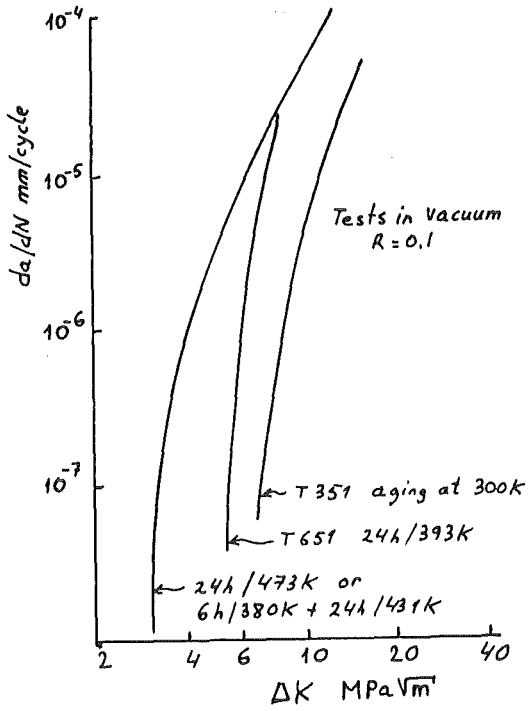

Fig. 63
FCGR data for 7075 alloy with different heat treatments. Tests were carried out in vacuum /52/.

The aluminium alloy 5083 is widely used for cryogenic application in the LNG (liquid natural gas) industry. Magnesium is the major alloying element of this alloy which gives a moderate-to high-strength, non-heat treatable alloy. Alloys in this series possess good welding characteristics and good resistance to corrosion in marine atmospheres. The measured FCGR of the bulk material in annealed condition is given in Fig. 64.

At cryogenic temperatures the material show enhanced crack growth resistance. The effect of the humidity is obvious.

Figure 65 represents the data for 5083 welds with 5183 filler material gained at ambient and at 78 K. The crack growth rate is lower at 78 K and at low ΔK regime, whereas the data merge with the ambient at high ΔK levels.

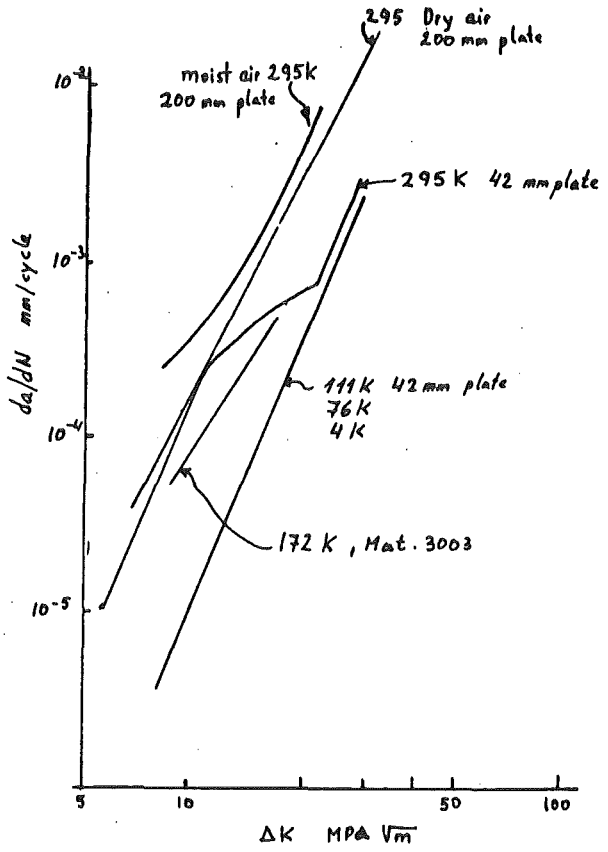

Fig. 64
Ambient and cryogenic FCGR data of the material 5083 in annealed condition. Data were taken from /53/.

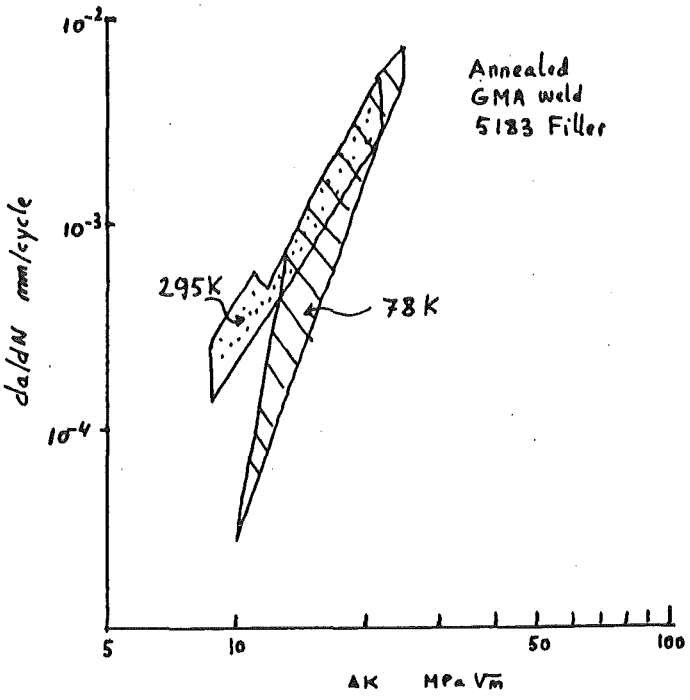

Fig. 65
Ambient and cryogenic FCGR data of the weld material 5083 in annealed condition. Filler material 5183. Data were taken from /53/.

3.3.2 Titanium alloys

Titanium alloys have particular characteristics which make them different from other alloy types such as Aluminium or steel. Certain titanium alloys, when properly processed, are almost free of inclusions or second phase particles. The microstructures of Ti-alloys are often duplex in nature, containing an intimate mixture of the high temperature β-phase (bcc) and the low temperature α-phase (hcp). In general, the alloys fall into three major categories α, α/β or β. Certain alloying elements influence the phase diagram of Ti significantly concerning the α-rich and β-rich phases. Elements such as Oxygen and Aluminium stabilize the α-phase, whereas Vanadium stabilizes the β-phase. The effect of oxidation at high service temperatures on cyclically loaded titanium alloys are detrimental. Above 873 K, simultaneous oxide film formation and growth and oxygen dissolution into the metal forming a gas saturated layer are expected. This has a very adverse effect on low cycle fatigue behaviour. The fatigue properties depend also upon the α-grain size, the smaller the α-grain size the greater the fatigue resistance /54/. The crack growth rates are affected significantly by variables such as microstructure, environment, temperature, interstitial content and load ratio. At ambient for a given titanium alloy, FCGR varies by as much as an order of magnitude in response to heat treatment, with the usual trend being that FCGR is the smaller the larger the microstructural size /55/. The typical influence of load ratio R on crack growth rates in an air environment is shown in Fig. 66.

In comparing FCGR in air with those obtained in vacuum it has been observed that air environments increase FCGR compared to vacuum. This difference in growth rates is attributed to the interaction of interstitial oxygen with the base metal, which may modify the local plastic behaviour and fracture strain in the vicinity of the crack tip /57/.

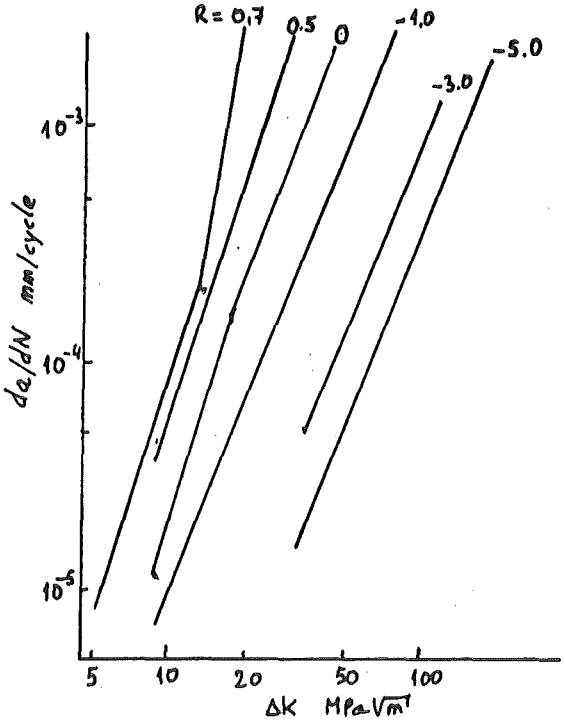

Fig. 66
Ambient FCGR as a function of ΔK for various R ratios. Data were taken from /56/.

FCGR investigations in dependence on temperature (Fig. 67) indicate a pronounced environmental effect, particularly at low ΔK levels where time dependent effects such as oxidation, would be expected to predominate.

Ti-6Al-4V shows the ability to withstand structural loads in cryogenic regime as successfully demonstrated by the use of this material as liquid hydrogen tanks in space industry /59/. This material is attractive for such uses because of its high toughness and high modulus compared to the best known aluminium alloy. As indicated in Fig. 67 the 4 K FCGR of Ti-6Al-4V is shifted to low crack growth rates compared to the ambient and elevated temperature results.

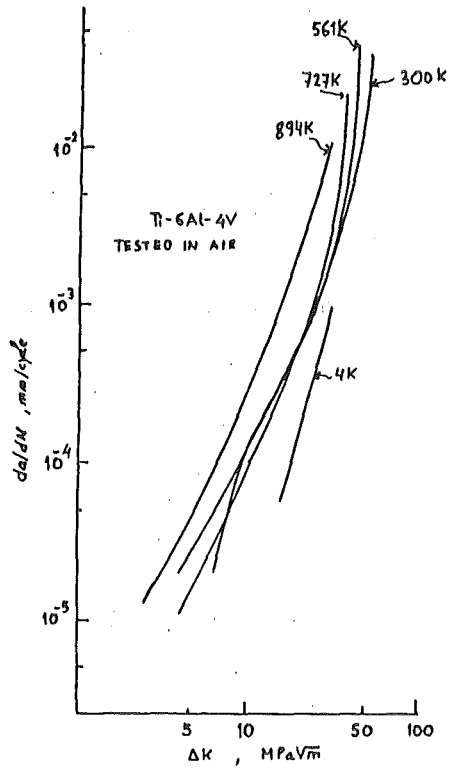

Fig. 67 FCGR ΔK for various temperatures. For elevated temperatures data were taken from /58/ and for 4 K from /26/.

3.3.3 Copper and copper alloys

The structural applications of copper are limited, causing a lack of data on crack growth behaviour. Lukas /60/ measured a threshold value of about 2.5 MPa√m at 173 K. In addition, increasing the grain size of the copper leads to lower crack growth rates. Observations by the same author /61/ show that for fine grain sized coppers the fatigue strength is higher than for coarse grain sized copper.

On the other hand a good data base concerning the fatigue strength properties of commercially available copper and copper base alloys exist. Table 10 summarizes the fatigue strength characteristics of some important copper and copper base alloys. The data were established with reversed bending tests at R = -1.

Table 10 Fatigue strength properties of commercial available copper and copper alloys. Data refer to ambient measurements.

Material		Tensile strength MPa	Number of cycles x 10^6	Fatigue strength MPa	Endurance ratio	reference
Electrolytic tough pitch copper	Annealed Flat product grain size 25 µm	240	100	75	0.31	
	CW 21 %	295	100	90	0.31	/62/
	37 %	350	100	90	0.26	
	60 %	385	100	100	0.26	
	Annealed Rod product grain size 40 µm	220	300	65	0.30	
	CW 36 %	345	300	120	0.35	/63/
OFHC - copper	CW 29 %	360	300	120	0.33	/64/
Phosphorus deoxidized copper low residual phosphorus	CW 21 %	290	100	90	0.31	
	37 %	320	100	110	0.34	/65/
	60 %	360	100	100	0.28	
CuSn 10 Tin Bronze	Annealed grainsize 35 µm	445	100	175	0.39	
	15 µm	485	100	225	0.46	
	CW 21 %	600	100	225	0.46	/66/
	50 %	750	100	205	0.27	
	69 %	850	100	205	0.24	
Copper Nickel alloy CuNi10Fe1	quoted as hard	380	100	150	0.39	/67/
Copper Nickel alloy CiNi30Fe	annealed	410	100	140	0.34	/68/
	CW 33 %	575	100	245	0.43	/69/

This table shows also that the mechanical properties such as the tensile strength depends strongly on grain size. The grain size affects also the fatigue strength consequently. Investigations have revealed that the yield strength of copper depends on the grain size according to the Hall Petch relation /69/. Ultra fine grain size copper (grain size ~ 0.1 µm) increases the ambient yield strength of high purity copper up to 480 MPa /69/. Another characteristics of the high purity copper is the absence of a real endurance limit.

At cryogenic temperatures the fatigue strength increases due to the enhanced yield strength behaviour. For OFHC copper in annealed condition, Fig. 68 shows the temperature dependence of the fatigue life. This diagram reveals the significant positive effect of the temperature decrease.

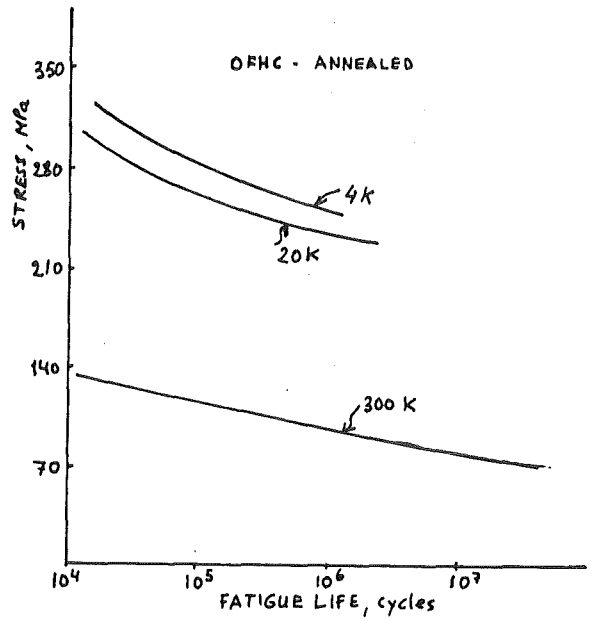

Fig. 68
OFHC-copper fatigue strength vs. number of cycles at various temperatures. Data were taken from /70/.

Figure 69 gives the fatigue data of annealed electrolytic tough pitch copper and the effect of cryogenic temperatures.

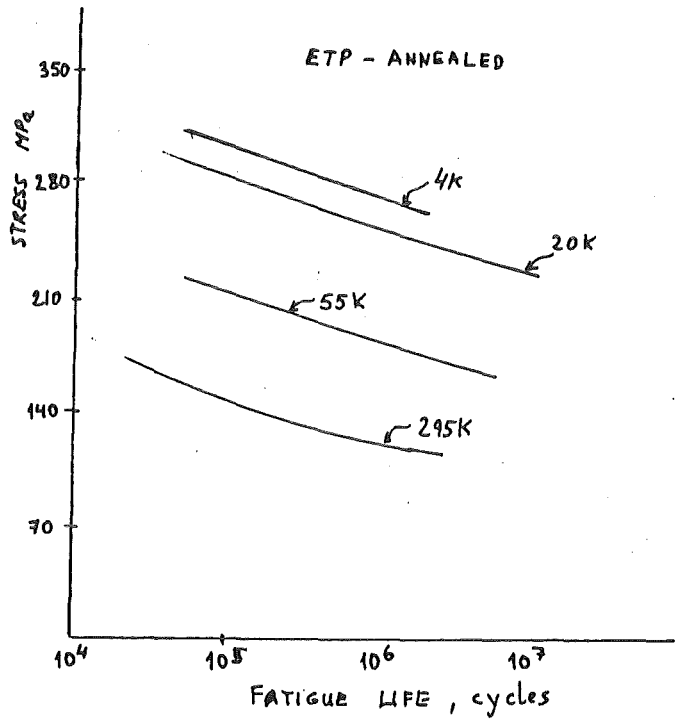

Fig. 69
ETP-copper fatigue strength vs. number of cycles at various temperatures. Data were taken from /70/.

3.3.4 Nickel base alloys

Nickel base alloys exhibit high strength and high corrosion resistance at elevated temperatures. Whenever structural problems at elevated temperatures exist use of nickel base alloys can be a solution. Main industrial applications of these alloys are their use in heat exchanging units and as materials for turbine blades and disks working at elevated temperatures. Besides the strength these materials need also resistance to fatigue loading including both high cycle fatigue from vibration or rotation bending and low cycle fatigue arising from the steep thermal gradients occuring during rapid start-up and shut-down of machineries. A material with superiour high temperature qualification

is the Nimonic 901 (chemical composition Cr = 13 %, Fe = 38 %, Mo = 6 %, Ti = 3 %, C < 0.1 and Nickel in balance). Figure 70 gives the results of the low cycle fatigue investigations.

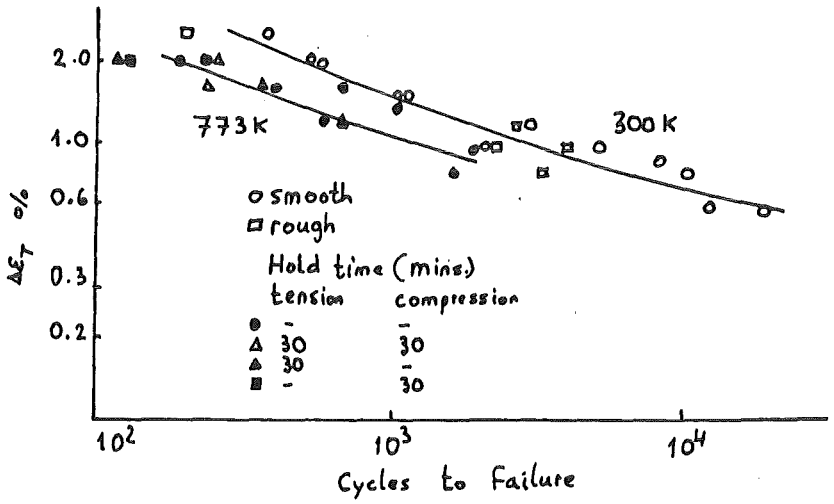

Fig. 70
LCF lifetime curves at ambient and at 773 °K. Data were taken from /71/.

It is apparent that, at the same total strain amplitude, specimens tested at 773 K exhibit ~ 40 % of the lifetime determined at ambient. High cycle fatigue specimens with the same material tested at both ambient and 773 K indicate that cracking initiates at carbides.

FCGR measurements were carried out in air at R = 0.1 and R = 0.5. The results are shown in Figures 71 and 72.

Almost no difference exists between 573 K and 298 K in the stage II regime at both R-values. At 773 K a slight increase in crack growth and a small change in slope could be found. In the threshold region at 773 K a very pronounced drop to a threshold value is apparent at R = 0.1 and R = 0.5. Here again the environmental effect (oxidation) plays an important role according to /71/.

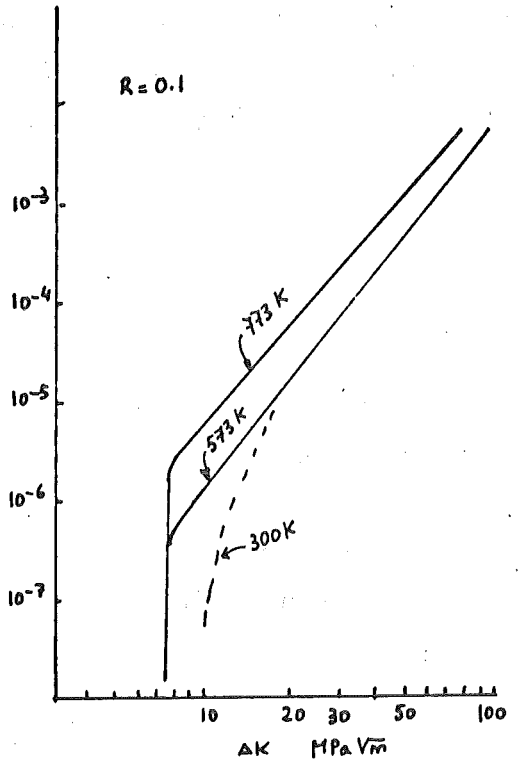

Fig. 71
FCGR of Nimonic 901 tested at different temperatures and at R = 0.1. Data were taken from /71/.

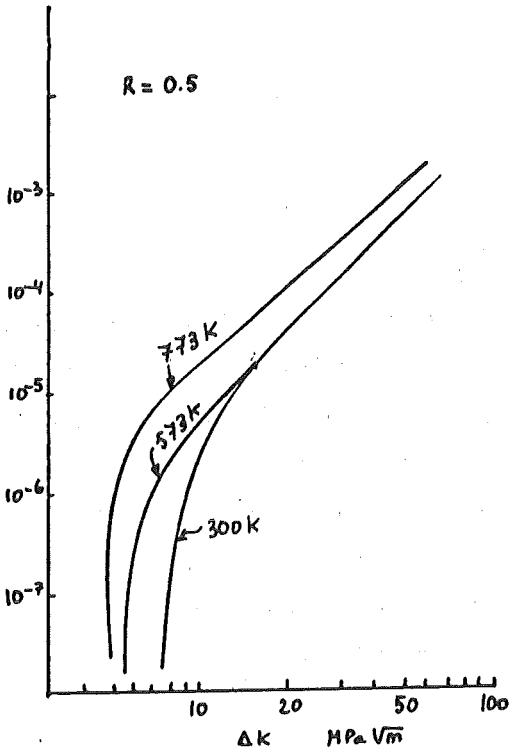

Fig. 72
FCGR of Nimonic 901 tested at different temperatures and at R = 0.5. Data were taken from /71/.

The effect of the environment is determined for the Nickel base alloy inconel alloy 718 (Cr = 18.5 %, Ni = 52.5 %, Mo = 3.0 %, Nb = 5.1 %, Ti = 0.9 %, Al = 0.5 %, C = 0.04 %) in /72/. Figure 73 shows the results of FCGR tests in air and helium at 923 K. The air environment significantly increases the crack growth rate /72/.

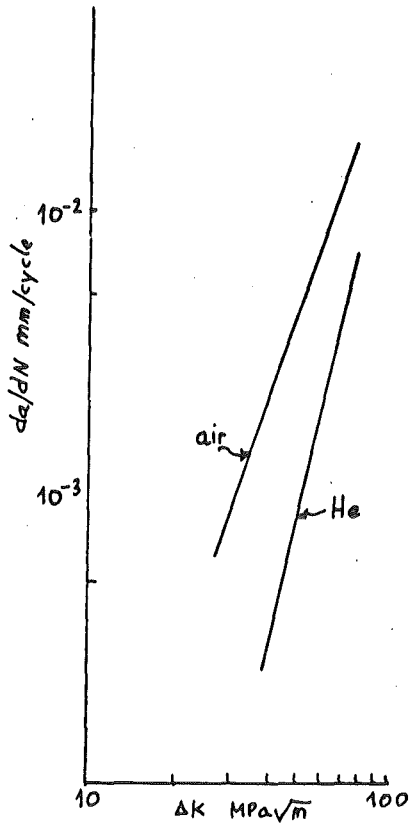

Fig. 73
FCGR of inconel 718 at 923 K in air and helium atmospheres. Data were taken from /72/.

Nickel base alloys are also extensively utilized for cryogenic applications. Inconel X750, an austenitic nickel base superalloy was investigated concerning its FCGR at cryogenic regime /73/. The material chemical composition is given as Ni ≈ 73 %, Cr ≈ 15 %, C < 0.04 %. The results of FCGR indicate that the growth rate of fatigue cracks at ambient is at least equal to or in most cases substantially greater than at 4 K. Figure 74 represents the results of FCGR investigations of material X750 at ambient and 4 K.

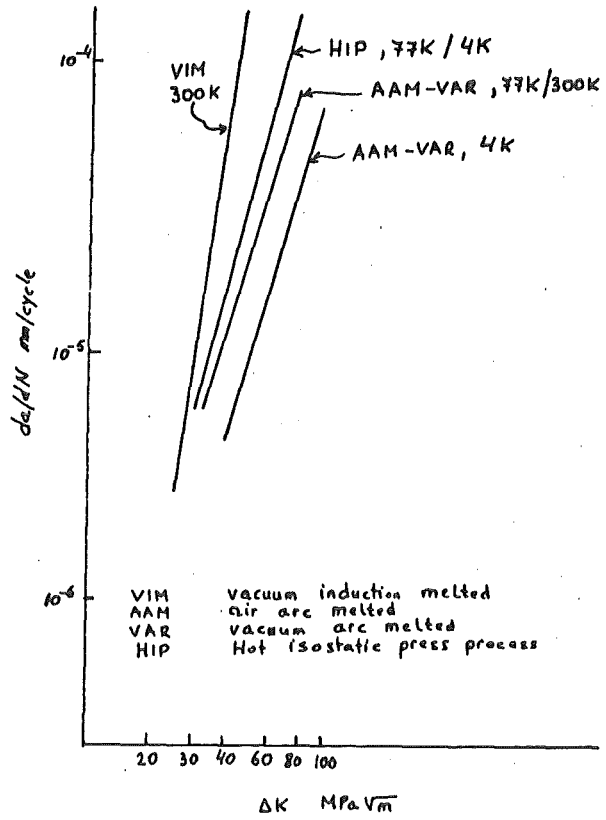

Fig. 74 FCGR results of inconel X750 at ambient and at 4 K. The band shows the influence of different manufacturing processes and heat treatment of the materials. Data were taken from /73/.

3.4 Low cycle fatigue data of structural alloys

Application of structural materials in low cycle regime necessitate strain-controlled cyclic investigations. In the following the low cycle fatigue results of important structural materials are outlined. All tests are fully reversed bending tests with R = -1. The results of structural ferritic steels HY-80 - HY-230 with yield strengths between 560 MPa and 1600 MPa are shown in Fig. 75. The 95 % confidence line of the results gives the scatterbased of the investigated materials. As a comparison the structural material 316 LN is also given in this diagram. The tests with this austenitic material were also carried out at R = -1, but in axial loaded condition /74/.

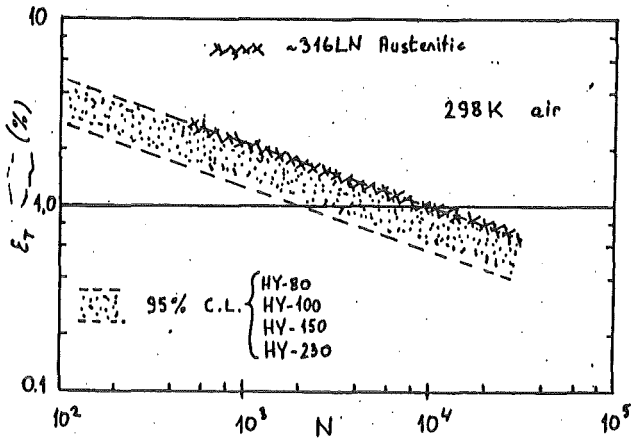

Fig. 75
Total strain vs. cycles to failure for ferritic materials /75/ and for the material 316 LN /74/.

Similar tests carried out with structural aluminium alloys reveal at ambient and under air environment results which are nearly identical with the structural steel tests. Fig. 76 gives the results of the tested aluminium series.

Nickel base alloys and copper alloys were also investigated at ambient and under air environment, Fig. 77. The chemical composition of gun metal is given as 87 % Cu, 8.4 % Sn, 3.5 % Zn and 0.7 % Ni; for superston (an aluminium bronze) the chemical composition is given as 74.6 % Cu, 7.4 % Al, 12.5 % Mn, 3.3 % Fe and 2.1 % Ni. Monel is a Nickel base alloy with ~ 70 % Ni and 30 % Copper. There is a marked difference between the two copper base alloys. The 95 % confidence line of inconel 718 and Monel is also somewhat similar to the previously described tests of ferritic steels.

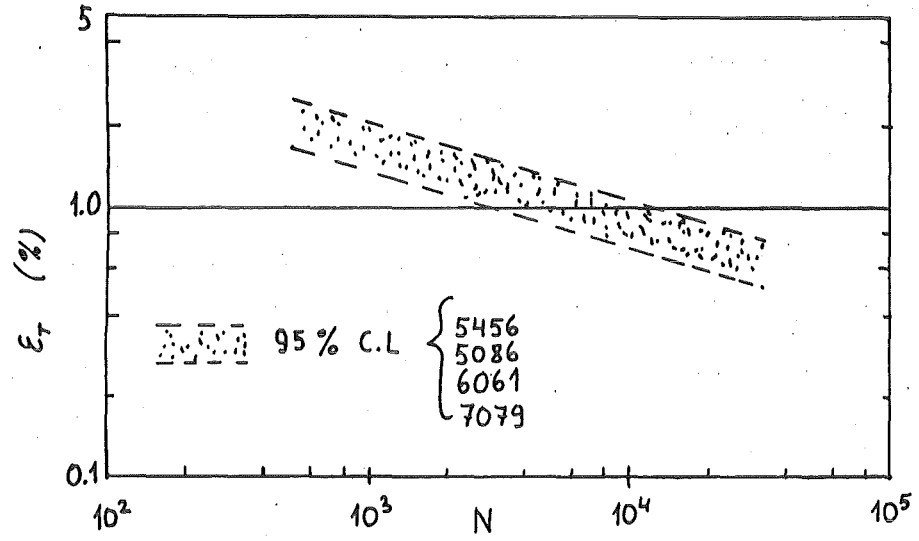

Fig. 76 Total strain vs. cycles to failure for different aluminium alloys. Data were taken from /75/.

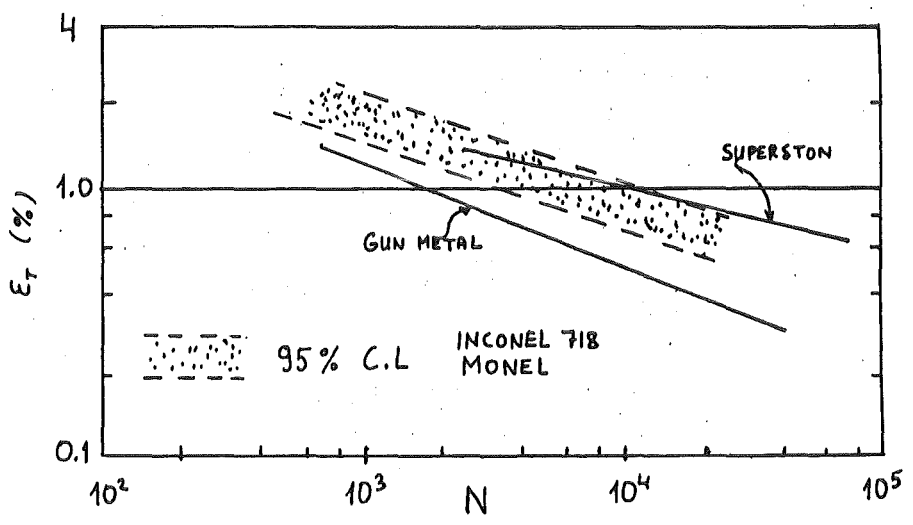

Fig. 77 Total strain vs. cycles to failure for nickel base and copper base alloys. Data were taken from /75/.

3.5 Fatigue of engineering plastics

The trend towards lighter and higher strength structures shifted the interest recently to the engineering plastics and their use in mechanical systems. Especially the fibre reinforced plastics are attractive for structural applications. Therefore, fatigue response of these materials has become icreasingly important. Earlier investigations of polymer materials under reversed (R = -1) bending mode generated S-N curves, which revealed the superious overall fatigue resistance of epoxy resins. Figure 78 shows the representative curves of various plastics measured at ambient and with 30 Hz frequency.

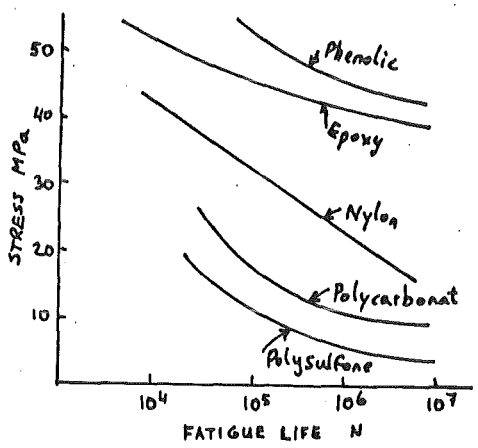

Fig. 78
Stress vs. cycle number plots for engineering plastics. After Riddel /76/.

The different damping characteristics of the polymers make them sensitive to the frequency. During cyclic loading the polymers heat up and a thermally induced damage mechanism may be apparent in addition to the mechanical damage. When crack propagation rates are compared, the relative ranking of the different polymeric materials with regard to fatigue strength is reversed (Fig. 79): Fatigue cracks are seen to propagate most rapidly in the epoxy resin.

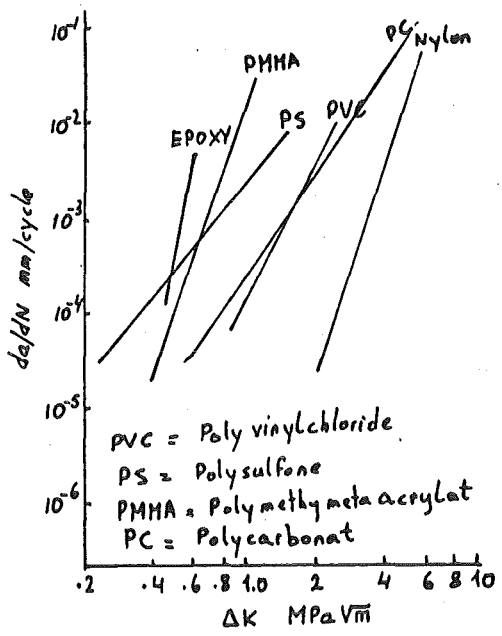

Fig. 79
FCGR data of different polymere materials at ambient. After Hertzberg et al. /77/.

According to the above findings the epoxy resins have high crack growth rates compared to polymers such as Nylon or Polycarbonat. The superiour FCGR behaviour of Nylon or Polycarbonats can be attributed to the cystalline regions, which retard the crack advance. This behaviour, however, can be quite different at low temperatures since these materials loose their viscoelastic properties during cool down. Recent fatigue strength investigations carried out at 77 K /78/ reveal that the 95 probability of survival of epoxy resin Cy 222/HY 979 is approximately ~ 70 % of the ultimate strength for unnotched specimens and ~ 50 % for notched (CT) specimens.

Fibre reinforcment of the epoxy changes the fatigue behaviour considerably and in general. Fatigue depends on the type of used fibres. Ambient results of tensile fatigue (R ≈ 0.1) tests with different fibres are shown in Fig. 80.

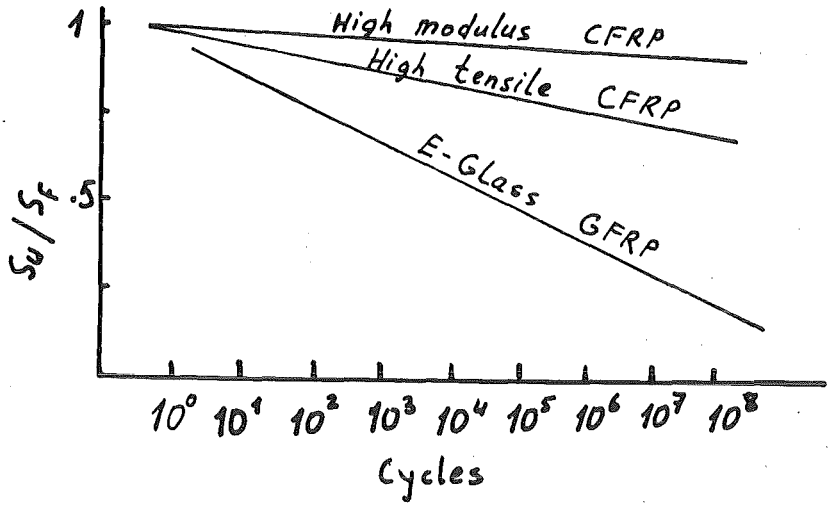

Fig. 80
Normalized S/logN curves for unidirectional reinforced epoxy with different fibres and $0^o/90^o$ laminate results for carbon fibre reinforced epoxy. After Jones /79/.

These results reveal the fact that with increased modulus of the fibres the fatigue strength of the composition are also increased. This behaviour is valid for tests carried out with a load ratio of R > 0. Under purely comparession/tension condition (R = -1) the fatigue resistance decreases drastically. For example, carbon reinforced epoxy retains only ~ 30 % of its strength for R = -1 condition /6/. This fact should be considered during design of structures made of composites.

4. Consideration of fatigue data in design

One of the most important questions in engineering design is the establishment of allowable stress limits for the materials considered. Safety factors for static conditions, frequently used in many guide books consider the experience gained for many years, and engineers are used to work with such factors. The establishment of safety factors against fatigue failure is a hard task because of the multitude of parameters involved which affect the structure during its service. The factors that can influence the fatigue initiation and the fatigue crack growth behaviour are:

i) Material variables;
composition, inclusion content, microstructure, processing.
ii) Environmental variables;
environmental chemistry, temperature, pressure.
iii) Loading variables;
load spectrum , load range, stress ratio, frequency, thickness, type of loading (uniaxial, bending, torsional or complex).

In the classical approach for designing against fatigue, the laboratory gained S-N data are corrected in accordance with the influences given above. The hidden philosophy behind the S-N design criterion approach is the "safe-life"-philosophy. The "safe-life"-philosophy relies on the provision of a valid S-N or ε-N data base. These data are then multiplied by a factor to provide the design curve. The data base can be gained either from material failures or failure of a structural detail expressed by stress range and cycles. The safety factor can vary according to the application; it can be increased e.g. for non-redundant parts whose fatigue failure results in catastrophic failure of the entire structure.

One suggestion for the correction of test data was given by Juvinal /80/. Taking account of Table 11 and Fig. 10, the number

of cycles N_T, determined in a fatigue test is multiplied by three factors to calculate the design life N_D:

$$N_D = K_D \cdot K_T \cdot K_S \cdot N_T$$

Table 11 Life reduction factors for standard rotating bending fatigue test data.

Factor	Type of load		
	Bending	Torsion	Axial
K_T	1.0	0.58	0.9
K_D, where Thickness < 10 mm	1.0	1.0	1.0
10 mm < Thickness < 50 mm	0.9	0.9	1.0
K_S	From Fig. 10		

For certain severe cases, the above correction delivers design lifes 20 times lower than the laboratory S-N test data. This seems to be very conservative but in certain design rules this practice has been already adopted and is today´s design guide against fatigue failure. The standard pressure vessel design code (ASME section VIII Div. 2 App. 5, Art 5-1) recommends as a design rule a factor of 20 on cycles and a factor of 2 on stress. The allowable design stress is then established by using the smaller value, This low value of allowable design stress is not surprising. Triaxial S-N-fatigue tests carried out in the past for mild steels /81/ delivered a value of about two for the ratio of uniaxial to triaxial loading.

Although the fatigue design rules for certain machinery and components, as stated above, is today´s practice, there is considerable disagreement for allowable stress limits in complex cases such as weldments. There is also a lack of a generally accepted fatigue design philosophy. Instead for each structural detail (Butt welds, Fillet welds etc.) a mandatory design

stress range exists, which is only valid for the special material and for the special use. There is even considerable difference of opinion around the world as to the appropriate fatigue design criteria. Figure 81 shows for several countries the marked variation in fatigue design criteria used for a single fillet welded joint and a design life of $2 \cdot 10^6$ cycles. The material was here a low alloyed ferritic steel.

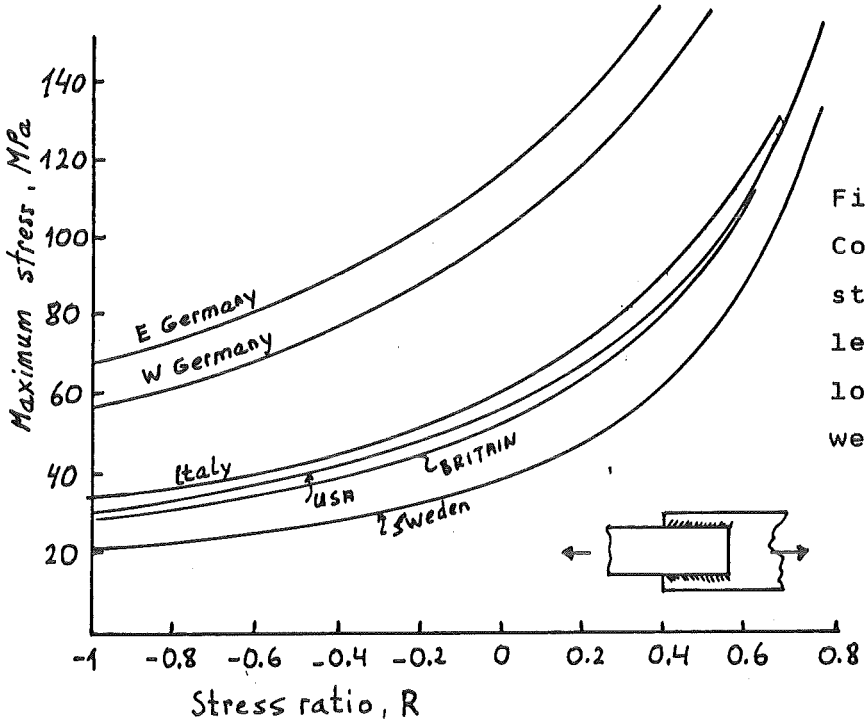

Fig. 81
Comparison of design stresses at $2 \cdot 10^6$ cycles for longitudinal load carrying fillet welded joints /82/.

The difference in maximum allowable design stress is about a factor of 3.5. Different levels of reliability result from such criteria. Therefore with improved fatigue information and better loading prediction the way is still open to achieve greater design economy in both live, time and money.

The limitations of safe-life assessment led to the development of the fatigue design philosophy "damage tolerance", which includes modern fracture mechanics. Its great advantage is the degree of certainty for the assessment. The advances in non-destructive inspection and fracture mechanics methodology are the

basis for development of this philosophy. The damage tolerance approach takes strongly into account that a structural member starts its service with preexisting defects (cracks, flaws, fissures etc.). The attractiveness of the "damage tolerance" philosophy is its ability at least in theory to calculate the remaining life of a structure under operation.

The procedure of assessment consists of simple steps which can be calculated easily.

i) Detection of an initial crack or service related crack and its measurement. This leads to a crack length assessment of size a.

ii) Calculation of the stress intensity range for the particular crack size and crack location. The equation used is of the form

$$\Delta K = Y . \Delta\sigma \sqrt{a} \qquad (18)$$

$\Delta\sigma$ is the applied cyclic stress field. Its magnitude and the distribution can be calculated by Finite Element Analysis. The factor Y is a function of crack size, geometric constraints and crack location.

iii) Materials data base concerning the FCGR, which can be measured.

iv) Integration of Paris Law (see 2.2) and the determination of the crack growth increment for the applied cycle number.

Out of these calculation a maximum tolerable crack size can be determined and the prediction of the components life is possible.

However, difficulties and limitation are encountered with each of the above steps and the "damage tolerance" method should be further developed.

These difficulties are summarized as follows:

i) The crack inspection is done by non destructive test (NDT) methods. The methods are: dye penetrant, radiography, eddy current, acoustic emmission, ultrasonic. Each of these methods has its own limitation. To have success in inspection, the simultaneous use of several different methods is necessary in many cases. The effectiveness of inspection depends on many factors, including material (ferritic or austenitic, weld- or bulk material), surface condition, section size and section geometry. Today under optimum conditions, cracks of order 0.1 mm may be detected, but it is much likely that pre- and in-service detection cannot guarantee crack sizes below 1 mm or more. The practice of complex austenitic structures such as the Euratom Large Coil case showed the detection limit of weld defects to be > 2 mm in size /84/. On the other hand, the exact determination of the initial crack size is very important, because the FCGR integration is very sensitive to the initial crack size, due to the exponential nature of the law.

ii) Specific ΔK determination depends on the local orientation of the crack and the structure geometry. The computation procedure is very complex because ΔK varies around the periphery of a two dimensional crack. Local plasticity makes the ΔK characterization even more difficult, because of the complex elastoplastic parameters. The stress distribution around the crack is triaxial and its determination is not easy. The FCGR power law with an exponent of 2 - 4 makes ΔK a senstitive parameter in the crack growth assessment.

iii) The curves da/dN vs. ΔK for the particular material have non linear region in near threshold and threshold regime. The definition and the use of the curve in this regime is difficult and the calculation is very sensitive to small variations. The laboratory test data should be translated

to the specific environment and loading conditions used. The data scatter and a realistic confidence level should be considered for such measurements. In certain instances round robin tests (same material tested in different laboratories) could be adequate to gain relevant data for the particular material.

Considering these points, it seems that the "damage tolerance" philosophy requires more experience and practical background to become a useful tool for the engineer. These difficulties make necessary to introduce also safety factors on stress and cycles. For tokamak type cold structures, the general suggestions made up to now result in a safety factor of two on stress /83/. More relevant studies, tests and experience will show the actual limitations of the materials use under cyclic conditions.

A proposal to incorporate the "damage tolerance" philosophy for structures operating at 4 K can be made tentatively according to the present data base. It is reasonable to calculate the weld metal fatigue response, because the weldments in general are accepted as the weakest point in a structure. The reason for this can be given by the following arguments. First, the weldments bear already weld process related defects. This means that the weld section is in a precracked situation from the very beginning of operation. Second, the weld metal fracture toughness properties are in general lower than the bulk metal properties. Therefore, it seems appropriate to use the weld metal data instead of the bulk metal data.

As an example, the 4 K residual fatigue crack growth life of the austenitic stainless steel type 316 LN as weld metal was calculated (Fig. 82).

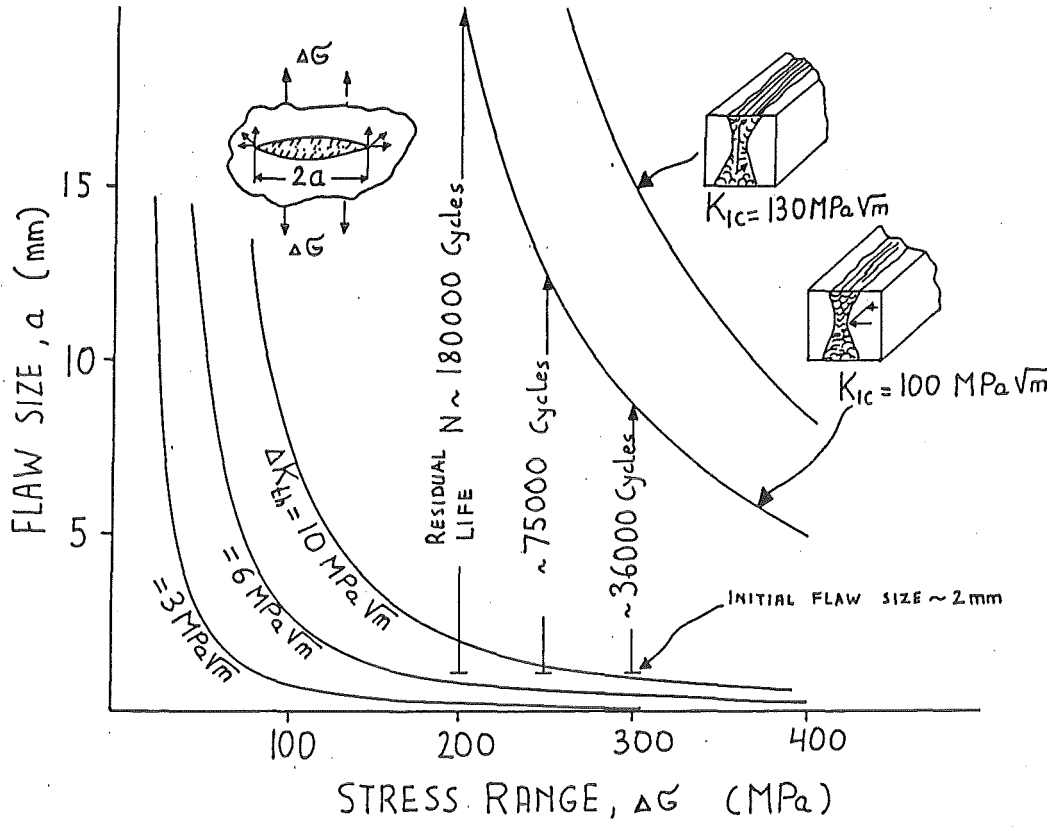

Fig. 82 4 K fatigue response of austenitic type 316 LN weld metal. Tested weldment was a double U-type joint.

The three distinct curves for the threshold conditions are calculated using the fracture mechanics concept for defects with a penny shaped crack morphology. The equation according to /12/

$$\Delta K_{th} = \frac{2}{\pi} \cdot \Delta\sigma \cdot \sqrt{\pi} \cdot \sqrt{a} \qquad (19)$$

gives the relationship between stress range, crack size and the threshold stress intensity range. The upper curves of Fig. 82 show the weld metal fracture toughness performance. The data for K_{IC} (100 MPa$\sqrt{m}$ and 130 MPa$\sqrt{m}$), have been taken from recent measurements /32/. The difference is due to the crack orientation in the weld metal. As shown, the root section of the weld metal reveals the lowest fracture toughness value. In Fig. 82 the static collapse of the structure due to crack advance is calculated

by using the equation

$$a_{cr} = \left(\frac{K_{Ic}}{2\,\sigma_{max}\sqrt{\pi}} \right)^2 \qquad (20)$$

where a_{cr} is the critical crack size and σ_{max} the stress maximum. A safety factor of 2 on stress has been assumed /32/.

Using now the integrated form of the Paris equation (see Fig. 82) one is able to calculate the residual life of a cracked component. The values for n and C_0 are measured at 4 K and taken from /29/:

$n = 3.75$

$C_0 = 3.54 \times 10^{-13}$ m/cycle

$Y = 1.2$

Starting with 2 mm flaw size (2a = 2 mm) the equation delivers a residual life of 180,000 cycles for $\Delta\sigma$ = 200 MPa. This value decreases to 36,000 cycles at 300 MPa stress range. Figure 82 gives also further information concerning the materials threshold level. Increasing the threshold level from ΔK_{th} = 6 MPa$\sqrt{m}$ to ~ 10 MPa$\sqrt{m}$ gives safe operation for the component being considered, because below this value no crack propagation is expected for the given boundary conditions. Increasing the threshold value by material improvement is one way to prevent cyclic damage. The other way is to reduce the probable flaw sizes during the fabrication, which is a question of good workmanship, quality control, and proper selection of the processing. In practice both ways should be tried to increase the safety of a component under cyclic load.

5. References

/1/ Timoshenko, Stephen P.: "History of strength of materials", Mc Graw-Hill Book Company, New York, 1953.

/2/ Kennedy, A.J.: "Process of creep and fatigue in metals", Oliver & Boyd Ltd., London 1962.

/3/ Teed, P.L.: "The properties of metallic materials at low temperature", Chapman & Hall, Ltd., London, 1950.

/4/ Heywood, R.B.: "Designing against fatigue", Chapman Hall, Ltd., London 1962.

/5/ Forrest, P.G.: "Fatigue of metals", Pergamon Press, New York 1962.

/6/ Piggot, M.R.: "Load bearing fibre composites", Pergamon Press, Oxford 1980.

/7/ Yao, J.T.P. and W.H. Munse: The welding journal 41, No. 4, 1962, p. 182s.

/8/ Manson, S.S. and M.H. Hirschberg: "Fatigue: An Interdisciplinary Approach", Syracuse University Press, Syracuse, N.Y. 1964, p. 133.

/9/ Olivier, R. and W. Ritter: "Catalogue of S-N-curves of welded joints in structural steels. Part 1: Butt Joints" DVS Berichte 56/1, 1979.

/10/ Westergaard, H.M.: Trans, ASME J. Appl. Mech. 61, 1939 p. 49.

/11/ ASTM Designation E 647-78 T, ASTM STP 738, 1981, p. 321.

/12/ Hertzberg, R.W.: Deformation and fracture mechanics of Engineering Materials, John Wiley & Sons, New York (1976).

/13/ Paris, P.C.: "Fatigue - An Interdisciplinary Approach", Proceedings 10th Sagamore Conference, Syracuse University Press, Syracuse, N.Y., 1964, p. 107.

/14/ Tobler, R.L. and R.P. Reed: Adv. in Cryo. Eng., Plenum Press Vol. 22, 1975, p. 35.

/15/ Forman, R.G., Kearney, V.E. and R.M. Engle: J. Basic Eng. Trans., ASME 89, 1967, p. 459.

/16/ Trebules, V.W., Roberts R. and R.W. Hertzberg: ASTM STP 536, 1973, p. 115.

/17/ Barsom, J.M.: ASTM STP 536, 1973, p. 147.

/18/ Barsom, J.M.: Journal ob Basic Engineering, Trans. ASME series B, Vol. 93 No. 4, Nov. 1971.

/19/ Bucci, R.J.: ASTM STP 738, 1981, P. 5.

/20/ Imhof, E.J. and J.M. Barsom: ASTM STP 536, 1973, p. 182.

/21/ Weber, J.H. and R.W. Hertzberg: Met. Trans. 4, 1973, p. 595

/22/ Bucci, R.J., Greene B.N. and P.C. Paris: ASTM STP 536, 1973, p. 206.

/23/ Sandifer, J.P. and G.E. Bowie: ASTM STP 648, 1978, p. 185.

/24/ Mc.Henry, H.I. and A.W. Pense: ASTM STP 520, 1973, p. 345.

/25/ Sadananda, K. and P. Shahinian: Journal of Eng. Mat. and Technology, Transactions of the ASME, Vol. 100, No. 4, Oct. 1978, p. 381.

/26/ Tobler, R.L. and R.P. Reed: Adv. in cryo. eng. Vol. 22, 1975, p. 35.

/27/ Nakajima, H., Shoji T., Kikuchi M., Niitsuma H., and M. Shindo: ASTM STP 738, 1981, p. 139.

/28/ Metzner, M.: KfK investigations 1984, to be published.

/29/ Nyilas, A., Krauth H., Metzner M., and D. Munz: Proc. of Fatigue 84, 2nd int. conf. on fatigue and fatigue thresholds, Birmingham 1984, p. 1637.

/30/ Gideon, D.N., Favor R.JH., Grover H.J., and G.M. McCluse: Adv. in Cry. Eng. Vol. 7, 1961, p. 503.

/31/ Grindberg, N. M., Aleksenko E.N., Yushchenko K.A., and L.G. Kulikova: Cryogenics, July 1982, p. 348.

/32/ Nyilas A., Krauth H., and E. Lohse: DVS Berichte 75, 1982, p. 200.

/33/ Morris, J.W., and E.N.C. Dalder: RXD Kobe steel, Eng. Reports, Vol. 34, 1984, p. 1.

/34/ Tobler, R.L., McHenry H.I., and R.P. Reed: Adv. in Cryo. Eng., Plenum Press, Vol. 24, p. 560.

/35/ Tobler, R.L. and R.P. Reed: Adv. in Cryo. Eng., Plenum Press, Vol. 22, 1975, p. 35.

/36/ Tobler R.L. and R.P. Reed: Adv. in Cry. Eng., Vol. 22, 1975, p. 35.

/37/ Katz, Y., Bussiba A., and H. Mathias: Fracture and the role of microstructure, Vol. II, Proc. of ECF 4, Editor K.L. Maurer, Leoben, 1982, p. 503.

/38/ Liaw, P.K., Logsdon W.A., and M.H. Attar: Cryogenics, 23, 1983, p. 523.

/39/ Whipple, T.A., McHenry H.I., and D.T. Read: Welding Journal 60, 4, 1981, p. 72s.

/40/ Shiraishi, K., 1982 IEA Workshop on special materials for fusion, Culham Lab..

/41/ Reed, R.P., Tobler R.P., and R.P. Mikesell: Adv. in Cry. Eng. Vol. 22, 1975, p. 68.

/42/ Phase II Detailed Design Analysis Report for LCP prepared by General Electric under UCC contract 22X-31745C.

/43/ Vol. II Structural Analysis of the Phase II Analyses Report for LCP prepared by GD-Convair Division for UCC under contract 22X-31746C; GD Report 91Z0080-1.

/44/ Wells, J., Kossowski R., Logsdon W., and M. Daniel: "Structural Materials for Cryogenic Application", Materials Research for Superconducting Machinery, Vol. VI, NBS-ARPA, Sept. 1976, p. 112.

/45/ IEA Workshop on special materials for fusion, Culham Lab., 1982.

/46/ Staal, H.U.: Netherlands Energy Research Foundation Report, ECN-90, March 1981.

/47/ Stahlberg R.: Arch. Eisenhüttenwesen 49, Nr. 1, 1978, p 1.

/48/ Hawthorne J.R.: Fatigue Environment and Temperature Effects, Ed. J.J. Burke and V. Weiss, 1983, Plenum Press, New York, p. 195.

/49/ Dalder E.N.C.: Technical meeting between LLNL and KfK, March 1984.

/50/ Rhodes D., Nix K.J., and J.C. Radon: Fracture and the role of microstructure, Vol. II, Proc. of ECF4, Editor K.L. Maurer, Leoben, 1982, p. 443.

/51/ Evans B.: 5th Int. Conf. Materials and Process, Sampe, Paper 8, Montreaux, June 1984.

/52/ Petit J., Renaud P., and P. Violan: Fracture and the role of microstructure, Vol. II, Proc. of ECF 4, Editor K.L. Maurer, Leoben, 1982, p. 426.

/53/ Mann D.: Ed. LNG Materials & Fluids (1. Revised Edition) Cryogenic Division, National Bureau of Standards, US Dept. of Commerce, 1977.

/54/ Lucas J.J.: Titanium Science and Technology, Vol. 3, p. 2081, Plenum Press, New York, 1973.

/55/ Robinson J.L. and C.J. Beevers, Metal Sci, J., Vol. 7, 1973, p. 153.

/56/ Yuen A., Hopkins S.W., Leverant G.R., and C.A. Rau: Met. Trans. Vol. 5A, 1974, p. 1833.

/57/ Swanson J.W. and H.L. Marcus: Met. Trans., Vol. 9A, 1978, p. 291.

/58/ Sallade P.L.: Masters Thesis, Univ. of Connecticut, CT. 1970.

/59/ Wigley D.A.: Mech. Properties of Materials at Low Temperatures, Plenum Press, 1971.

/60/ Lukas P.: "Models for ΔK_{th} and Near-Treshold Fatigue Crack Growth", 2nd Int. Conf. on fatigue and fatigue thresholds, Fatigue 84, Invited Lecture, Birmingham 1984.

/61/ Lukas P. and L. Kunz: Mat. Sci. Eng., 62, 1984, p. 149.

/62/ Butts A. ed. Copper, The science and technology of the metal, its alloys and compounds, Reinhold Publishing Corp., New York (1954) p. 369.

/63/ Andersen A.R., Swan E.F., and Palmer E.W.: Proc. A.S.T.M. Vol. 46 (1946) p. 678.

/64/ Andersen A.R. and Smith C.S.: Proc. A.S.T.M. Vol. 41 (1941) p. 846.

/65/ Burghoff H.L. and Blank A.I.: Proc. A.S.T.M. Vol. 48 (1948) p. 709.

/66/ Metals Handbook, Vol. 1, 8th ed. Am. Soc. for Metals, Cleveland, Ohio, (1961), p. 1028.

/67/ Gross M.R. and Schwab R.C.: US Navy Marine Eng. Lab. Annapolis, Md. R and D Rept. No. 232/66 (1966) (AD 633 771).

/68/ Czyryca E.J. and Schwab R.C.: Naval Ship Res. and Dev. Center, Annapolis, Md. Rept. No. 2445 (1967) (AD 656 574).

/69/ Burghoff H.L. and Blank A.I.: Proc. A.S.T.M., Vol. 47 (1947) p. 695.

/70/ NBS Monograph 101, Low Temp. mech prop. of copper and selected copper alloys, US Dept. of Commerce.

/71/ Scarlin R.B., Melton K.N., and W. Hoffelner: Fracture and the role of microstructure, Vol. II, Proc. of ECF 4, Editor K.L. Maurer, Leoben, 1982, p. 689.

/72/ Florean S. and R.H. Kane: Nickel Topics, Vol. 34, No. 2, 1981, p. 6.

/73/ Logsdon W.A.: Adv. in Cry. Eng., Vol. 22, 1975, p. 47.

/74/ Degallaix S., Faillard R., and J. Foct: Proc. of 2nd Int. Conf. on Fatigue and Fatigue Thresholds, Ed. C.J. Beevers, Birmingham, 1984, p. 49.

/75/ Gross M.R.: Naval Eng. Journal, Oct. 1963, p. 783.

/76/ Riddel M.N.: Plast. Eng. 30 (4), 1974, p. 71.

/77/ Hertzberg R.W. and J.A. Manson: Fatigue in Engineering Plastics, Academic Press, New York, 1980.

/78/ Hartwig G.: Adv. in Cryo. Eng., Plenum Press Vol. 24, 1977, p. 17.

/79/ Jones, C.J., Dickson R.F., Adam T., Reiter H., and B. Harris: 2nd Int. Conf. on Fatigue and Fatigue Thresholds, Ed. C.J. Beevers, Birmingham, 1984, p. 1076.

/80/ Juvinall R.C.: Engineering Considerations of Stress, Strain and strength, Mc Graw Hill, 1967.

/81/ Welter G and J.A. Choquet: Welding Res. Supplement, 1963, p. 565s.

/82/ Munse W.H.: ASTM STP 648, D.W. Hoeppner, Ed., 1978, p. 89.

/83/ Hooper R.J. and B.L. Hunter: "Structural Design Procedures for FED Magnets", 9th Symp. Eng. Prob. Fusion Res., Chicago, 1981, p. 539.

/84/ Nyilas A. and H. Krauth: To be published in Int. Cryo. Mat. Conf. proceedings, Kiew, 1984.